

Searches for long-lived particles at the Large Hadron Collider at CERN

February 4, 2018

Abstract: Searches for long-lived particles (LLPs) beyond the Standard Model at the Large Hadron Collider — particles that can have non-negligible lifetimes and decay to SM particles within detectors but substantially displaced from the interaction vertex — constitute a rich, challenging, and increasingly fascinating avenue via which new physics may be discovered at the LHC. Members of the ATLAS, CMS, and LHCb experiments in conjunction with theorists, phenomenologists, and those working on dedicated experiments such as Moedal, MilliQan, MATHUSLA, CODEX-b, and FASER, here report upon the state of LLP searches at the LHC; propose a set of simplified models for LLP searches; survey the existing searches, the experimental coverage of LLP signatures, and enumerate gaps in this coverage; identify high-priority studies to be performed by the experimental collaborations to ensure that LLP signatures are not missed in detector upgrades planned for the upcoming high-luminosity era at the LHC; propose recommendations for new triggering strategies for LLPs in ATLAS, CMS, and LHCb; list ideas for new searches for LLPs; propose a set of recommendations for the presentation of search results to ensure future reinterpretation and recasting for LLP searches; discuss new frontiers for LLP searches such as those involving dark sector QCD-like theoretical ideas; and describe the often unexpected experimental challenges inherent in LLP searches, including atypical or non-standard background sources.

Is your name missing? Let us know!

James Beacham (editor) *Ohio State University, Columbus, OH, USA*

Brian Shuve (editor) *Harvey Mudd College, Claremont, CA, USA*

Giovanna Cottin (Simplified Models & Reinterpretations chapter editor) *National Taiwan University, Taipei, Taiwan*

David Curtin (Simplified Models & Experimental Coverage chapter editor) *University of Toronto, Toronto, ON, Canada*

Jared Evans (Simplified Models & Experimental Coverage chapter editor) *University of Cincinnati, Cincinnati, OH, USA*

Zhen Liu (Simplified Models & Reinterpretations chapter editor) *Fermilab, Batavia, IL, USA*

Michael Ramsey-Musolf (Simplified Models chapter editor) *University of Massachusetts, Amherst, MA, USA*

Jessie Shelton (Simplified Models chapter editor) *University of Illinois, Urbana, IL, USA*

Xabier Cid Vidal (Experimental Coverage chapter editor) *Universidade de Santiago de Compostela, Santiago, Spain*

Albert de Roeck (Experimental Coverage chapter editor) *CERN, Geneva, Switzerland*

Heather Russell (Experimental Coverage chapter editor) *McGill University, Montreal, QC, Canada*

Jose Zurita (Experimental Coverage chapter editor) *Karlsruher Institut für Technologie, Karlsruhe, Germany*

Germany

Yangyang Cheng (Upgrades chapter editor) *Cornell University, Ithaca, NY, USA; and FNAL, Batavia, IL, USA*

Sabine Kraml (Reinterpretations chapter editor) *LPSC Grenoble, Grenoble, France*

Andre Lessa (Reinterpretations chapter editor) *Universidade Federal do ABC, SP, Brazil*

Oliver Buchmueller (Simplified Models WG convener) *Imperial College, London, UK*

Juliette Alimena (Reinterpretations WG convener, Backgrounds chapter editor) *Ohio State University, Columbus, OH, USA*

Will Buttinger (Reinterpretations WG convener) *CERN, Geneva, Switzerland*

Jared Evans (Reinterpretations WG convener) *University of Cincinnati, Cincinnati, OH, USA*

Sascha Mehlhase (Backgrounds WG convener and chapter editor) *Ludwig-Maximilians-Universität Munich, Munich, Germany*

Martino Borsato (Backgrounds chapter editor) *Universidade de Santiago de Compostela, Santiago, Spain*

Andreas Albert *RWTH Aachen University, Aachen, Germany*

Bobby Acharya *Abdus Salam International Centre for Theoretical Physics, Trieste, Italy*

Cristiano Alpigiani *University of Washington, Seattle, WA, USA*

Simone Amoroso *CERN, Geneva, Switzerland*

Andrea Coccato *INFN e Universita Genova, Genova, Italy*

Eric Conte *GRPHE, Université de Haute-Alsace, IUT Colmar, France*

Yanou Cui *University of California, Riverside, CA, USA*

Alessandro Davoli *SISSA, Trieste, Italy*

Andrea De Simone *SISSA, Trieste, Italy*

Nishita Desai *CNRS-Université de Montpellier, Montpellier, France*

Sven Dildick (contributor) *Texas A&M University, College Station, TX, USA*

Benjamin Fuks *LPTHE, CNRS and Institut Universitaire de France, Paris, France*

Stefano Giagu *Sapienza Universita e INFN, Roma, Rome, Italy*

Andrew Haas *New York University, New York, NY, USA*

Kristian Hahn *Northwestern University, Evanston, IL, USA*

Jan Heisig *RWTH Aachen University, Aachen, Germany*

Gavin Hesketh (Reinterpretations WG convener) *University College London, London, UK*

Tao Huang (contributor) *Texas A&M University, College Station, TX, USA*

Philip Ilten *University of Birmingham, Birmingham, United Kingdom*

Thomas Jacques *SISSA, Trieste, Italy*

Ted Kolberg *Florida State University, Tallahassee, FL, USA*

Revital Kopeliansky *Indiana University, Bloomington, IN, USA*

Lawrence Lee, Jr. *Harvard University, Cambridge, MA, USA*

Henry Lubatti *University of Washington, Seattle, WA, USA*
Michelangelo Mangano *CERN, Geneva, Switzerland*
Matthew McCullough *CERN, Geneva, Switzerland*
Philippe Mermod *Universite de Geneve, Geneva, Switzerland*
David Morse *Northeastern University, Boston, MA, USA*
Stephen Mrenna *Fermilab, Batavia, IL, USA*
Christian Ohm *KTH Royal Institute of Technology, Stockholm, Sweden*
Hideyuki Oide *INFN e Universita Genova, Genova, Italy*
Rachel Christine Rosten *institute*
Ennio Salvioni *Technical University of Munich, Garching, Germany*
Ryu Sawada *University of Tokyo, Tokyo, Japan*
Michele Selvaggi *CERN, Geneva, Switzerland*
Emma Torro Pastor *University of Washington, Seattle, WA, USA*
Marco Trovato *Northwestern University, Evanston, IL, USA*
Yuhsin Tsai *University of Maryland, College Park, MD, USA*
Carlos Vasquez Sierra *Nikhef, Amsterdam, Netherlands*
Monica Verducci *INFN Sezione di Roma Tre, Rome, Italy*
Gordon Watts *University of Washington, Seattle, WA, USA*

Contact editors: lhc-llp-admin@cern.ch

Contents

1	<i>Introduction</i>	7
	1.1 <i>Goals of the White Paper</i>	7
2	<i>Simplified Models Yielding Long-Lived Particles</i>	9
	2.1 <i>Goals of the Present Simplified Model Framework</i>	11
	2.2 <i>Existing Well-Motivated Theories for LLPs</i>	12
	2.3 <i>The Simplified Model Building Blocks</i>	14
	2.4 <i>A Simplified Model Proposal</i>	20
	2.5 <i>Proposal for a Simplified Model Library</i>	26
	2.6 <i>Future Opportunities and Challenges</i>	29
3	<i>Experimental Coverage of Long-Lived Particle Signatures</i>	31
	3.1 <i>Survey of the Current Experimental Long-Lived Program</i>	32
	3.2 <i>Overview of Gaps</i>	50
4	<i>Trigger and Detector Upgrades</i>	53
	4.1 <i>The ATLAS and CMS experiments</i>	53
	4.2 <i>LHCb Upgrade</i>	73
	4.3 <i>Current and Proposed Dedicated LLP Detectors</i>	83
5	<i>Reinterpretation and Recommendations for the Presentation of Search Results</i>	85
	5.1 <i>Introduction</i>	85
	5.2 <i>Options for Presenting Experimental Results</i>	87
	5.3 <i>Reinterpretation using Simplified Models</i>	89
	5.4 <i>Recasting Examples for Specific Searches</i>	93

5.5	<i>Handling long-lived particles in DELPHES-based detector simulations</i>	109
5.6	<i>Recasting Inside the Experimental Collaborations</i>	114
5.7	<i>Reinterpretation with Prompt Analysis</i>	115
5.8	<i>Our Proposals for the Presentation of Results</i>	116
6	<i>Frontiers: Dark Showers and Quirky Signatures</i>	119
6.1	<i>Dark Showers</i>	119
6.2	<i>Quirks</i>	119
7	<i>Conclusions</i>	121
A	<i>Appendix: Discussion of Backgrounds for LLP Searches</i>	123
A.1	<i>Introduction</i>	123
A.2	<i>Known long-lived particles</i>	123
A.3	<i>Real particles generated in the detector</i>	123
A.4	<i>Real particles generated outside the detector</i>	124
A.5	<i>Fake particle signatures</i>	126
A.6	<i>Algorithmically induced fakes</i>	126
A.7	<i>Summary</i>	127

1

Introduction

Put introduction to the long-lived particle search program at the LHC. Brief overview of theory motivation (on a general level, with citation dumps) as well as the general challenges and opportunities of experimental searches for LLPs (again, broad brush with lots of citations).

1.1 Goals of the White Paper

In recent years, there has been a proliferation of work on LLP both on the theory and experiment side. This is due to the success of experimental techniques to reconstruct LLPs in earlier runs of the LHC and the theoretical development of well-motivated models that give rise to a range of LLP signatures. It is also in part due to the lack of positive signals of new particles in other, more conventional LHC searches, giving heightened urgency and importance in the coverage of LLP signatures.

To this end, the document serves to assess the current status of LLP searches at the LHC, determining where searches currently have good coverage of LLP searches and where there can be improvements. It also evaluates the impact of possible new triggers or upgrades on the performance of LLP searches in advance of the final decisions for Phase 2 upgrades. Finally, it provides recommendations for the presentation of search results to broaden the impact of existing and planned searches, and to chart a course for the near-future development of the program.

More concretely,

1. We develop a minimal (but expandable) simplified models framework for the LLP program that incorporates the best-motivated LLP theories and models
2. We use the simplified models framework to assess the sensitivity of current searches and identify the highest priority gaps in coverage
3. These in turn inform the development of triggers and decisions about upgrade technologies, and we summarize the impact of possible new upgrades (including existing and planned dedicated detectors such as Moedal, MilliQan, MATHUSLA, ...)

4. Provide a summary of recommendations for the presentation of new LLP searches
5. Identify the new frontiers of LLP searches in which more research and development is needed, particularly in the area of high-multiplicity LLP searches (dark showers)

Simplified Models Yielding Long-Lived Particles

Long-lived particles (LLPs) arise in many well-motivated theories of physics beyond the Standard Model (SM), ranging from well-established scenarios such as the minimal supersymmetric Standard Model (MSSM) to newer theoretical frameworks such as neutral naturalness and hidden sector dark matter. Macroscopic decay lengths of new particles naturally arise from the presence and breaking of new symmetries, which can be motivated by cosmology (such as dark matter and baryogenesis) [1, 2, 3, 4, 5, 6, 7, 8, 9, 10, 11, 12], neutrino masses [13, 14, 15, 16, 17, 18, 19], as well as solutions to the hierarchy problem [20, 21, 22, 23, 24, 25, 26, 27, 28]; indeed, LLPs are generically a prediction of new weak-scale hidden sectors [29, 30, 31, 32, 33, 34, 35, 36, 37]. A comprehensive search program for LLPs is therefore critical to fully leverage the LHC’s immense capability to illuminate the physics of the weak scale and beyond.

LLPs present both major opportunities and major challenges for searches at the LHC. On the one hand, SM backgrounds are small for signals originating far from the collision point, making prospects for discovering displaced signals much better than for similar prompt signals in many scenarios. On the other hand, searches for LLPs demand specialized techniques at all stages of the analysis, from the trigger level to reconstruction to background estimation. Background estimation in particular presents unique challenges: the spectacular nature of LLP decays, together with low signal rates, means backgrounds are dominated by very rare processes which are difficult to model and sometimes cannot be reliably simulated. Because LLP searches involve aspects of detector response that cannot be reliably simulated by theorists with public Monte Carlo tools (and, indeed, may not be reliably simulated by tools internal to experimental collaborations as well), it is notoriously difficult for individuals outside of the experimental collaborations to accurately apply search results to new theoretical models. This potentially limits the future applicability of current searches to models that are developed in the future.

This document builds on the exceptional success of the existing LHC program for LLPs. We propose a systematic framework for future LLP searches that aims to ensure that experimental results are (i) *powerful*, covering as much territory as possible; (ii) *efficient*,

reducing unnecessary redundancy among searches; (iii) *flexible*, so that they are broadly applicable to different types of models, and (iv) *durable*, providing a common framework for Monte Carlo simulation of signals, and facilitating the communication of results of LLP searches so that they may be compared and applied to new models for years to come. We elaborate on these goals in Section 2.1. We expect that this common framework will help illuminate gaps in coverage and highlight areas where new searches are needed, and we undertake such a study in Section ??.

The simplified models framework has proven to be a highly successful approach for accomplishing the above goals for signatures featuring prompt decays of new particles [38] or dark matter produced at colliders [39]. Simplified models are so successful because the majority of search sensitivity is driven by only a few broad aspects of a given beyond-SM (BSM) signature such as the production process, overall production rate, and decay topology. Meanwhile, the sensitivity of searches is typically insensitive to other properties such as the spin of the particles involved [40, 41, 42, 43].

Our aim here is to construct an initial basis of simplified models representative of theories giving rise to final states with one or two LLPs¹. The simplified model approach is very powerful for LLP signatures: the typically lower backgrounds for displaced signatures allow searches to be highly inclusive with respect to other objects in the event or the identification of objects originating from the displaced vertex. This enables a single analysis to have sensitivity to a wide variety of possible models for LLP production and decay. Our efforts build on earlier work proposing simplified model programs for LLPs motivated by particular considerations such as supersymmetry (SUSY) or dark matter (DM) [44, 45, 46, 47, 48, 49].

We organize our simplified models in terms of **LLP channels** characterized by a particular LLP production mode and a particular decay mode. Because the production and decay positions of LLPs are physically distinct², it is possible to factorize and consider separately their production and decay.³ For each LLP channel, the lifetime of the LLP is taken to be a free parameter. We emphasize that the LLP channel defined here is *not* the same as an experimental signature that manifests in the detector: a single channel can give rise to many different signatures depending on where (or whether)⁴ the LLP decays occur inside the detector, while a single experimental search for a particular signature could potentially cover many simplified model channels. In this document, we focus on the construction and simulation of a concrete basis of LLP simplified model channels; a partial mapping of existing searches into our basis of simplified models is discussed in Section ??, along with the highest-priority gaps in current coverage and proposals for new searches.

As discussed in the existing simplified models literature, simplified models have their own limited range of applicability [38,

¹ Some models predict moderately higher LLP multiplicities, but the coverage of such signatures from 1-2 LLP searches is good provided the LLPs do not overlap in the detector. Our proposed simplified models are not, however, representative of high-multiplicity signatures such as dark showers (see Section 2.6).

² Stable LLPs, which for neutral LLPs appear as missing E_T [39], and for charged/colored LLPs appear as stable tracks or R -hadrons, can be covered in this framework by taking the decay length $c\tau \rightarrow \infty$. External detectors can also be used to search for ultra-long-lived neutral or milli-charged particles [50, 51, 52, 53].

³ In addition to production and decay, a third consideration is the propagation of particles through the detector. While particles that do not possess color charge undergo straightforward propagation, colored states, *e.g.*, SUSY R -hadrons, or particles with exotic charges such as magnetic monopoles or quirks, typically engage in a more complicated and often very uncertain traverse through the detector. The subtleties with colored LLPs will be discussed more in subsection 2.4.3. A trickier question is how to best simulate such states: since charged or colored LLPs interact with the detector material, there must be an interface between the detector simulation software and the program implementing decay. See Section ?? for a more detailed discussion.

⁴ The range of detector stability.

[39]. For example, the presentation of search results in terms of simplified models often assume 100% branching fractions into particular final states. In a UV model where the LLP decays in a very large number of ways, none of the individual simplified model searches may be sufficient to constrain it. Similarly, if the LLP is produced in a UV model with other associated objects that spoil the signal efficiency (for example, the production of energetic, prompt objects collimated with the LLP such that the signal fails isolation or displacement criteria; this is particularly important for high-multiplicity or dark-shower scenarios), then the simplified model result does not apply. Nevertheless, the simplified models framework allows us to organize possible production modes and signatures in a systematic way and identify if there are any interesting signals or parts of parameter space that are missed by current searches. Search results presented in terms of simplified models also cover a wide range of UV models. Therefore, we present a proposal for simplified models here with the understanding that there exist scenarios where UV models remain important for developing searches and presenting results.

The basis of simplified models presented here is a starting point, rather than a final statement: the present goal is to provide a set of simplified models that covers many of the best-motivated and simplest models containing singly- and doubly-produced LLPs (and, by extension, many models with 3-4 relatively isolated LLPs as well). Simplified models by design do not include all of the specific details and subtle features that may be found in a given complete model. Therefore, the provided list is meant to be expandable to cover new or more refined models as the LLP search program develops. For instance, extending the simplified model framework to separately treat final states with heavy flavor particles is of high interest (in analogy with the prompt case [54, 55, 56]); see Section 2.6 for a discussion of this and other future opportunities. High-multiplicity signatures such as dark showers or emerging jets present different experimental and theoretical issues. Also, a broader set of simplified models may be needed to present the results of experimental searches and to allow ready application of experimental results to UV models of interest.

2.1 Goals of the Present Simplified Model Framework

The purpose of the simplified model framework is to provide a simple, common language that experimentalists and theorists can use to describe theories of LLPs and the corresponding mapping between models and experimental signatures. We therefore want our simplified model space to:

1. Use a minimal but sufficient set of models to cover a wide range of the best-motivated theories of LLPs;
2. Furnish a simple map between models and signatures to enable

- a clear assessment of existing search coverage and possible gaps;
- 3. Expand flexibly when needed to incorporate theories and signatures not yet proposed;
- 4. Provide a concrete Monte Carlo signal event generation framework;
- 5. Facilitate the re-interpretation of searches by supplying a sufficiently varied set of standard benchmark models⁵ for which experimental efficiencies can be provided for validation purposes.

Note that points #1 and #5 are somewhat in tension with one another: we wish to have a compact set of models that can be the subject of systematic study in terms of experimental signatures, but expressing experimental results in terms of only this set of simplified models may make it challenging to re-interpret experimental searches for UV models that are not precisely described by one of the simplified models. In this section, we prioritize having a minimal set of simplified models for the purpose of studying experimental coverages and generating new search ideas, while we defer a discussion of simplified models in the presentation and reinterpretation of search results to Section ??.

In the following sections, we construct a proposal for a minimal basis of simplified models for events with one or two LLPs. We begin with a discussion of the theories that dominate the predictions for LLPs at the LHC, and identify a set of ‘umbrella’ models that yield LLPs in Section 2.2. We next identify the relevant (simplified) production and decay modes for LLPs in Section 2.3, emphasizing that each production mode has a characteristic set of predictions for the number and nature of *prompt* objects accompanying the LLP. In Section 2.4 we combine these production and decay modes into our simplified model basis and highlight how different umbrella models naturally populate the various LLP channels. Section 2.5 and Appendix ?? presents a framework and instructions for how the best motivated simplified model channels can be simulated in Monte Carlo using a new model library that is currently under development.

2.2 Existing Well-Motivated Theories for LLPs

Here we provide a brief distillation of many of the best-motivated theories with LLPs into five over-arching categories, focusing in particular on those that give rise to single and double production of LLPs at colliders. We emphasize that each of these categories is a broad umbrella containing many different individual models containing LLPs; in many cases, the motivations and model particulars among theories within a particular category may be very different, but tend to predict similar types of LLPs. In all cases, long lifetimes typically arise from some combination of hierarchies of scales in

⁵ Note that in general more benchmark models will be needed for enabling reliable re-interpretation than are strictly necessary for discovering a new particle, *i.e.*, it is important to consider both whether two simplified models share a common signature in a search, and also whether they look similar enough to have similar reconstruction efficiencies

interactions that mediate decays; small couplings; and phase space considerations (such as small mass splittings between particles).

The UV umbrella models we consider are:

- **Supersymmetry-like theories (SUSY).** This category contains models with multiple new particles carrying SM gauge charges and a variety of allowed cascade decays. LLPs can arise as a result of approximate symmetries (such as R -parity [25] or indeed SUSY itself in the case of gauge mediation [57]) or through a hierarchy of mass scales (such as highly off-shell intermediaries in split SUSY [58], or nearly-degenerate multiplets [29, 30, 59], as in anomaly-mediated SUSY breaking [31]). Our terminology classifies any non-SUSY models with new SM gauge-charged particles, such as composite Higgs or extra-dimensional models, under the SUSY-like umbrella because of the prediction of new particles above the weak scale with SM charges. In this category, LLP production is typically dominated by SM gauge interactions, whether of the LLP itself or of a heavy parent particle that decays to LLPs.
- **Higgs-portal theories (Higgs).** In this category, LLPs couple predominantly to the SM-like Higgs boson. This possibility is well-motivated because the SM Higgs field provides one of the leading renormalizable portals for new gauge-singlet particles to couple the SM, and the experimental characterization of the Higgs boson leaves much scope for couplings of the Higgs to BSM physics [60, 61]. The most striking signatures here are exotic Higgs decays to low-mass particles [62] (as in many Hidden Valley scenarios [32, 33]), which can arise in models of neutral naturalness [23, 21, 63] and dark matter [64]. The Higgs is also special in that it comes with a rich set of associated production modes in addition to the dominant gluon fusion process, with vector-boson fusion (VBF) and Higgs-strahlung (VH) production modes allowing novel opportunities for triggering on and suppressing backgrounds to Higgs-portal LLP signatures. Indeed, in many scenarios where LLPs are produced in exotic Higgs decays, associated production modes can be the only way of triggering the event.
- **Gauge-portal theories (ZP).** This category contains scenarios where new vector mediators can produce LLPs. These are similar to Higgs models, but where the vector mediator is predominantly produced from $q\bar{q}$ -initiated final states without other associated objects. Examples include models where both SM fermions and LLPs carry a charge associated with a new Z' (for a review, see Ref. [65]), as well as either Abelian or non-Abelian “dark” photon or dark Z models [66] in which the couplings of new vector bosons to the SM are mediated by kinetic mixing. Scenarios with LLPs coupled to new gauge bosons are well motivated by theories of dark matter, particularly models with

significant self-interactions [67, 68, 69] and/or sub-weak mass scales [70, 71, 72, 73, 74].

- **Dark-matter theories (DM):** Non-SUSY and hidden-sector DM scenarios are collected in this category, which encompasses models where the cosmological dark matter is produced as a final state in the collider process. Examples of multi-component dark matter theories include models of strongly interacting massive particles (SIMP) [75], inelastic dark matter [76], and models with DM coannihilation partners [77, 78, 47]; in many of these models, the collider phenomenology and LLP lifetime can be tied to the DM relic abundance. The main feature distinguishing this category from the Higgs and gauge scenarios above is that dark matter, i.e., missing transverse momentum (\cancel{E}_T), is a necessary and irreducible component of such signatures [32, 33, 7, 79, 80, 81, 82, 83, 47, 49, 84, 85].
- **Heavy neutrino theories (RH ν):** Models where new weak-scale states are responsible for SM neutrino mass generation [86, 87, 88, 89, 90] typically predict long-lived TeV-scale right-handed neutrinos that can be probed at the LHC [91, 92, 93, 94, 95, 13, 17, 18, 96]. Examples of well-motivated, UV-complete models that do this include the neutrino minimal SM (ν MSM) [97, 98] and the left-right symmetric model [99, 100, 101, 102]. Characteristic features of models in this category are singly-produced LLPs via SM neutral and charged current interactions, and lepton-rich signatures in terms of prompt and displaced objects (often in association with quarks); in extended models like left-right symmetric models, production through new right-handed W and Z bosons can lead to production of between 1 and 4 LLPs, and cascade decays between right-handed neutrinos can lead to phenomena such as doubly displaced decays. RH neutrinos can also be produced via Higgs decays [15, 16, 18, 103, 104, 105].

In developing our simplified model framework below, we will construct maps between these UV model categories and the simplified model channels to illuminate some of the best-motivated combinations of production and decay modes for LLPs. This allows us in upcoming work to focus on the most interesting channels and assess their coverage in the work of the Experimental Coverage Working Group reported in Section ??.

2.3 The Simplified Model Building Blocks

As discussed above, production and decay can largely be factorized in LLP searches. This allows us to specify the relevant production and decay modes for LLP models separately; we then put them together and map the space of models into the umbrella categories of motivated theories.

2.3.1 Production Modes

Motivated by our over-arching UV frameworks, we can identify a minimal set of interesting production modes for LLPs. These production modes determine LLP signal yield both by relating the LLP production cross section to meaningful theory parameters such as gauge charges or Higgs couplings, and by determining the kinematic distribution of the LLP. Additionally, a given production mechanism will also make clear predictions for the number and type of *prompt* objects accompanying the LLP(s). These prompt accompanying objects (AOs) can be important for both triggering on events with LLPs and for background rejection, particularly when the LLP has a low mass or decays purely hadronically. [MAKE PSEUDO-FEYNMAN DIAGRAMS]

- **Direct Pair Production (DPP):** Here the LLP is dominantly pair-produced non-resonantly from SM initial states. This is most straightforwardly obtained when the LLP is charged under a SM gauge interaction. In this case, an irreducible production cross section is then specified by the LLP gauge charge and mass. DPP can also occur in the presence of a (heavy) *t*-channel mediator (e.g., an initial quark-antiquark pair may exchange a virtual squark to pair produce bino-like neutralinos); in this case the production cross section is a free parameter.
- **Heavy parent (HP):** In this case the LLP can be produced in the decay of a heavy parent particle that is itself pair produced from the pp initial state. The production cross section is essentially a free parameter, and is indirectly specified by the gauge charges and masses of the heavy parent particles. Heavy parent production gives very different kinematics for the LLP than direct pair production production, and will often produce additional prompt accompanying objects in the rapid cascade decays of the parents.
- **Higgs (HIG):** The LLP is produced through its couplings to the SM-like Higgs boson. This case has an interesting interplay of possible production modes. The dominant production is via gluon fusion, which features no associated objects beyond initial state radiation (ISR); owing to its role in electroweak symmetry breaking, however, the Higgs has associated production modes (VBF, VH), each with its own characteristic features. The best prospects are for LLP masses below $m_h/2$, in which case the LLPs can be produced on-shell in SM-like Higgs boson decays. LLPs with heavier masses can still be produced via an off-shell SM-like Higgs, albeit at lower rates. The LLP can be pair produced or singly produced through the Higgs portal depending on the model, and may also be produced in conjunction with missing energy. The cross section (or, alternatively, the Higgs branching fraction into the LLP) is a free parameter of the model. The Higgs mass can also be taken as a free parameter: there ex-

ist many theories that predict new exotic scalar states (such as the singlet scalar extension to the SM [64]), and these new states can be produced through the same production modes as the SM Higgs.

- **Heavy resonance (ZP):** Here the LLP is produced in the decay of an on-shell resonance, such as a heavy Z' gauge boson initiated by $q\bar{q}$ initial state. Note that production via an off-shell resonance is kinematically similar to the direct production (DPP) above. As with HIG, the LLP can be pair-produced or singly-produced (potentially in association with missing transverse momentum). In ZP models, ISR is the dominant source of accompanying prompt objects. Models with new heavy scalars could conceivably fall into either ZP or HIG; the main determining factor according to our organizational scheme is whether the scalar possesses Higgs-like production modes such as VBF and VH. Note that heavy resonance decays to SM particles also occur in these models and, searches for such resonances [106, 107, 108, 109, 110, 111, 112] may complement the sensitivity for decays to LLPs.
- **Charged current (CC):** In models with weak-scale right-handed neutrinos, the LLP can be produced in the leptonic decays of W/W' . Single production is favored. Prompt charged leptons from the charged-current interaction are typical prompt objects accompanying the LLP.

It is important to note that each of the above production mechanisms has its own “natural” set of triggers to record the signal. For example, the Higgs production portal can be accompanied by forward jets or leptons that are characteristic of VBF or VH production; similarly, the charged-current production processes often result in prompt charged leptons and the heavy-parent production comes with associated hard objects from the heavy parent decay. However, the reader should be cautioned that this does not necessarily mean that the “natural” trigger is the *optimal* trigger for a particular signal: for example, the Higgs production modes suggest the use of VBF- or VH-based triggers, but if the LLP decays leptonically, it might be more efficient to trigger on the lepton from the LLP decay. Thus, the final word on which trigger is most effective for a given simplified model depends on the production mode as well as the nature and kinematics of the LLP decay.

The generic presence of associated prompt objects (such as VBF or central jets, lepton, missing momentum, etc.) in many LLP production modes indicates that they may offer valuable handles to extend sensitivity for LLPs to otherwise hard-to-reach parts of parameter space.

2.3.2 Decay Modes

We now characterize a list of LLP decay modes. As we attempt to construct a minimal, manageable set of decay-mode building

blocks, it is important to keep in mind that a given experimental search for LLPs can frequently be sensitive to a variety of possible LLP decay modes. As a result, it is not always necessary to divide LLP signatures into as many exclusive processes as might otherwise be needed for prompt signatures.

The fact that LLP searches can be sensitive to many LLP decay modes is, in part, because LLPs that decay far from the collision point offer fewer avenues for particle identification, (*e.g.*, for an LLP decaying inside of the calorimeter, most decay products are reconstructed as missing energy, or an energy deposition in the calorimeter); consequently, particle identification criteria are typically relaxed in comparison to requirements on searches involving only a single primary vertex. Indeed, these “loose” collider objects can differ significantly from the corresponding “tight”, prompt objects. Also, since backgrounds for LLP searches are often small, tight identification and/or reconstruction criteria typically found in exclusive prompt analyses are no longer needed to suppress backgrounds. For example, ATLAS has a displaced vertex search sensitive to dilepton and multitrack vertices that are relatively inclusive with respect to other objects originating from near the displaced vertex [113]. Similarly, CMS has an analysis sensitive to events with one each of a high-impact-parameter muon and electron without reconstructing a vertex or any other objects [114]. For these examples, the specific decay mode of the LLP may not be too important so long as certain objects (such as muons) are present or the decay occurs in a specific location, and so many LLP decay modes could be represented by only a few simplified models. An even more extreme example in this regard is the search for highly-ionizing tracks sensitive to electrically and color-charged LLPs. While the searches are primarily targeted to detector-stable particles (heavy stable charged particles or R -hadrons) they can also be used to probe intermediate lifetimes for which only a certain fraction of LLPs traverse the tracker before decaying (see *e.g.* [84]). Apparently the search is largely independent of the decay mode.

In some cases, however, the topology of a decay does matter. One potentially important factor that influences the sensitivity of a search to a particular model is whether the LLP decays into two SM objects vs. three, because the kinematics of multi-body decay are distinct from two-body decay and this may affect the acceptance of particular search strategies. An additional simplified model featuring a 3-body decay of the LLP may consequently be needed to span the space of signatures.

Below, we describe an irreducible set of decay modes that can be used to characterize LLP signatures for various LLP charges (including neutral, electrically charged, and colored). For each, we also provide an explicit example for how the decay would appear in a particular UV model. **We emphasize that the following decay modes are defined loosely with the understanding that their signatures will also be representative similar and/or related decay**

modes, for example $2j$ can also be a proxy for $3j$ because searches for multi-body hadronic LLP decays can be sensitive to both. It should also be noted that we are not recommending searches to be optimized to the exact, exclusive decay mode because that could suppress sensitivity to related but slightly more complicated decay chains.

- **Diphoton decays:** The LLP can decay resonantly to $\gamma\gamma$ (like in Higgs-portal models or left-right symmetric models [115]) or to $\gamma\gamma + \text{invisible}$ (in dark matter models). This latter mode stands as a proxy for other $\gamma\gamma + X$ decays where the third object is not explicitly reconstructed. *Example: a singlino decaying to a singlet (which decays to $\gamma\gamma$) and a gravitino in Stealth SUSY [24].*
- **Single photon decays:** The LLP decays to $\gamma + \text{invisible}$ (like in SUSY models). The SUSY signal mandates a near-massless invisible particle, while other models allow for a heavy invisible particle, as can arise in theories of dark matter [116, 81]. *Example: a bino decaying to photon plus gravitino in gauge-mediated models of SUSY breaking [117].*
- **Hadronic decays:** The LLP can decay into two jets (jj) (like in Higgs and gauge portal models, or RPV SUSY), $jj + \text{invisible}$ (SUSY, dark matter, or neutrino models), or $j + \text{invisible}$ (SUSY). Here, “jet” (j) means either a light-quark parton, gluon, or b -quark. This also encompasses decays directly into hadrons (for example, LLP decay into π^+ plus an invisible particle [29, 30, 31]). *Example: a scalar LLP decaying to $b\bar{b}$ due to mixing with the SM Higgs boson, as in models of neutral naturalness.*
- **Semileptonic decays:** The LLP can decay into a lepton + 1 jet (such as in leptoquark models) or 2 jets (like in SUSY or neutrino models). *Example: a right-handed neutrino decaying to a left-handed lepton and an on- or off-shell hadronically decaying W boson (or W' boson in a left-right symmetric model).*
- **Leptonic decays:** The LLP can decay into $\ell^+\ell^- (+\text{invisible})$, or $\ell^\pm + \text{invisible}$ (as in Higgs-portal, gauge-portal, SUSY, or neutrino models). ℓ may be any flavor of charged lepton, but the decays are lepton flavor-universal and (for $\ell^+\ell^-$ decays) flavor-conserving. *Example: a wino decaying to a neutralino and an on- or off-shell leptonic Z boson in SUSY.*
- **Flavored leptonic decays:** The LLP can decay into $\ell_\alpha + \text{invisible}$, $\ell_\alpha^+ \ell_\beta^-$ or $\ell_\alpha^+ \ell_\beta^- + \text{invisible}$ where flavors $\alpha \neq \beta$ (as in SUSY or neutrino models). *Example: a neutralino decaying to two leptons and a neutrino in R-parity-violating SUSY; or a right-handed neutrino decaying to two leptons and a neutrino.*

In all cases, both the LLP mass and proper lifetime are free parameters. Therefore, the case of detector-stable particle is automatically included by taking any of the above decay modes and setting

$c\tau \rightarrow \infty$.⁶ We emphasize that, depending on the location of the LLP within the detector, these decay modes may or may not be individually distinguishable: a displaced dijet decay will look very different from a displaced diphoton decay in the tracker, but nearly identical if the decay occurs in the calorimeter. We are identifying here promising channels, as distinct from detector signatures.

As an example of how the above listed decay modes cover the most important experimental signatures, we consider a scenario of an LLP decaying to top quarks. This scenario is very well-motivated (for instance, with long-lived stops on SUSY) and might appear to merit its own decay category of an LLP decaying to one or more top quark. However, the top quark immediately decays to final states that *are* covered in the above list, giving a semileptonic decay ($t \rightarrow b\ell^+\nu$) and a hadronic decay ($t \rightarrow bj$), and so the above model-independent LLP decay modes cover this important scenario. Similarly, 4-body and higher LLP decays are typically covered by the above inclusive definitions of decay modes; this motivates not overly optimizing experimental searches to the specific, exclusive features of a particular decay mode.

While it would be ideal to have separate experimental searches for each of the above decay modes (when distinguishable), it is rare for specific models to allow the LLP to decay in only one manner; instead, as in the LLP decay to top quark example above, a number of decay modes are typically allowed with corresponding predictions for the branching fractions. As another example, if a LLP couples to the SM via mixing with the SM Higgs boson, then the LLP decays via mass-proportional couplings giving rise to b - and τ -rich signatures. If, instead, the LLP decays through a kinetic mixing as in the case of dark photons or Z bosons, then the LLP can decay to any particle charged under the weak interactions, giving rise to a relatively large leptonic branching fraction in addition to hadronic decay modes. This allows some level of prioritization of decay modes based on motivated UV-complete models; for example, the Higgs-portal model prioritizes searches for heavy flavor quarks and leptons in LLP decay. Ultimately, however, it is desirable to retain independent sensitivity to each individual decay mode as much as possible. Indeed, for each decay mode listed above, models exist for which the given decay mode would be the discovery channel.

Invisible Final-State Particles: Where invisible particles appear as a product of LLP decay, additional model dependence arises from the unknown nature and mass of the invisible particle. The invisible particle could be a SM neutrino, DM, a lightest superparticle in SUSY, or another beyond-SM particle. The phenomenology depends strongly on the mass splitting, $\Delta \equiv M_{\text{LLP}} - M_{\text{invisible}}$. If $\Delta \ll M_{\text{LLP}}$ (*i.e.*, $M_{\text{LLP}} \sim M_{\text{invisible}}$), the spectrum is squeezed and the decay products of the LLP are soft. This could, for instance, lead to signatures such as disappearing tracks or necessitate the use of ISR jets to reconstruct the LLP signature. If the mass splitting is large,

⁶ As mentioned earlier in this limit the decay mode becomes irrelevant. However, an exception is the search for particle that are stopped inside the detector material and decay out-of-time.

$M_{\text{invisible}} \ll M_{\text{LLP}}$, then the signatures lose their dependence on the invisible particle mass.

We suggest three possible benchmarks: a squeezed spectrum with $\Delta \ll M_{\text{LLP}}$; a massless invisible state, $\Delta = M_{\text{LLP}}$ (which also includes the case where the invisible particle is a SM neutrino); and an intermediate splitting corresponding to a democratic mass hierarchy, $\Delta \approx M_{\text{LLP}}/2$.

2.4 A Simplified Model Proposal

In this section, we present a compact set of simplified model channels that, broadly speaking, covers the space of theoretical models in order to motivate new experimental searches. Such a minimal, compact set may not be optimal for reinterpretation of results (where variations on our listed production and decay modes may influence signal efficiencies and cross section sensitivities), but rather provides a convenient characterization of possible signals to ensure that no major discovery mode is missed. These models may therefore serve as a starting point for systematically understanding experimental coverage of LLP signatures and devising new searches, but may need to be extended in future for the purposes of facilitating reinterpretation. We undertake an in-depth discussion of these topics in the Section ??.

We classify LLPs according to their SM gauge charges, as these dictate the dominant or allowed LLP production modes and can give rise to different signatures (for example, disappearing tracks and hadronized LLPs). We separately consider LLPs that are: (a) neutral, (b) electrically charged but color neutral, and (c) color charged.

All of the following models have the LLP mass and lifetime as free parameters. For heavy parent production, the parent mass is an additional parameter, while for invisible decays, several different benchmarks for mass splittings between LLP and invisible final state may have to be separately considered as described in Section 2.3.2. The cross section may have a theoretically well-motivated target value depending on UV model parameters, but phenomenologically can generally be taken as a free parameter.

We emphasize that in spite of the many simplified model channels proposed below, a small number of experimental LLP searches can have excellent coverage over a wide range of channels (for certain lifetime ranges). Ultimately, the goal in future work will be to identify whether there are other searches that could have a similarly high impact on the space of simplified models, and identify where the gaps in coverage are.

2.4.1 Neutral LLPs

The simplified model channels for neutral LLPs are shown in Table 2.1. X indicates the LLP.

In our proposal, which we expect to be the first iteration of the

simplified model framework, it is sufficient to consider as “jets” each of the following: $j = u, d, s, c, b, g$. It is worth commenting that b -quarks pose unique challenges and opportunities. Since b -quarks are themselves LLPs, they appear with an additional displacement relative to the LLP decay location. They also often give rise to soft muons in their decays, which could in principle lead to additional trigger or selection possibilities. However, these subtleties can be addressed in further refinements of the simplified models; we discuss this further in Section 2.6. Similarly, we consider e , μ , and τ to be included in the header of “leptons”, with the proviso that searches should be designed where possible with sensitivity to each.

When multiple production modes are specified in one row of the table, this means that multiple especially well-motivated production channels give rise to similar signatures. Typically only one of these production modes will actually need to be included when developing a search, but we sometimes include multiple different production modes as individuals may variously prefer one over the other.

In each entry of the table, we indicate which umbrella category of well-motivated models (Section 2.2) can predict a particular (production) \times (decay) mode. An asterisk (*) on the umbrella model indicates that \cancel{E}_T is required in the decay. A dagger (†) indicates that this particle production \times decay scenario is not present in the *simplest and most minimal* implementations of the umbrella model, but could be present in extensions of the minimal models. While the Higgs signatures are best motivated for the SM-like 125 GeV Higgs, exotic Higgses of other masses can still have the same production modes and so m_H can be taken as a free parameter.

We remind the reader that the production modes listed in Table 2.1 encompass also the associated production of characteristic prompt objects. For example, the Higgs production modes not only proceed through gluon fusion, but also through vector boson fusion and VH production, both of which result in associated prompt objects such as forward tagging jets, leptons, or missing momentum. All of the production modes listed in Table 2.1 could be accompanied by ISR jets that aid in triggering or identifying signal events. It is therefore important that searches are designed to exploit such associated prompt objects whenever they can improve signal sensitivity, especially with regard to triggering.

To demonstrate how to map full models onto the list of simplified models (and vice-versa), we consider a few concrete cases. For instance, if we consider a model of neutral naturalness where X is a long-lived scalar that decays via Higgs mixing (for instance, X could be the lightest quasi-stable glueball), then the process where the SM Higgs h decays to $h \rightarrow XX, X \rightarrow b\bar{b}$ would be covered with the Higgs production mechanism and a dijet decay. Entirely unrelated models, such as the case where X is a bino-like neutralino in $h \rightarrow XX, X \rightarrow jjj$ could be covered with the same simplified model

Production \ Decay	$\gamma\gamma(+\text{inv.})$	$\gamma + \text{inv.}$	$jj(+\text{inv.})$	$jj\ell$	$\ell^+\ell^-(+\text{inv.})$	$\ell_\alpha^+\ell_{\beta\neq\alpha}^- (+\text{inv.})$
DPP: sneutrino pair	[†]	SUSY	SUSY	SUSY	SUSY	SUSY
HP: squark pair, $\tilde{q} \rightarrow jX$ or gluino pair $\tilde{g} \rightarrow jjX$	[†]	SUSY	SUSY	SUSY	SUSY	SUSY
HP: slepton pair, $\tilde{\ell} \rightarrow \ell X$ or chargino pair, $\tilde{\chi} \rightarrow WX$	[†]	SUSY	SUSY	SUSY	SUSY	SUSY
HIG: $h \rightarrow XX$ or $\rightarrow XX + \text{inv.}$	Higgs, DM*	[†]	Higgs, DM*	RH ν	Higgs, DM* RH ν^*	RH ν^*
HIG: $h \rightarrow X + \text{inv.}$	DM*, RH ν	[†]	DM*	RH ν	DM*	[†]
ZP: $Z(Z') \rightarrow XX$ or $\rightarrow XX + \text{inv.}$	Z', DM^*	[†]	Z', DM^*	RH ν	Z', DM^*	[†]
ZP: $Z(Z') \rightarrow X + \text{inv.}$	DM	[†]	DM	RH ν	DM	[†]
CC: $W(W') \rightarrow \ell X$	[†]	[†]	RH ν^*	RH ν	RH ν^*	RH ν^*

Table 2.1: **Simplified model channels for neutral LLPs.** The LLP is indicated by X . Each row shows a separate production mode and each column shows a separate possible decay mode, and therefore every cell in the table corresponds to a different simplified model channel of (production) \times (decay). We have cross-referenced the UV models from Section 2.2 with cells in the table to show how the most common signatures of complete models populate the simplified model space. The asterisk (*) shows that the model definitively predicts missing momentum in the LLP decay. A dagger ([†]) indicates that this particle production \times decay scenario is not present in the *simplest and most minimal* implementations of the umbrella model, but could be present in extensions of the minimal models. When two production modes are provided (with an “or”), either simplified model can be used to cover the same experimental signatures.

because most hadronic LLP searches do not have exclusive requirements on jet multiplicity. Similarly, a hidden sector model with a dark photon, A' , produced in $h \rightarrow A'A'$, $A' \rightarrow f\bar{f}$ would also give rise to the dijet signature when f is a quark, whereas it would populate the $\ell^+\ell^-$ column if f is a lepton. Finally, a scenario with multiple hidden sector states X_1 and X_2 , in which X_2 is an LLP and X_1 is a stable, invisible particle, could give rise to signatures like $h \rightarrow X_2 X_2$, $X_2 \rightarrow X_1 jj$ that would be covered by the same Higgs production, hadronic decay simplified model; however, we see how \cancel{E}_T can easily appear in the final state, and that the LLP decay products may not all be hadronic. Therefore, the simplified models in Table 2.1 can cover an incredibly broad range of signatures, but only if searches are not overly optimized to particular features such as \cancel{E}_T and resonant LLP reconstruction⁷.

2.4.2 Electrically Charged LLPs: $|Q| = 1$

For an electrically charged LLP, we need to consider far fewer production modes because of the irreducible gauge production associated with the electric charge. We still consider a heavy parent scenario where the heavy parent has a QCD charge, as this could potentially dominate the production cross section, see *e.g.* [44]. We summarize our proposals in Table 2.2.

Note that we lump all resonant production into the Z' simplified

⁷ This should not, of course, be interpreted as saying that searches shouldn’t be done that exploit these features. Instead, our position is that experiments should bear in mind the range of topologies and models covered by each cell in Table 2.1 when designing searches, and that some more inclusive signal regions should be established where possible.

model. The reason is that the SM Higgs cannot decay into two on-shell charged particles due to the model-independent limits from LEP on charged particles masses, $M \gtrsim 75 - 90$ GeV (see, for example, Ref. [118]). Similarly, there are fewer decay modes because of the requirement of charge conservation.

For concreteness, we recommend using $|Q| = 1$ as a benchmark for charged LLPs for the purpose of determining allowed decay modes. Although other values of Q are possible, these often result in cosmologically stable charged relics or necessitate different decay modes than those listed here. LLPs with $|Q| = 1$ are also motivated within SUSY [29, 30, 31] and within Type-III seesaw models of neutrino masses [119, 120, 121, 122]. We note that there exist already dedicated searches for heavy quasi-stable charged particles with non-standard charges [123, 124]; because those searches are by construction not intended to be sensitive to the decays of the LLP, the existing models are sufficient for characterizing these signatures and they do not need to be additionally included in our framework.

For massive particles with $|Q| = 1$ with intermediate or large lifetimes such that the LLP traverses a significant part (or all) of the tracker the highly-ionizing track of the LLP provides a prominent signature. This can be exploited for an efficient background suppression while keeping identification and/or reconstruction criteria as loose and, hence, inclusive as possible. In particular, for decay-lengths of the order of or larger than the detector size the signature of highly-ionizing tracks and anomalous time-of-flight (*i.e.* searches for heavy stable charged particles) constitute an important search strategy covering a large range of lifetimes present in the parameter space of theoretically motivated models. While the searches for heavy stable charged particles are largely inclusive with respect to additional objects in the event they depend strongly on the velocity of the LLP. For $\beta \rightarrow 1$ one loses the discriminating power against minimally ionizing particles, while for too small velocities, $\beta \lesssim 0.5$, the reconstruction becomes increasingly difficult due to timing-issues. It is therefore important to include the heavy parent production scenario which covers a much larger kinematic range than direct production alone resulting in a much wider range of signal efficiencies [46].

While the signatures in Table 2.2 form a minimal set, they also encompass some scenarios that merit special comment. One of these is the disappearing track signature [29, 30, 31], in which a charged LLP decays to a nearly degenerate neutral particle; the lifetime is long due to the tiny mass splitting. Formally, these are included in the chargino or slepton pair production modes in Table 2.2 with decays to $\ell + \text{inv.}$ or $q\bar{q}' + \text{inv.}$ taken in the limit where the splitting between charged LLP and the invisible final state is of $\mathcal{O}(200)$ MeV. In the case of a hadronic decay, X decays to a soft pion that is very challenging to reconstruct and so the track simply disappears. This is an important scenario that is already the topic of existing searches [125, 126]. As the degeneracy between the charged

Production \ Decay	$\ell + \text{inv.}$	$jj(+\text{inv.})$	$jj\ell$	$\ell\gamma$
DPP: chargino pair or slepton pair	SUSY DM*	SUSY DM*	SUSY	[†]
HP: $\tilde{q} \rightarrow jX$	SUSY	SUSY	SUSY	[†]
ZP: $Z' \rightarrow XX$	Z', DM^*	Z', DM^*	Z'	[†]
CC: $W' \rightarrow X + \text{inv.}$	DM*	DM*	RH ν	[†]

Table 2.2: Simplified model channels for electrically charged LLPs, $|Q| = 1$.

The LLP is indicated by X. Each row shows a separate production mode and each column shows a separate possible decay mode, and therefore every cell in the table corresponds to a different simplified model channel of (production) \times (decay). We have cross-referenced the “well-motivated” UV models from Section 2.2 with cells in the table to show how the most common signatures complete models can be linked to the simplified model space. The asterisk (*) shows that the model definitively predicts missing momentum in the LLP decay. A dagger ([†]) indicates that this particle production \times decay scenario is not present in the *simplest and most minimal* implementations of the umbrella model, but could be present in extensions of the minimal models. When two production modes are provided (with an “or”), both production simplified models can be used to cover the same experimental signatures.

LLP and neutral state is relaxed, other signatures are possible; this parameter range is well motivated both by SUSY and DM models with coannihilation [77, 78, 47].

Finally, we comment on the challenges of simulating the charged LLP simplified models. Because the LLP interacts with the detector material before the decay, the simulation of the LLP propagation is important in correctly modelling the experimental signature. The subsequent decay of the LLP must either be hard-coded into the detector simulator, or allow for an interface with programs such as `Pythia 8` to implement the decays. It is currently an outstanding problem to generally model all of the possible decay modes. We discuss this further in Section ??.

2.4.3 LLPs with Color Charge

LLPs with charges under the strong interactions are more constrained than even electrically charged LLPs. Because of the non-Abelian nature of the strong interactions, the gauge pair production cross section of the LLP is specified by the LLP mass and its representation under the color group, $SU(3)_C$. We do not include production via a heavy parent particle here because that cross section is unlikely to dominate the total production rate at the LHC.

A complication of the QCD-charged LLP is that the LLP hadronizes prior to its decay. We comment on a few aspects of hadronization for LLPs that are charged under the standard model $SU(3)_C$ gauge group. First, the modeling of hadronization is directly related to many properties of the long-lived parton, such as electric charge, flavor, spin, etc. Many LLP searches at the LHC are particularly sensitive to the electric charge of the long-lived BSM hadrons (referred to henceforth as *R*-hadrons in keeping with the standard SUSY nomenclature). For instance, only the charged *R*-hadrons can

Production \ Decay	$j + \text{inv.}$	$jj(+\text{inv.})$	$j\ell$	$j\gamma$
Production	$j + \text{inv.}$	$jj(+\text{inv.})$	$j\ell$	$j\gamma$
DPP: squark pair or gluino pair	SUSY	SUSY	SUSY	†

Table 2.3: **Simplified model channels for LLPs with color charge.** The LLP is indicated by X. Each row shows a separate production mode and each column shows a separate possible decay mode, and therefore every cell in the table corresponds to a different simplified model channel of (production) \times (decay). We have cross-referenced the “well-motivated” UV models from Section 2.2 with cells in the table to show how the most common signatures complete models can be linked to the simplified models. A dagger (†) indicates that this particle production \times decay scenario is not present in the *simplest and most minimal* implementations of the umbrella model, but could be present in extensions of the minimal models. When two production modes are provided (with an “or”), both production simplified models can be used to cover the same experimental signatures.

be found in heavy stable charged particle search, and for some vertex reconstruction based searches the LLP is either required to be neutral or has a higher efficiency in the absence of a prompt track stub associated with the LLP. Event generators such as Pythia8 [127] has routines to simulate R -hadronization and is believed to provide a reasonable estimate of these distributions. For example, Pythia8 estimates that the neutral R -hadron fraction from a gluino (color-octet fermion, \tilde{g}) is approximately 54%, while the neutral R -hadron fraction for a stop (scalar top partner) is estimated to be 44% [45].

R -hadrons that interact with detector materials can result in higher energy losses, dE/dx , than conventional hadrons and even in a change of electric charge. For instance, some estimates [128, 129] suggest that heavy, meta-stable gluinos would initially mostly form mesons, e.g., $(u\tilde{g}\bar{d})$, but drop to the lower-energy, neutral, singlet baryon $\tilde{\Lambda} = (\tilde{g}uds)$ state when interacting with the protons and neutrons within the calorimeters. To take into account the possibility of the charge being stripped off when passing through the detectors, the experimental searches for heavy stable charged particles includes a tracker-only signal region, where activity in the muon system is not used [130, 131]. Within GEANT4 [132] there is a modeling of how an R -hadron propagates through the detector material [133].

If the R -hadron decays, especially via a multi-body decay, it can be more accurate to decay the LLP using the full matrix element with event generators such as Madgraph5 [134, 135]. In this case, the Pythia8 R -hadronization routine cannot be used, as the BSM colored particle is already decayed and its daughters are color connected to other parts of the event. As the corrections from these color connections provide $\mathcal{O}(\Lambda_{QCD})$ changes to the momentum of the final state particles, it is typically reasonable to ignore effects of color connection unless the kinetic energy transferred to the daughters in the LLP rest frame is not large relative to Λ_{QCD} . For example, in the case of compressed decays, a careful treatment of the hadronization of the displaced decay products, which thus far has not been performed in the literature, would be needed.

As with electrically charged LLPs, colored LLPs interact with the detector material prior to decay. Similarly, the subsequent decay of the LLP must either be hard-coded into the detector simulator, or allow for an interface with programs such as `|Pythia 8` to implement the decays. It is currently an outstanding problem to generally model all of the possible decay modes. We discuss this further in Section ??.

2.5 *Proposal for a Simplified Model Library*

The simplified models outlined in the above sections provide a common language for theorists and experimentalists to study the sensitivity of existing searches, propose new search ideas, and interpret results in terms of UV models. Each of these activities demands a simple framework for the simulation of signal events that can be used to evaluate signal efficiencies of different search strategies and map these back onto model parameters. Requiring individual users to create their own MC models for each simplified model is impractical, redundant, and invites the introduction of errors into the analysis process.

In this section, we propose and provide a draft version of a *simplified model library* consisting of model files and Monte Carlo (MC) generator cards that can be used to generate events for various simplified models in a straightforward fashion. Because each experiment uses slightly different MC generators and settings, this allows each collaboration (as well as theorists) to generate events for each simplified model based on the provided files. Depending on how the LLP program expands and develops over the next few years, it may become expedient to go a step further and add to the simplified model library sets of events in a standard format (such as the Les Houches format) that can be directly fed into event-generator and detector-simulation programs; given the factorization of production and decay of LLPs that is valid for all but QCD-charged LLPs, this could involve two mini-libraries: a set of production events for LLPs, a set of decays for LLPs, along with a protocol for “stitching” the events together.

The current version of the library can be found here: [\[provide link\]](#). In Appendix ?? we also provide tables that list how to simulate each LLP simplified model channels with one of the specified base models. The library currently focuses on models of neutral LLPs; charged and colored LLPs are included in several of the models, but simulating the full range of decays listed in Sections [2.4.2-2.4.3](#) requires more careful collaboration with detector simulation and other MC programs to ensure that they can actually be used in experimental studies. This work is ongoing; see Section ?? for more details.

We provide model files in the popular Universal FeynRules Output (UFO) format [\[136\]](#), which is designed to interface easily with parton-level simulation programs such as `MadGraph5_aMC@NLO` [\[135\]](#).

The goal is to cover as many of the simplified models of Section 2.3 with as few UFO models as possible; this limits the amount of upkeep needed to maintain the library and develops familiarity with the few UFO models needed to simulate the LLP simplified models. We then give specific instructions for how to simulate each simplified LLP channel using the UFO models. **NOTE: as this document is still in draft form, the library is not yet complete. If you need a simplified model that has not yet been filled in, or would like to contribute to completion of the library, please contact the organizers listed in the simplified model repository.**

2.5.1 Base Models for Library

In order to reproduce the simplified model channels of Section 2.3, we need a collection of models that:

- Includes additional gauge bosons and scalars to allow vector- and scalar-portal production of LLPs;
- Includes new gauge-charged fermions and scalars to cover direct and simple cascade production modes of LLPs;
- Includes a right-handed-neutrino-like state with couplings to SM neutrinos and leptons;
- *Recommended, but optional:* Allows for the decays of the LLP particle through all of the decay modes listed in Section 2.3, either through renormalizable or higher-dimensional couplings. If couplings that allow LLP decay are included in the UFO model, then the decays can be performed directly at the matrix-element level in programs such as `MadGraph5_aMC@NLO` [135] and accompanying packages such as `MadSpin` [137]. If the couplings needed for LLP are not in the UFO model, then LLPs can be left stable at the matrix element level and decays implemented via `Pythia 8.2` [127, 138], which allows for the straightforward implementation of decays but without taking into the angular distribution of decay products.

Fortunately, an extensive set of UFO models is already available for simulating the production of beyond-SM particles. We note that extensions or generalizations of only four already-available UFO models are needed at the present time:

1. **The Minimally Supersymmetric SM (MSSM):** the use of this model is motivated by and allows for the simulation of SUSY-like theories. The model contains a whole host of new particles with various gauge charges and spins. Therefore, an MSSM-based model allows for the simulation of many of the simplified model channels. In particular, we note that existing UFO variants of the MSSM that include gauge-mediated supersymmetry breaking (GMSB) couplings (including decays to light gravitinos) and R -parity violation (to allow for the decay of otherwise stable light-

est SUSY particles) already cover most of the SUSY-motivated LLP scenarios.

2. **The Hidden Abelian Higgs Model (HAHM):** this UFO model contains new scalars and gauge bosons and so can be used to simulate both Higgs-portal and gauge-portal (ZP) theories. The model consists of the SM supplemented by a “hidden sector” consisting of a new U(1) gauge boson and corresponding Higgs field. The physical gauge and Higgs bosons couple to the SM via kinetic and mass mixing, respectively. The HAHM allows for straightforward simulation of Higgs-portal production of LLPs, as well as Z' models and many hidden sector scenarios. The UFO implementation is from Ref. [139].
3. **The Left-Right Symmetric Model (LRSM):** this UFO model is best for simulating UV theories with right-handed neutrinos ($RH\nu$). The UFO model supplements the SM by an additional $SU(2)_R$ symmetry, which gives additional charged and neutral gauge bosons. The model also contains a right-handed neutrino which is the typical LLP candidate, which can be produced via SM W , Z , or the new gauge bosons.
4. **Dark Matter Simplified Models (DMSM):** these UFO models are best for simulating UV theories in the dark-matter class (DM). These UFO models have been created by the LHC-DM working group [39]. They typically consist of a new, beyond-SM mediator (such as a scalar or a Z') coupled to invisible DM particles. With minimal modification, the would-be-DM particles can be made unstable and decay at a LLP. These models are particularly good for simulating LLP production via a heavy resonance (ZP), and can also simulate continuum production of LLPs in the limit where the mediator is taken to be light and off-shell.
Work on modifying the DM-simplified models is ongoing; volunteers to assist with this task are welcome!

If additional decay modes are needed beyond those in the specified simplified models, then the library can be updated to include the new couplings mediating the decay. Alternatively, the LLPs can be left stable in the parton-level generator and decayed down the pipeline in programs such as Pythia.

A detailed list of processes that can be used to simulate each simplified model channel is provided in Appendix ???. Because the library is only meant to be used to simulate events for determining acceptances, the signal cross section is not important and so, for example, SM gauge interactions can be used as proxies for much weaker exotic interactions. Similarly, the spins of the particles are generally of subdominant importance: replacing the direct production of a fermion with the direct production of a scalar will not fundamentally alter the signature. As long as results are expressed in terms of sensitivity to cross sections and not couplings, the results can be qualitatively (and in some cases, quantitatively) applied

to any similar production mode regardless of spin. However, we caution the reader that changing the spin of the LLP (or its parent) can change the angular distribution, and since in some cases LLP searches are typically more sensitive to aspects of event geometry than prompt searches, the second-order effects of spin could have more of an effect than for prompt simplified models.

2.6 Future Opportunities and Challenges

We conclude our discussion of simplified models by returning to topics that we glossed over in an attempt to provide a compact set of models that cover what is currently the most motivated and interesting theory space. The presented framework is only the first step of a simplified models program that is comprehensive in terms of generating LHC signatures and also allowing straightforward reinterpretation of experimental results for UV models. The framework we have developed with separate, modular components for LLP production and decay is amenable to expansion, and we encourage members of the theory and experimental communities to continue to do so over the coming years to ensure maximal utility of the simplified models framework.

One significant simplification we have undertaken in our framework is to define a “jet” as any of $j = u, c, d, s, b, g$. In reality, different partons give rise to different signatures, especially when one of the “jets” is a heavy-flavor quark. b - and c -jets have some useful distinguishing features, such as the fact that the underlying heavy-flavor meson decays at a displaced vertex and that there are often associated soft leptons resulting from meson decays. In particular, it is possible that the soft muons associated with B -meson decays could be used to enhance trigger and reconstruction prospects for LLPs decaying to b -jets. However, heavy quarks also constitute one of the major backgrounds for LLP searches, and so LLPs decaying to b - and c -jets may necessitate dedicated treatment in future. Similarly, LLP decays to τ leptons may merit further specialized study.

Another property of the current framework is that it is restricted to LLP signatures of low multiplicities. By “low multiplicity”, we mean collider signatures with one or two LLPs. Searches inspired by these models are also suitable for scenarios with three or four LLPs per event (which include models with dark Higgs decays into lepton jets [79], or left-right symmetric models [96]), since the LLP signatures are typically extremely rare and so only one or two typically need to be selected to greatly suppress backgrounds. As the multiplicity grows, however, the simplified model space we have presented requires modification. This is both because the individual LLPs grow softer, making them harder to reconstruct on an individual level, and they become less separated in the detector, which makes isolation and identification of signal a challenge. On the other hand, the high LLP multiplicity may allow for new han-

dles for further rejecting backgrounds. In extreme cases, signals can even mimic pile-up [140]. High multiplicity signatures therefore require dedicated modeling, and we defer the study of these signatures to the Dark Showers section, Section [ref-needed].

Finally, we conclude by noting that simplified models are built to provide a general framework to cover a broad swath of models. Any simplified model set-up, however, cannot cover every single UV model without becoming as complex as the UV model space itself. There will always be very well-motivated models that predict specific signatures that are challenging to incorporate into the simplified model framework outlined here: experimental searches for these signatures should still be done where possible, but we encourage theorists and experimentalists alike to think carefully about how to design such searches so as to retain maximal sensitivity to simplified models that may give rise to similar signatures.

Mention something about charged/colored LLPs?

3

Experimental Coverage of Long-Lived Particle Signatures

The goal of this chapter is to assess the capabilities of the existing long-lived particle (LLP) searches at ATLAS, CMS and LHCb, and to identify any potential gaps in coverage. We address this chapter to a reader interested in understanding the coverage of LHC on LLPs, but assume little to no background on the search strategies, thus we include a high level of detail regarding the current analyses. While we focus on the current existing studies, we acknowledge the landscape for new physics models and LLP signatures can be broader than the ones described here.

Backgrounds to most of these studies are typically small, as there are no irreducible SM processes that mimic the exact signature. The rare backgrounds that can fall within the signal regions, such as cosmic muons,

beam halo, detector noise, and cavern backgrounds, will be discussed in detail in Chapter "X". As rare as these backgrounds are, their rate is not completely negligible, and the difficulty of modeling them usually requires additional cuts (on the LLP mass, or selecting a specific decay mode) to ensure the search can be effectively "background-free".

Triggering for LLP searches is particularly challenging. With the exception of certain dedicated ATLAS triggers in the calorimeters or muon systems, there are no L1 triggers that pick up on the displaced nature of the LLP decay directly, and standard objects like leptons or high-energy jets have to pass L1 trigger thresholds in order for the event to be recorded. Hence the design of customized LLP triggers is to be encouraged, as they can probe otherwise inaccessible regions of parameter space.

The detailed review of all existing searches is presented in subsection [3.1](#). This survey of the current experimental coverage aims to highlight the highest-priority searches needed, which are shown in subsection [3.2](#). In all cases, we focus on the latest version of each analysis, notably we will typically present searches based on data taken at $\sqrt{s} = 13$ TeV, and discussing searches using Run I data only when the newer version is not yet available, or when there are conceptual differences between two versions of the same study.

3.1 Survey of the Current Experimental Long-Lived Program

In this subsection, we examine the existing searches in detail to identify current gaps in coverage. As long-lived particles travel macroscopic distances, many of the search strategies rely in the identification of *displaced* objects, that is, standard model particles (leptons, photons, hadrons, taus, jets) that are produced at a location away from the

primary vertex (PV). The production location of these displaced objects is referred to as a displaced vertex (DV). Borrowing the jargon from prompt searches, we will consider the following categories for the analogous displaced objects: all-hadronic (jets), leptonic, semi-leptonic, and photonic. The remaining searches will fall in the “other long-lived exotics” category, mostly consisting of non-standard tracks (disappearing tracks, heavy stable charged particles, quirks, etc), but also including some trackless signals, such as stopped particles and Strongly Interactive Massive Particles (SIMPs). This classification is somewhat arbitrary and the categories are not exclusive, but it facilitates the LLP search taxonomy.

3.1.1 All hadronic decays

ATLAS has several searches for displaced decays with hadronic objects: two objects decaying in the hadronic calorimeter (HCAL) [141, 142]; decays within the muon system (MS) or inner detector (ID) [143]; ID decays in association with large missing energy [144]; and ID decays in association with large missing energy, jets, or leptons [113]. CMS has an inclusive search for displaced jets using 13 (8) TeV data [145] ([146]), which also covers semileptonic decays. LHCb has searches for both one [147] and two [148] DVs in their detector. Here we restrict ourselves to summarize the hadronic channels, while those studies including leptons [113, 145] will be revisited in sections 3.1.2 and 3.1.3 for the fully-leptonic and semi-leptonic cases, respectively.

The reconstruction of displaced tracks in the ATLAS ID [149] follows a two step procedure. In the first iteration, the default track identification algorithm is applied, which uses hits in the pixel system, SCT (Semiconductor Tracker), and TRT (Transition Radiation Tracker) to reconstruct tracks with a small impact parameter. The hits not associated to a track during the first pass are used in a second run of the track finder, with loose requirements on the transverse and longitudinal impact parameters (d_0 and z_0) and the number of silicon hits that are shared (or not) with another track, called the *large radius tracking* (LRT) algorithm¹.

The ID decay searches where the DV is accompanied by additional, prompt objects select events with standard triggers [144, 113]. The 13 TeV search [144] uses a standard E_T^{miss} trigger and an offline requirement of $E_T^{\text{miss}} > 250 \text{ GeV}$. The ID vertex is required to have at least 5 tracks and $m_{\text{DV}} > 10 \text{ GeV}$. The 8 TeV search [113]

¹

Applying this large radius tracking procedure is CPU-intensive, and thus it is only run once per data-processing campaign, on a subset of specially-requested events [149].

covers a larger range of topologies. Like the 13 TeV search, the ID vertex is required to have 5 tracks and $m_{\text{DV}} > 10 \text{ GeV}$. In addition to the ID vertex, the event must have either $E_T^{\text{miss}} > 180 \text{ GeV}$ or contain 4, 5, or 6 jets with $p_T > 90, 65, \text{ or } 55 \text{ GeV}$. These searches are interpreted in the context of gluino or squarks decays into leptons, jets and missing energy, for the following supersymmetric (SUSY) scenarios: R-Parity Violating (RPV) and General Gauge Mediation (GGM) and split SUSY, in the latter case R-hadrons² are considered. The specific scenarios set the final state topology (jet and lepton multiplicity, small/large MET, etc).

For LLPs decaying in the HCAL or MS, dedicated *CalRatio* and *MuonRoI* triggers are employed [141, 142, 143, 150], allowing the searches to place limited requirements on the non-displaced portion of the event. The efficiency of these triggers is 50-70% for decays within the particular region being considered, and negligible outside them. The results of these analyses are interpreted in terms of a $\Phi \rightarrow ss$ model, where Φ is a heavy scalar boson with $100 < m_\Phi < 1000 \text{ GeV}$ and s is a long-lived, neutral scalar decaying to hadrons with branching fractions dictated by the Yukawa coupling. This corresponds to the HIGGS production mode in the Simplified Model Library (see chapter "Y").

The *CalRatio* trigger selects events with at least one trackless jet that has a very low fraction of energy deposited in the ECAL³. These *CalRatio jets* are characteristic of a LLP that decays within HCAL. The 13 TeV analysis [141] requires two *CalRatio* jets, where the exact *CalRatio* criteria are determined using a boosted decision tree (BDT) to optimally discriminate the displaced decay signature from QCD jets. Using the simplified $\Phi \rightarrow ss$ model with $400 < m_\Phi < 1000 \text{ GeV}$ and $50 < m_s < 400 \text{ GeV}$, good sensitivity is observed for $c\tau$ between 0.1 and 10 m. The 8 TeV result also requires two *CalRatio* jets, and shows sensitivity for $100 < m_\Phi < 900 \text{ GeV}$ and $10 < m_s < 150 \text{ GeV}$. Notably, SM Higgs boson ($\Phi = 125 \text{ GeV}$) decays to LLP pairs are constrained to be below 10% branching ratio in the most sensitive $c\tau$ ranges, with exact limits dependent on the LLP mass.

The *MuonRoI* trigger selects events with clusters of level-1 Regions of Interest (RoIs) in the MS that are isolated from activity in the ID and calorimeters. It is efficient for LLPs that decay between 3–7 m transversely or 5–13 m longitudinally from the PV, for LLP masses greater than 10 GeV. After trigger selection, the analysis requires either two reconstructed DVs in the MS [151] or one ID vertex and one MS vertex. This ID–MS combination provides increased sensitivity to shorter lifetimes than an analysis only considering MS vertices, and shows good sensitivity to $100 < m_\Phi < 900 \text{ GeV}$ and $10 < m_s < 150 \text{ GeV}$. SM Higgs boson decays to LLP pairs are constrained below 1% in the most sensitive $c\tau$ regions. The efficiency degrades for benchmarks with higher LLP boosts or very low mass LLPs, as fewer tracks are reconstructed.

With the exception of [113] and [144], which require prompt

² R-hadrons form when BSM colored particles hadronize due to a lifetime larger than the hadronization scale. In split-SUSY, as R-parity is conserved, the R-hadrons are typically long-lived.

³ The variable used to discriminate between *CalRatio* jets and standard jets is $\log_{10}(E_{\text{HAD}}/E_{\text{EM}})$, and the trigger selects trackless jets with $\log_{10}(E_{\text{HAD}}/E_{\text{EM}}) > 1.2$, which corresponds to an EMF of 0.067.

activity in addition to the DV and have comparatively high trigger thresholds, these analyses require 2 DVs, and thus are insensitive to models that produce a single DV. All in all, these searches constrain $c\tau$ between 0.1 and 100 m for rates as low as 50 fb and masses down to approximately 10 GeV in the HIGGS model.

The CMS analysis is based on a dedicated offline *displaced jet tagging* algorithm using tracker information to identify pairs of DVs. The triggers used here are based on large values of $H_T = \sum |p_{T,j}| > 350/500$ GeV for the 8 / 13 TeV data. The sum runs over all jets with $p_{T,j} > 40$ GeV & $|\eta_j| < 3.0$, while vetoing jets with more than two tracks with 2D transverse impact parameters with respect to the beam below 1 mm. Only events with two or more displaced jets are kept in the analysis, while those with only one are used as a control sample to estimate the prompt jet misidentification rate. For $c\tau < 3$ mm, the algorithm is inefficient as more than two tracks tend to have impact parameters less than 1 mm; for $c\tau > 1$ m the search is inefficient as most decays occur too displaced to form reconstructable tracks. The requirements on H_T and on $p_{T,j}$ make the search inefficient for low LLP masses. A key difference between the 8 TeV [146] and 13 TeV [145] analyses is that the former explicitly reconstructs the DV, while the latter does not. CMS interprets the signal in several benchmark models, and for two neutral LLPs produced via an off-shell Z and decaying democratically into light jets (**Jet-Jet** model) the trigger efficiencies for $c\tau = 30$ mm are reported to be (2,41,81,92)% for (50, 100, 300, 1000) GeV masses. Indeed, a phenomenological recast of the 8 TeV analysis [152] in terms of 125 GeV Higgs rare decays sets very mild bounds for LLP masses below $m_h/2$ [153].

The LHCb studies [148, 147] trigger directly on DVs (transverse distance > 4 mm) with four or more tracks, vetoing dense material regions. Jet reconstruction is then performed offline with standard algorithms. This approach focuses on a scalar particle decaying to two neutral LLPs, π_v . The parent particle can be either the 125 GeV Higgs itself [147] or a Higgs-like scalar with mass in the 80-140 GeV range [148]. The search is performed for π_v masses between 25 and 50 GeV and lifetimes between 0.6 and 15 mm. It is expected that LHCb will extend their coverage to shorter lifetimes by improving the understanding of the material and to lower masses by using fat-jets and jet-substructure to access larger boosts [154]. A direct comparison between LHCb, ATLAS and CMS reach for dark pions can be seen in figure 3.1.

To summarize, searches in hadronic final states fail to comprehensively cover LLP parent masses (Φ) below about 100 GeV due to the typically large $p_{T,j}$ requirements at the trigger level. The exception is the DV reconstruction at LHCb. Additionally, singly produced LLPs with hadronic decays are overlooked at longer lifetimes and lower masses⁴. A straightforward extension to current analyses is to use any other existing trigger (VBF, leptons, E_T^{miss} , ...) and perform the displaced track reconstruction offline, which is already

⁴ Note that the presence of one LLP in the event can either mean that it was singly produced, or that several neutral LLPs with very long-lifetimes were produced, and only one decays within the detector. In this respect, highly-inclusive searches for single LLPs decaying in the ATLAS muon systems have been proposed [155], finding that backgrounds are appreciable and need to be controlled using data-driven methods.

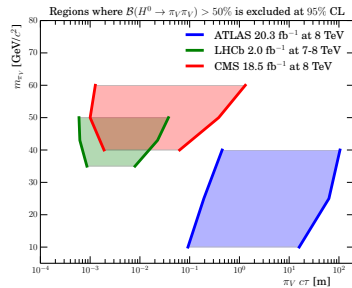


Figure 3.1: Comparison of the ATLAS [113], CMS and LHCb [147] reach for dark pions π_V decaying into jets. The CMS result is taken from the recast done in reference [153] of the 8 TeV analysis [152]. In the shaded regions the $\text{BR}(H \rightarrow \pi_V \pi_V)$ is constrained to be below 50%. Note that the ATLAS reach extend to higher masses, the plot was produced using the benchmark scenarios presented in [113], hence the meaningful bound is on the lifetimes. Taken from [147].

done in some ATLAS studies [113]. In particular, this implies that for the benchmark case of a 125 GeV Higgs as a parent for decays into LLPs, the current Higgs triggers would pick out signal events with reasonable efficiency. Some of these triggers also provide fairly clean objects for off-line use (e.g leptons) and thus reaching lower LLP masses is possible. As there is no theoretical preferred range for light neutral LLPs, aiming at the most extensive coverage forces us to push down the LLP mass / p_T thresholds. In that context a dedicated *online* reconstruction of DVs will allow for a reduction on the p_T threshold, allowing to reach lighter LLP masses.

3.1.2 Leptonic decays

Both ATLAS and CMS have searches for a pair of leptons coming from a DV [113, 156, 157]. CMS also has a search requiring exactly ⁵ one isolated muon and one isolated electron with large transverse impact parameter ($0.2 < d_0 < 10$ cm), but without any other additional requirement or veto (including that the reconstructed tracks do not need to point to a common vertex [114]). This loose selection makes the search sensitive to a variety of new physics scenarios.

Light and boosted LLPs can decay into collimated light leptons, dubbed *lepton-jets* [73], which are searched for at both CMS [146] and ATLAS. ATLAS has searches for both displaced [158, 159] and prompt lepton-jets [160]. The LHCb collaboration also looks for light, neutral LLPs going into $\mu^+ \mu^-$ pairs by studying B -meson decays to kaons, for exclusive decay channels for both neutral [161] and charged [162] B -mesons, as well as dark photons that decay to muon pairs [163].

The ATLAS search for displaced leptons [113] triggers on muons without an ID track, electrons, or photons (electrons with a large transverse impact parameters d_0 tend to be missing a track at trigger level and are reconstructed as photons) with fairly hard offline p_T criteria – requiring either one muon of 50 GeV, one electron of 110 GeV, one photon of 130 GeV, or two electrons, photons, or an electron and photon with p_T cuts for both objects in the 38-48 GeV

⁵ Hence, events with additional isolated leptons are discarded.

range. The DV is formed from opposite sign leptons, irrespective of flavor, and needs to be more than 4 mm transversely away from the PV of the collision. DVs in regions with dense detector material are vetoed to avoid converted photon backgrounds (e.g., $\gamma p \rightarrow e^+ e^- p$). This search is sensitive to events with a reconstructed DV mass $m_{DV} > 10$ GeV, but high offline p_T requirements for the leptons restrict the sensitivity to low mass LLPs.

The CMS studies trigger on leptons reconstructed using information from either the tracker [156] or the muon chambers [157] (the latter uses only muons). In the tracker-based analysis, the LLP is reconstructed by forming pairs of charged leptons (μ need to have opposite signs), with p_T cuts of (26, 36, 21) GeV for the muons, leading and subleading electron respectively, yielding slightly larger efficiencies in the muon channel. The transverse impact parameter d_0 needs to be 12 times larger than its uncertainty σ_d (approximately corresponding to a distance $\gtrsim 200$ μm to reject prompt backgrounds). In the muon-system based analysis, muon candidates are reconstructed using the hits in the muon chambers, while trying to avoid biases from a loose beamspot constraint in the seeding step. These candidates are referred to as *re-fitted stand-alone* (RSA) muons, and they need to fulfill $p_T > 26$ GeV, $|\eta| < 2$, be separated by $\Delta R > 0.2$. More importantly, these candidates are rejected if they can be matched to a $p_T > 10$ GeV track in the inner tracker, which efficiently excludes prompt muons and also renders this study fully complimentary to the tracker-based one. Both these searches are interpreted in terms of decays of H(125) ($H \rightarrow XX, X \rightarrow l^+l^-$) and RPV squarks, their combination covering proper lifetimes of $0.01\text{--}10^5$ cm for Higgs, and $0.1\text{--}10^4$ cm for the SUSY case. The difference in the lower reach of $c\tau$ being due to the larger boost factor the Higgs enjoys.

Furthermore, CMS has a search for one electron and one muon, each with large transverse impact parameter ($200\mu\text{m} < d_0 < 10$ cm) [114]. Events are selected using a dedicated trigger for displaced $e - \mu$ pairs that applies a p_T cut on the leptons but unlike standard triggers places no restriction on the maximum d_0 or distance from the PV. Events with exactly one muon and exactly one electron are kept, and then divided in "prompt", "displaced control" and "signal" regions, for $|d_0| < 100$ μm , 100 $\mu\text{m} < |d_0| < 200$ μm and $|d_0| > 200$ μm respectively. This selection makes the signal region almost free of leptons coming from SM processes, with rare τ leptons, B -mesons or D -mesons as the largest remaining background. Although the results are interpreted in the context of long-lived RPV stops, this search has been shown to be sensitive to many scenarios, including long-lived staus in gauge mediated SUSY breaking [164]. On the other hand, models where long-lived particles decay either to only muons or only to electrons (e.g., $\tilde{\mu} \rightarrow \mu \tilde{G}$) are unconstrained by this search. Additionally, same-sign lepton signatures and signatures with a prompt third lepton are possible [164] and could be covered by variants of the CMS search.

Due to the generality of τ -specific models, looking for hadronic tau channels is also desirable.

The searches for lepton-jets are focused on small LLP masses and distinctly boosted signatures, and thus we treat them separately. The ATLAS 8 TeV search [158] considers three types of lepton-jets: those containing only muons, only electrons/pions, or a mixture of the two. The muon and electron/pion lepton-jets can contain either two or four leptons, while the mixed lepton-jet must contain two muons and a jet consistent with a displaced electron/pion pair. As these signatures contain relatively soft leptons, the ATLAS 8 TeV analysis uses a trigger that requires three muon tracks in the MS with $p_T > 6$ GeV. A caveat to this trigger is the level-one requirement of three separate muon RoIs, which makes this trigger only sensitive to topologies with two lepton-jets in which one lepton-jet has a wide enough opening angle between two muons to create two level-one RoIs. For the electron lepton-jets, when the electrons decay in the HCAL they are indistinguishable from a hadronic decay and thus the CalRatio trigger is used.

In the 13 TeV ATLAS analysis [159] a *narrow-scan* muon trigger is used instead. This trigger starts off by selecting events with one muon with $p_T > 20$ GeV, then requires a second muon with $p_T > 6$ GeV within $\Delta R = 0.5$ of the leading muon.

Both the 8 and 13 TeV ATLAS searches are interpreted for Higgs-like scalar particles (with masses of 125 and 800 GeV) that decay effectively into either 2 or 4 lepton pairs, with each lepton pair assumed to come from a low-mass “dark” photon, γ_D . The ATLAS result excludes exotic Higgs branching ratios below 10% for dark photon lifetimes $2 < c\tau < 100$ mm. Note that here γ_D is also allowed to decay to pions, thus the results can also be interpreted for hadronically and semi-leptonically decaying LLPs.

The CMS lepton-jet search has only been performed with the 8 TeV dataset[146], and is a search for fully muonic lepton-jets. Events are selected with a di-muon trigger with standard isolation requirements. Further selection requires at least four standard muons, forming a minimum of two opposite charged pairs. CMS uses as a benchmark a model with scalars decaying into either lighter scalars or dark photons, with varying scalar and dark photon mass. For the case of a 125 GeV Higgs they can exclude an exotic branching ratio of 7%, comparable with the ATLAS results, as can be seen in figure 3.2. We note that this study employs both prompt and displaced muons.

LHCb has a search that looks for the direct production of dark photons [163], as opposed to dark photon production in decays of the Higgs. As a result of the direct production, dark photons do not tend to be highly boosted in the transverse direction. Events are required to have a single muon with $p_T > 1.8$ GeV, or two muons with a product of transverse momenta $\gtrsim (1.5 \text{ GeV})^2$. For the prompt dark photons search, events are reconstructed at trigger level so that all online reconstructed particles are recorded,

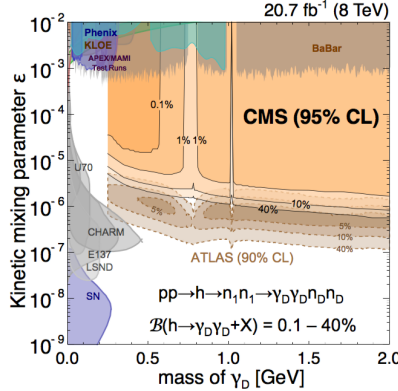


Figure 3.2: Comparison of the lepton-jet searches at ATLAS [158] and CMS [146] on the dark photon scenario [79] vis-a-vis dark photon limits coming from low-energy experiments.

while the rest of event information is discarded [165]. The displaced search constrains previously uncovered dark photon parameter space around masses of ~ 300 MeV, while the prompt search constrains entirely new territory above 10 GeV.

The LHCb searches for displaced leptons in rare B meson decays rely on standard techniques to identify the B^\pm decay vertex and the kaons and pions in the event, and the $m(\mu^+ \mu^-)$ variable is scanned for excesses. The $X \rightarrow \mu^+ \mu^-$ vertex is not required to be displaced from the B^\pm vertex, and thus the constraints apply to both prompt and long-lived particles. The analysis probe LLP masses of 214 (250) MeV $< m_X <$ 4350 (4700) MeV for the $B^0 \rightarrow K^* \mu^+ \mu^-$ ($B^+ \rightarrow K^+ X, X \rightarrow \mu^+ \mu^-$) process, with the mass range being limited by kinematics.

To summarize, the lepton searches rely on fairly standard lepton identification, with vertex reconstruction being performed mostly offline. Searches for leptonically-decaying LLPs typically enjoy low trigger thresholds and good sensitivity to LLP production rates. A major outstanding challenge, however, are LLP decays to τ leptons, which lie at the interface between hadronic and leptonic searches. Such decays are very well motivated from the theoretical point of view, as a Higgs-like scalar would decay about 300 times more into $\tau^+ \tau^-$ if kinematically allowed, and also one could have large rates into e.g. $\tau^+ \mu^-$. A displaced hadronic τ is a striking object, and most likely will have few backgrounds. Hence, limits on exclusive displaced τ s would be of upmost importance⁶.

As the leptonic searches explicitly require opposite sign (OS) leptons, the same sign (SS) lepton signature (motivated from Majorana neutrinos, see the LHCb search in Section 3.1.3, or heavy, doubly charged LLPs) is currently neglected.

Lepton-jet searches currently cover only final states with at least two LLPs and some muons in the final state⁷, and the same statement currently applies to both the LHCb searches for dark photons and for LLPs produced in B -meson decays. It would be beneficial to have additional searches with one lepton-jet or low-mass,

⁶ We note that if the τ originate from outside the tracker, the hadronically decaying taus are indistinguishable from other displaced hadrons. For instance, in the ATLAS Muon RoI study [143] the results are interpreted for a model with a scalar particle with Higgs-like couplings to SM fermions, which includes a branching fraction into $\tau^+ \tau^-$. However, if the τ originates from the ID, the low number of tracks associated to it (1-3) will not fulfill the requirements of the ATLAS study to having 5 or more tracks associated to a DV.

⁷ The ATLAS 8 TeV search included a search channel with two electron-only lepton-jets, but the performance was poor and it was excluded from the final result.

leptonically-decaying LLP (which are motivated in hidden sectors and Majorana neutrinos, for example in Refs. [17, 83]). In addition, the status of coverage in the intermediate mass transition region between “standard” displaced lepton pairs and lepton-jets is unclear, and may potentially harbor a gap.

The Heavy Neutral Lepton (HNL) scenario is an important physics case that leads to multi-lepton displaced signatures from W decays, with nice prospects at ATLAS and CMS [166]. While previous searches were not sensitive to this scenario due to either high- p_T requirements or the requirement of two DVs in the same event, the presence of a prompt lepton from the W allows to relax on these in a dedicated analysis.⁸ The identification of two leptons from the vertex is a powerful discriminant against backgrounds from metastable particle decays and hadronic interactions in material. This permits a better exploration of the lower HNL mass range ($3 - 6$ GeV) than in the semi-leptonic channel (see Section 3.1.3) despite the lower branching ratio. It should be noted that the ambition is to probe mixing to all three neutrino flavours, requiring the capability to reconstruct displaced leptons of all flavours, including taus.

3.1.3 Semi-Leptonic decays

As semi-leptonic signatures include aspects of both hadronic and leptonic LLP decays, many of the previously discussed searches can partially cover these cases, and some do so explicitly. For instance, the ATLAS search for electrons and muons accompanied by tracks [113], the inclusive CMS search for DVs [145] (there is an specific model interpretation called B -lepton addressing precisely this channel), and the large impact parameter $e - \mu$ pair by CMS [114] are all inclusive with respect to other hadrons produced in the LLP decay, provided the leptons are sufficiently isolated⁹. In addition, LHCb has dedicated searches for semi-leptonically decaying LLPs [167] and semi-leptonic decays of long-lived Majorana neutrinos [168]. The two CMS searches [145, 114] need no further explanation for how they cover semi-leptonic LLPs, but we now describe the rest of these searches in some detail.

The ATLAS search for a vertex with a lepton accompanied by tracks [113] uses the same trigger as the dilepton vertex search described earlier. The DV is required to have a lepton as well as at least four additional displaced tracks associated with it, and the invariant mass of the tracks must exceed 10 GeV. Thus, the search in principle can have sensitivity down to masses $\gtrsim 10$ GeV, although the very high p_T threshold for the displaced electron(photon)/muon typically limits sensitivity for low-mass LLPs: the vertex must contain a muon with $p_T > 55$ GeV or an electron with $p_T > 125$ GeV.

The LHCb search for semi-leptonic LLP decays selects events with a muon trigger, then requires a DV offline [167]. The results

⁸ Note that the displaced large transverse impact parameter $e - \mu$ CMS search [114] fails to cover this scenario due to the aforementioned lepton veto, which kills the tri-lepton signals discussed in Ref. [166].

⁹ Note that the lepton isolation affects most of the semi-leptonic searches.

are interpreted in terms of four distinctive topologies: single LLP production in association with a new particle, and double LLP pair production either from Higgs decays or via squark pair production. Material regions are vetoed, leaving the main backgrounds as heavy flavor either produced directly or from W/Z decays. The signal discrimination is obtained from a multivariate analysis based on the muon p_T and impact parameter, and subsequently the search is optimized on the LLP reconstructed mass and the muon isolation. This study is sensitive to lifetimes between 1.5 and 30 mm, as can be seen in Figure 3.3.

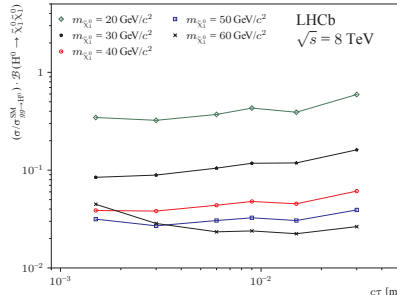


Figure 3.3: LHCb reach for displaced semi-leptonic decays. Taken from ref [167].

The LHCb search for Majorana neutrinos [168] looks for the production of a Majorana neutrino, N , produced in leptonic B decays, $B^\pm \rightarrow \mu^\pm N$, followed by the decay $N \rightarrow \mu^\pm \pi^\mp$, whether prompt or at a DV¹⁰. A same-sign muon requirement greatly reduces backgrounds to the search. The sensitivity of the search is limited by the restriction to muons in the final state (so models that predominantly decay to e or τ are not constrained), as well as the same-sign lepton requirement that restricts sensitivity to only lepton-number-violating LLP decays. More inclusive searches looking for additional N production modes [170] or searches targeting decays of heavier mesons like B_c [171] could also improve the sensitivity to semi-leptonically decaying LLPs.

When considering the application of inclusive, hadronic or leptonic searches to semileptonic LLP decays, it is important to understand how the simultaneous presence of leptons and jets in the signal can degrade the sensitivity. For instance, prompt jet searches will veto non-standard jets at the “cleaning” stage. Lepton isolation criteria can severely reduce the signal acceptance for a highly-boosted LLP decaying into a lepton and a jet, and they might also veto extra tracks in the events. Thus, boosted semileptonic decays (as might be found in the displaced decay of a low-mass right-handed neutrino produced via W decay) may not be covered by existing searches. Another important issue is that the lepton-jet studies express their results in terms of specific dark photon models¹¹, which makes it complicated to apply the results to other models. We refer the reader to Sec. ?? for a further discussion of this topic.

The signature of HNLs from W decays with displaced semi-leptonic HNL decays is an important item on the search agenda

¹⁰ Some care is required in interpreting the results of the search on a model with a Majorana neutrino, as the original theory interpretation is problematic [169].

¹¹ Recall that these searches also consider the $\gamma_D \rightarrow \pi^+ \pi^-$ decay mode.

of ATLAS, CMS and LHCb [172, 166, 173, 174]. The semi-leptonic channel has the highest branching ratio (about 50% in the relevant mass range [175]) and offers the best discovery prospects at LHC experiments for HNL masses up to 30 GeV as long as a DV mass cut of around 6 GeV is made to mitigate backgrounds. This 6 – 30 GeV mass range corresponds to a non-perturbative regime for the hadronisation of the HNL decay products. As the number of charged hadrons significantly affects the DV reconstruction efficiency, the validation of event generator outputs for this process is an important issue currently being addressed by the community. The ability of LHCb to trigger directly on the HNL decay products and better reconstruct displaced tracks can in some cases compensate for its lower acceptance and luminosity, as exemplified by a recent search for DVs made one one muon and several tracks [176, 174]. This possibly enables LHCb to better probe the more challenging tau channel. Fig. ?? shows the overall expected reach of LHC searches in the HNL coupling strength (muon channel) versus mass plane, using assumptions detailed in Ref. [173], similar to those in Refs. [172, 166]. An interesting aspect of the LHC HNL search programme is that backgrounds can be mitigated at high luminosities using the DV feature, making this signature particularly attractive at the HL-LHC.

The sensitivity of LHC experiments to HNLs is complementary to that of fixed-target experiments which probe lower couplings thanks to high-intensity beams albeit at lower mass ranges (HNLs from c and b decays). The CERN SPS provides great opportunities with the running NA62 experiment [177] and the planned SHiP experiment [178], which comprise a vacuum decay vessel and spectrometer tracker downstream of the target to reconstruct vertices of long-lived neutral particles. These are unbeatable for HNL masses up to 2 GeV, where they probe a region of the parameter space favoured in models which explain at once neutrino masses, matter-antimatter asymmetry and dark matter [179, 180, 181] (see Fig. ??).

3.1.4 Photonic decays

There are two ways in which photons coming from LLP decays do not resemble standard photons. First, they can not be traced back to the PV, thus giving rise to *non-pointing* photons. Second, they can arrive at the electromagnetic calorimeter at a slight different time than expected, referred to as *delayed* photons. We note that both these kinds of unusual photons can be vetoed when considering prompt photons, and thus the recasting of prompt searches typically provides weaker bounds on LLP scenarios. ATLAS has a search for non-standard photons [182] using the full 8 TeV dataset, which supersedes the 7 TeV analysis [183], while in CMS there are studies for delayed photons in the ECAL [184] and for non-pointing photons detected via their conversion to e^+e^- pairs [185]. The underlying topology in all these models is the neutralino decay into a

gravitino and a photon ($\chi_1^0 \rightarrow \gamma \tilde{G}$), ubiquitous in gauge-mediated supersymmetry breaking (GMSB) scenarios [186, 20]. Hence all these studies require to have large E_T^{miss} in the final state.

The ATLAS study benefits from the capability of the liquid-argon electromagnetic calorimeters to measure the flight direction and the time-of-flight of photons. Resolutions on Δz_γ , the separation between the PV of the event and the extrapolated origin of the photon, and $|\Delta t_\gamma|$, difference of the arrival time of the photon with respect to the prompt case, are as low as 15 mm and 0.25 ns, respectively. The trigger demands two photons within $|\eta| < 2.5$, with transverse energies E_T of 35 and 25 GeV. In addition, to guarantee the event comes from a proton–proton collision, a PV with 5 or more tracks with $p_T > 0.4$ GeV is requested. The offline selection requires two photons with $E_T > 50$ GeV and $|\eta| < 2.3$, not in the barrel-endcap transition region ($1.37 < |\eta| < 1.52$), at least one of them in the barrel ($|\eta| < 1.37$) and with less than 4 GeV energy deposit in the calorimeter in a cone of $\Delta R = 0.4$ around them (*isolation*). In addition, the events are binned in E_T^{miss} : the $E_T^{\text{miss}} < 20$ GeV bin contains the prompt backgrounds, the $25 \text{ GeV} < E_T^{\text{miss}} < 75$ GeV bin is used as the control region, and finally the signal analysis is performed in the $E_T^{\text{miss}} > 75$ GeV bin. This study covers lifetimes from 0.25 to 100 ns in the GMSB framework, the lower limit being a hard cut-off imposed experimentally, as the similarity between background and signal samples in that region makes discrimination rather difficult. The excluded signal rates in this range of lifetimes vary between 0.8 and 150 fb, with the best-constrained value obtained for $\tau \sim 2$ ns.

The CMS study of delayed photons [184] follows a similar approach to ATLAS. The main difference is that it demands only one photon with $p_T > 80$ GeV, but in addition two jets are required. Furthermore, in addition to E_T^{miss} , the vector sum of E_T^{miss} and E_T^γ , which is denoted $E_{T \text{ no}\gamma}^{\text{miss}}$, is used for background discrimination. (Non)-collisional backgrounds have small (large) E_T^{miss} and large (small) $E_{T \text{ no}\gamma}^{\text{miss}}$, while for the signal events both variables are large, hence they are both requested to be larger than 60 GeV. The time resolution is 0.372 ns, slightly worse than in the optimal scenario of the ATLAS search. Their reach in lifetimes lies in the 2–30 ns range, excluding signal rates of 10–30 fb.

The CMS study of non-pointing photons [185] relies on conversion to e^+e^- pairs. It requires two photons, two additional jets, and $E_T^{\text{miss}} > 60$ GeV. The photon trajectory is obtained from the conversion vertex as the line segment along the momenta of the e^+e^- track pair, and the impact parameter, $|d_{XY}|$, is defined as the closest distance between the photon and the beam axis, can be determined within approximately a mm. A comparison of the reach of these 8 TeV studies, as well as those using the 7 TeV dataset, can be found in Fig 3.4.

The gaps in these studies are straightforward to identify. The requirement of large E_T^{miss} is due to the fact that all of these studies

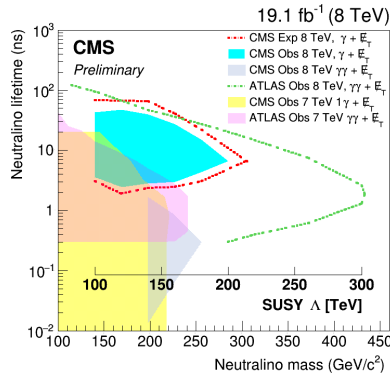


Figure 3.4: Summary of the $\gamma + E_T^{\text{miss}}$ searches from ATLAS and CMS, displayed assuming the same GMSB model. Taken from reference [184].

have an underlying theoretical picture of neutralinos decaying into gravitinos and photons, motivated from GMSB scenarios. Hence, these searches do not cover cases without the presence of missing energy, including LLPs that decay to $\gamma\gamma$, $l\gamma$ or $j\gamma$, although either mis-measurement of jets or the photon decay geometry could fake large missing energy to provide moderate constraints. With the exception of the CMS study which requires two additional hard jets, all of these analyses require two displaced photons. A single displaced photon signature can occur in motivated models: it can easily arise, for example, from a very slightly mixed electroweak triplet and singlet. Furthermore, as discussed in section 3.1.1, a single LLP in the detector also arises for very large lifetimes of neutral LLPs, which limits the reach at longer lifetimes.

3.1.5 Other exotic long-lived signatures

In this section we present the analyses that are based on exploiting properties of other exotic long-lived signatures, such as non-standard tracks. We summarize in detail the existing searches for heavy stable charged particles (HSCP), disappearing tracks (DT), stopped particles (SP) and monopoles, and describe existing ideas on how to look for quirks and SIMPs (Strongly Interacting Massive Particles).

3.1.5.1 Heavy Stable Charged Particles (HSCP)

The search for HS CPs at CMS [187, 188] and ATLAS [189, 130] rely on two key properties. First, particles that are massive and/or electrically charged with $Q \neq \pm e$ have a characteristic ionization loss (dE/dx) distinctively different than SM particles. This property can be measured in the tracker. Second, HS CPs are typically heavy and move with a speed smaller than the speed of light, $\beta = v/c < 1$. Thus, compared to a particle with $\beta \approx 1$, they require a longer time-of-flight (TOF) to reach the outermost components of the detector (calorimeters and muon chambers). As interactions of the HSCP with the material in the detector can change the electric charge of

the HSCP, both CMS and ATLAS perform separate *tracker-only* and *tracker + TOF* studies in the language of CMS¹². The event selection relies on standard single muon or large missing energy triggers. The offline selection relies on identifying the signal events from quality requirements on the tracks using discriminator variables built from track observables.

The theoretical interpretation of a signal or limit depends on whether the HSCP carries both color and electroweak charges. If it carries a color charge, the default benchmarks correspond to *R-hadrons*, namely HSCPs that hadronize with SM particles via the strong force, e.g: gluino-gluon, quark-squark states. In the absence of a color charge, the signal is exemplified by long-lived sleptons in the context of gauge-mediated SUSY. Both ATLAS [189] and CMS [188] studies employ these two scenarios¹³. Finally, CMS also looks for HSCPs coupling only to hypercharge (and hence possessing only couplings to γ and Z), while ATLAS has a search inspired by electroweakinos in SUSY: it considers the associated production of a neutral and an electrically charged LLP (chargino-neutralino), and thus only one HSCP plus missing energy are required.

The HSCP search conducted by LHCb [190] is slightly different. Instead of exploiting dE/dx and time-of-flight, they use the lack of radiation in the ring imaging Cherenkov detector (RICH). Events are required to pass a high- p_T single muon trigger ($p_T(\mu) > 15$ GeV). Two opposite sign “muons” are then required, each with p_T above 50 GeV and an invariant di-muon mass above 100 GeV, to suppress muons coming from DY production, the main background for this search. In addition, particles must have $\beta > 0.8$, set by the efficiency of the muon chambers to reconstruct slow particles. As electrons and hadrons interact more with the calorimeter than an HSCP, a deposit in the calorimeter of less than 1% of the momentum of the particle is required. The results are interpreted in the context of stau pair production.

To summarize, these searches present no obvious weak points. Standard triggers and tracking algorithms are used, and the analysis methods are well-understood and have been extensively validated against data. While the HSCP strategies are robust, we encourage the experimental collaborations to continue pursuing improvements for these searches. The small number of signal events that would be produced for HSCPs above current limits render the sensitivity highly dependent on the understanding of the background and the control of the systematics.

3.1.5.2 Disappearing tracks (DT)

Massive charged particles traveling in the detector can decay to a lighter, almost mass degenerate neutral state, emitting a SM charged particle (typically a pion or a muon). While at first glance a small mass gap naively seems like a hallmark of tuning, near degeneracies often occur naturally as a result of a symmetry. In fact, electroweak symmetry generically leads to small mass splittings be-

¹² ATLAS measures $\beta\gamma$ from dE/dX and β from time-of-flight and extracts an independent mass, m_β and $m_{\beta\gamma}$, from each measurement.

¹³ The ATLAS R-hadron searches using the 13 TeV dataset have recently been presented in reference [130].

tween components of a single electroweak multiplet. For example, $\mathcal{O}(100 \text{ MeV})$ splittings arise between the different components of an electroweak multiplet [30, 191] due to EW gauge boson loops¹⁴. If the SM particle is sufficiently soft it can not be reconstructed, and then a charged track seems to vanish: this is thus referred to as a disappearing track.¹⁵ The actual lifetime of the charged particle is highly sensitive to the precise value of the mass splitting. For instance, the well studied cases of a fermionic doublet with $Y = 1/2$ and a fermionic triplet with $Y = 0$, reminiscent of a Higgsino and Wino in supersymmetry, respectively, have mass splittings of $\Delta = 355$ and 166 MeV up to small corrections, but the corresponding $c\tau$ differ by almost an order of magnitude: 6.6 mm versus 5.5 cm ¹⁶. This is because the lifetime, $c\tau$, depends on the third power of the mass splitting in these scenarios [30, 191].

Before 2017, both ATLAS [192] and CMS [125] required a track to travel about 30 cm in order to be reconstructed, giving good coverage of the Wino scenario. These 30 cm correspond to four hits at ATLAS, three in the pixel layers plus one in the silicon tracker, and to seven hits in the pixel and trackers of CMS. The search uses a trigger requiring an ISR jet against which the charged particle recoils, along with the presence of large missing energy. The disappearing track is reconstructed offline and needs to fulfil a few quality criteria (isolation, p_T threshold, etc). A phenomenological study [48] had shown that reducing the distance from 30 to 10 cm would give coverage to the elusive Higgsino scenario, moving the expected reach up to 400 GeV , trumping over the expected mono-jet reach of 250 GeV [193, 194, 195]. Later ATLAS presented a study [196] using 13 TeV data and exploiting the presence of a new innermost pixel layer (IBL). This addition allows for all four hits to be in the pixel, with the outermost pixel layer now at 12.25 cm , granting sensitivity to lower values of $c\tau$. The summary for disappearing tracks at ATLAS for the Wino case can be seen in the left panel of Figure 3.5, while in the right panel we show the constraints for Higgsinos from reference [48].

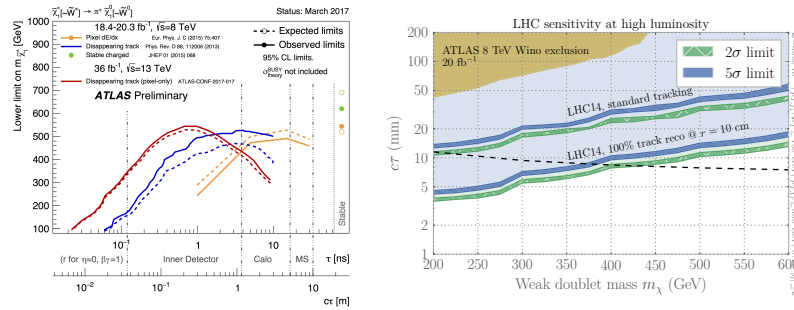


Figure 3.5: Summary of the status of Wino searches in ATLAS (left panel) and HL-LHC expected constraints on the Higgsino scenario (right). Taken from [197] and [48] respectively.

At LHCb the prospects for a disappearing track analysis with the present detector are poor. Currently, the momentum of the track can only be measured if the particle passes through the TT, which

¹⁴ For a single fermionic multiplet, the splitting can only be altered by higher-dimensional operators, and thus it is harder to vary Δ from the 1-loop EW value. For other cases, such as mixing with additional particles, the actual splitting can differ greatly than this 1-loop EW value.

¹⁵ If the charged particle could be reconstructed this case is often referred to as *kinked track*. However, as the kinked portion has a very large impact parameter, without a serious attempt to capture the kink these tracks too simply disappear.

¹⁶ While these values set a concrete physics target, we stress again that the mass splitting can be arbitrary in other corners of the BSM parameter space (even within SUSY). For instance, $\tilde{\tau} \rightarrow \tau \bar{\nu}$ (where the stau and sneutrino masses are free independent parameters) or for scalar particles (e.g. $H^+ \rightarrow \mu^+ H^0$), where the mass splitting and the overall mass scalar are set by arbitrary quartic couplings.

is about 3 m away from the IP. Particles decaying in the VELO or RICH1 system will not leave a fully-measurable track and will be swamped in a background of SM processes such as kaon decays, which would give a similar signature in the detector components before the magnet. Detector improvements (additional magnets, better PID at low momentum, additional layers) might lead to some sensitivity for $\mathcal{O}(\text{cm})$ lived tracks.

If the detector were improved (by e.g: adding station magnets, better PID at

To summarize, the search for disappearing tracks present a few drawbacks. Using an ISR-jet trigger means a price is paid in terms of signal sensitivity: reference [48] has shown that significantly lowering the p_T threshold of the jet (or directly triggering on the momentum of the disappearing track^{[17](#)}) would lead to a factor of 2 increase in the number of signal events. It is also clear that better access to lower lifetimes is needed; thus, adding new layers as close as possible to the beampipe (and/or having double layers instead of single ones) is a desirable feature.

¹⁷ While currently there are some proposals to trigger on tracks [198], those only apply to standard tracks. In particular, the new fast track reconstruction (FTK) system at ATLAS requires more than 10 hits [199, 200]

3.1.5.3 Stopped particles (SP)

If an HSCP is produced with very low kinetic energy, it can come to rest in the detector due to interactions with the detector materials. This most likely occurs in the calorimeters or the muon chambers as a result of their high densities. The HSCP can then decay at a later time when no collision is taking place (an out-of-time decay). This experimental restriction severely restricts the background processes, with the dominant backgrounds coming from cosmic rays, beam halo and instrumental noise.

In the Run-I analyses from ATLAS [201] and CMS [202], events are selected with a dedicated trigger selecting bunch crossings which are empty and have no bunches of protons nearby. The analyses require a jet with p_T (E) above 30 (50) GeV at ATLAS (CMS). ATLAS further supplements the hardware trigger by requiring $p_T(j) > 50 \text{ GeV}$, $|\eta| < 1.3$ and $E_T^{\text{miss}} > 50 \text{ GeV}$, rejecting instrumental noise. In addition, CMS has a search that triggers on out-of-time muons [203] using the 13 TeV dataset. The latter also employs the displaced stand-alone (DSA) muon reconstruction algorithm [204].

An offline selection procedure follows aimed at reducing the main backgrounds. Since, as mentioned, the particles are most likely stopped in the calorimeters or muon chambers, the information coming from the muon chambers is crucial to identify the signal events. Muons coming from cosmic rays can be identified due to their distinctive topology. Beam halo is the result of protons interacting with residual gas in the beampipe, the beampipe itself, or collimators upstream from the interaction point. Most particles will not travel far before being absorbed by various structures, but muons will travel parallel to the beam and can leave calorimeter deposits out of time with a proton–proton collision. However, these deposits will often present with corresponding horizontal tracks in

the muon systems and can thus be efficiently vetoed. Instrumental noise is rejected in CMS by exploiting the anomalous response in the HCAL.

HSCP searches are typically much more sensitive to any signature that can have a charge, so stopped particle searches are not expected to be a discovery mode for most simple new physics scenarios with charged LLPs. However, in case of a positive signal, HSCP searches might not provide much information. In such a case, SP searches allow to properly study the decays of the newly discovered LLP. Moving forward, as luminosity rises and the number of empty bunch crossings per fill decreases it might be worth considering how higher energy and triggering thresholds could control backgrounds and allow for access to novel physics decaying off-time from the rest of the event.

3.1.5.4 Magnetic Monopoles

ATLAS [123] has a dedicated search for highly ionizing particles (HIPs), which encompass a variety of new physics scenarios, such as magnetic monopoles, dyons (particles with both magnetic and electric charge), stable microscopic black holes, etc. For the sake of concreteness, we focus on magnetic monopoles but the interpretation in terms of other models is straightforward.

The main phenomenological feature is that magnetic charge is quantized in units of $g_D = 2\pi/e \approx 68.5$. Hence, a magnetic monopole behaves as a particle with at least 68.5 electron charges, leading to an unusually large ionization power in matter, so that they would quickly stop in the detector as HIPs lose energy at spectacular rates. Because of the large QED coupling of magnetic monopoles, a perturbative calculation of the cross section is invalid and there is no accurate determination of the production rate, but a naïve Drell-Yan production cross section is provided for the purposes of comparison. The specifics of the detector restrict the sensitivity of this search to magnetic charges $g < 2g_D$ because a large fraction of the monopoles stop in the beampipe. We note that larger magnetic charges can be tested by the MoEDAL experiment [205], which is described in detail in section 5.

ATLAS has a dedicated trigger for HIPs based on identifying relevant RoIs in the ECAL and subsequently counting the number of hits in the transition radiation tracker (TRT). As well, the fraction of TRT hits that are high-threshold (HT), meaning that they have an ionization larger than ~ 3 times that expected from a SM particle, is used as a discriminant. The analysis selects events based on the fraction of TRT-HT hits matched to an EM cluster deposit, and how the energy deposits are distributed in the different layers of the ECAL. It is important to note that due to the lack of a consistent theory, the signal simulation is performed by re-scaling Drell-Yan production at leading order and assuming no coupling to the Z-boson. The HIPs are assumed to have either spin-0 or 1/2. The spin does not affect the interaction with the material, but the

angular distributions are different according to angular momentum conservation; however, there is anyways no perturbative theoretical prediction for the angular distribution. Limits for $0.5 < |g|/g_D < 2$ are set for masses in the 890-1050 (1180-1340) GeV for the spin-0 (1/2) case.

The LHC coverage of magnetic monopoles in the $g_D - \sigma$ plane is displayed in fig 3.6.

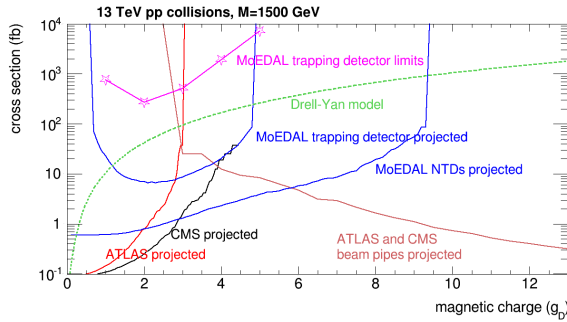


Figure 3.6: Comparison of the MoEDAL, ATLAS and CMS reach for magnetic monopoles. The curves assume 3 signal events and a total integrated luminosity of 50 fb^{-1} . Source: private communication from P. Mermod, updated version of existing figure in [206].

3.1.5.5 Quarks

Quarks are particles charged under both the SM and a new confining gauge group [207], referred to here as “infracolor” (IC). The defining property of quirks is that the tree-level quirk masses m_Q are above the confinement scale Λ_{IC} (this is like QCD but with no light-flavored quarks), so that there is never enough local energy density to pop new quirks out of the vacuum. A pair of a quirk and an anti-quirk can live in a quantum mechanical bound state that can separate by macroscopic distances $\ell \sim \frac{m_Q}{\Lambda_{IC}^2}$, remaining connected by an infracolor flux tube. The infracolor flux tube exerts a tension on each quirk that causes its trajectory to differ from the expected helicoidal ones for SM particles. Although well-motivated by hidden-valley models [32], we stress that quirks are not exclusive to hidden valleys, contrary to popular lore.

The collider phenomenology depends greatly on the size of ℓ . If ℓ is below the mm scale, the individual quirks are not distinguished from one another and the anomalous track can not be seen. However, the pair (which is overall neutral, and therefore does not bend in the tracker magnetic field) appears as a single highly ionizing straight track with missing energy aligned with it, the latter arising from miss-measuring the track momenta. The Do collaboration has searched for precisely this signature [208], requesting an additional jet for trigger purposes, finding lower bounds on quirk masses of 107, 119 and 133 GeV for SU(2), SU(3) and SU(5) gauge groups. However, no extensions of this search to higher mass have been performed at the LHC, and the existing HSCP searches require a fractional certainty on the tracks momenta that a straight track

cannot provide.

Conversely, if ℓ is very large then the existence of the confining force has no effect on the quirk motions, and HSCP searches apply directly to the quirk case, with quirks charged under QCD yielding R -hadrons and uncolored quirks leading to slepton-like signatures. We refer the reader to the HSCP section for more information.

For intermediate values of ℓ , there are interesting phenomenological prospects at the LHC that have been recently studied theoretically [209, 210], but for which there are no current public searches by the LHC collaborations. The first study [209] has recast monojet and HSCP searches, finding bounds up to 1.7 TeV for colored quirk masses. In addition, it has also proposed using the CMS dataset taken with zero magnetic field (0T). In this dataset, all SM particles are expected to follow a straight trajectory, but the quirks would still bend due to the string tension. The second study [210] has proposed a new algorithm to search for quirks, exploiting the fact that the quirk and anti-quirk pair should lie in the same plane with the highest sensitivity in the $\ell \sim 1 - 10$ mm range. This allows to avoid fitting the non-helicoidal trajectories, and has the potential to extend the sensitivity to quirks well beyond the current mono-jet and HSCP limits.

Because of the non-standard nature of the tracks, quirk phenomenology poses substantial challenges in their experimental reconstructions, and the lack of constraints on quirks have already attracted the attention of the ATLAS, CMS and LHCb experiments. It would be desirable to test how the phenomenological proposals in Refs. [209, 210] can perform in a realistic detector simulation of one of the LHC experiments.

3.1.5.6 Strongly interacting massive particles (SIMPs)

Strongly interacting massive particles (SIMPs) can be motivated by astrophysical observations of dark matter that do not fully agree with the WIMP paradigm (missing satellites, core vs cusp problem see e.g [211, 212, 213, 214]). These particles are assumed to interact strongly with baryons. Consequently, the experimental signature is little to no signal in the tracker and the ECAL, and large energy deposits in the HCAL. Such a final state with trackless jets also arises in the context of emerging jets [215], and ATLAS has a trigger for trackless jets in association with a soft muon (where the muon is required to exit level 1 of the trigger) [150]. Additionally, the Cal-Ratio trigger and associated search for displaced hadronic decays (addressed in Section 3.1.1) presents with a similar signature and could provide some coverage of this signature.

An LHC phenomenological study of SIMPs was carried out in ref. [216]. We summarize the main points of the study here. In their setup, SIMPs interact with the SM via an attractive potential (either scalar or vector mediator) coupling SIMP pairs with $q\bar{q}$ pairs. The proposed analysis selects events with high p_T back-to-back jets within the tracker, exploiting the charged energy fraction within

a jet to discriminate signal from background. The astrophysical experimental constraints on this scenario are compared with the expected reach of this search and that of monojets in figure 3.7. Currently there is an ongoing analysis in CMS pursuing this strategy.

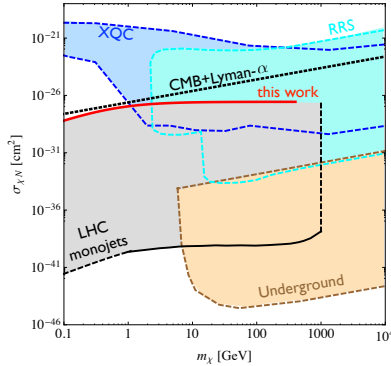


Figure 3.7: Astrophysical and collider constraints on a simple SIMP setup. Note that the relevance of the astrophysical constraints depends on the contribution of the SIMPs to the relic density. Taken from reference [216].

3.2 Overview of Gaps

1. All-hadronic

- Use associated object triggers (especially motivated by Higgs like VBF and VH)
- Try to push to lower masses & lifetimes
- Online reconstruction of hadronic displaced objects
- Exclusion limits for displaced hadronic taus. Opportunity for CMS displaced triggers?

2. Leptonic

- Intermediate region between low-mass (lepton-jets) and high-mass (resolved ATLAS/CMS searches)
- Continue to push to go to lower masses, p_T thresholds
- Tau leptons in LLP decay, in particular if they come from ID. Opportunity for CMS displaced triggers?

3. Semi-Leptonic

- Low masses (like Majorana neutrino)
- Making sure to cover all flavor combinations (for example, one CMS search only covers $e^\pm \mu^\mp$), as well as same-sign vs. opposite sign leptons
- Trigger on associated objects or use dilepton trigger if there are two LLPs?

4. Photonic

- No coverage for LLPs decaying into $l\gamma$, $j\gamma$ or without E_T^{miss} .
- Poor coverage (non-dedicated search) for single γ , only if two jets are present, needs recasting of CMS delayed photon study [184].
- Prompt photons searches useless, as they veto "non-standard" photons.
- No coverage for softer photons.

5. Other exotic long-lived signatures

- DTs: $c\tau \sim \text{mm}$ are very hard to probe. Unclear if ATLAS IBL will be present in HL-LHC run. What is the lowest distance new layers (or double layers) can be inserted at?

4

Trigger and Detector Upgrades

Introduction here.

4.1 The ATLAS and CMS experiments

The striking signatures of long-lived particles present unique experimental challenges in triggering, signal reconstruction, and background estimation. The planned upgrades to the ATLAS and CMS experiments for the high-luminosity LHC (HL-LHC) will give the detectors increased coverage in the forward regions, better spatial and timing resolutions, and other new features including track trigger and timing. The improved hardware capabilities, combined with software developments, give rise to tantalizing new prospects for future LLP searches. This section gives an overview of the upgrade scopes (Section 4.1.1), discusses their physics potential (Section 4.1.2 4.1.3), and presents new ideas for detector upgrade and LLP searches (Section 4.1.4).

Unless specified otherwise, the subsequent CMS experiment results are from its Technical Design Reports for the different sub-detector upgrades at HL-LHC, namely tracker(Ref. [217]), barrel calorimeter(Ref. [218]), endcap calorimeter(Ref. [add HGCAL TDR]), muon detectors(Ref. [219]), timing detector(Technical Proposal, Ref. [add timing TP]), and Level-1 Trigger(Interim Technical Design Report, Ref. [220]).

4.1.1 Detector and Trigger Upgrades for High-Luminosity LHC

The High Luminosity LHC (HL-LHC) will begin with the third long shutdown (LS3) of the LHC in the coming decade, where the machine and detectors will be upgraded to allow for pp running at a luminosity of $5 \times 10^{34} \text{ cm}^{-2} \text{ s}^{-1}$ in the nominal scenario, or even $7.5 \times 10^{34} \text{ cm}^{-2} \text{ s}^{-1}$ in the ultimate performance scenario. This will allow the ATLAS and CMS experiments to collect integrated luminosities ten times that of the current operations, which mounts to around 300 fb^{-1} per year and 3000 fb^{-1} during the projected HL-LHC lifetime of ten years (up to 4000 fb^{-1} . if the ultimate instantaneous luminosity can be achieved).

The HL-LHC conditions creates unique challenges in terms of high pile-up levels and high radiation dosage. About 140 pileup

events on average are expected in the nominal scenario, and up to 200 pileup events in the ultimate luminosity scenario. The radiation level will be unprecedented: for the design integrated luminosity of 3000 fb^{-1} , a 1 MeV neutron equivalent fluence of $2.3 \times 10^{16} n_{eq}/\text{cm}^2$ and a total ionizing dose (TID) of 12MGy (1.2 Grad) is expected at the centre of the detectors, where the innermost silicon pixel tracking layers will be installed.

To meet the challenges of the HL-LHC operating conditions, and to fully profit from its physics capabilities, comprehensive upgrade programmes are planned for both the ATLAS and CMS experiments. This section summarizes the main detector and trigger upgrade plans for both experiments.

4.1.1.1 Tracker

By the start of the HL-LHC, the inner trackers of both experiments will have to be replaced due to the significant radiation damage and performance degradation they would have suffered, and to cope with the more demanding operational conditions.

CMS Upgrade The CMS tracker is composed of the inner pixel detector and the outer tracker. At the HL-LHC, the CMS inner pixel detector will include four cylindrical barrel layers covering the region of $|z| < 200 \text{ mm}$, and forward extensions of up to twelve endcap disks on both sides, which will extend its $|\eta|$ coverage from the current value of 2.4 with three disks to 4. To maintain radiation hardness and reasonable occupancy, as well as to improve resolution, small, thin pixels will be used. In the CMS tracker TDR (Ref. [217]), pixels with a thickness of $150\mu\text{m}$ and $25 \times 100\mu\text{m}^2$ in size are used in the simulation. ($50 \times 50\mu\text{m}^2$ is an alternative option.)

The CMS outer tracker is composed of six cylindrical barrel layers in the central region, covering the region of $|z| < 1200 \text{ mm}$, complemented on each side by five endcap double-disks, in the region of $1200 < |z| < 2700 \text{ mm}$. Modules are installed between $r \sim 21 \text{ cm}$ and $r \sim 112 \text{ cm}$. Three sub-detectors are distinguished: the Tracker Barrel with pixel-strip modules, TBPS; the Tracker Barrel with strip-strip modules, TB2S; and the Tracker Endcap Double-Disks, TEDD. The inner rings of the TEDD disks use pixel-strip modules up to $r \sim 60 \text{ cm}$, and the rest use strip-strip modules. The outer tracker modules, called p_T modules, are composed of two single-sided closely-spaced (1 to 4 mm separation) small pitch sensors read out by a common set of front-end ASICs that correlate the signals in the two sensors and select the hit pairs (referred to as “stubs”) compatible with particles above the chosen p_T threshold. A p_T threshold of 2 GeV corresponds to a data volume reduction of roughly one order of magnitude, which is sufficient to enable transmission of the stubs at 40 MHz. The “stubs” are used as input to the hardware trigger at Level-1 (L1), which enables track finding at L1 for all tracks with a p_T of 2 GeV or above. To improve the “stub” finding efficiency

and also to reduce material, the inner three outer tracker barrel layers, the TBPS, are made with flat modules in the center and tilted modules in the regions with larger z .

ATLAS Upgrade

4.1.1.2 Calorimetry

Both the ATLAS and CMS calorimetry consist of electromagnetic calorimeters and hadronic calorimeters. Different materials and designs are used for the two experiments.

CMS Upgrade For the CMS detector, the scintillating crystals in its electromagnetic calorimeter (ECAL) barrel (EE) will be kept for duration of LHC. On the other hand, both frontend and backend electronics will be replaced(Ref. [218]), which allows for higher transfer rates and more precise timing. The target timing resolution for the upgraded ECAL electronics is ~ 30 ps for particles with $p_T > \sim 30$ GeV, which is the fundamental limit allowed by hardware and an order of magnitude smaller than the current limit. Current studies on the CMS hadronic calorimeter (HCAL) barrel radiation damage suggest there is no need for replacement at HL-LHC.

The CMS endcap calorimeter, including both the electromagnetic (EE) and the hadronic sections, will be replaced with a high granularity silicon-based calorimeter(HGCAL). The HGCAL, with fine granularity both lateral and longitudinal, enables 3D imaging in reconstructing energy clusters. The intrinsic high-precision timing capabilities of the silicon sensors will add an extra dimension to event reconstruction. The HGCAL is expected to provide timing resolution of few tens of ps for high energy particles with p_T of tens of GeV.

ATLAS Upgrade

4.1.1.3 Muon System

The muon system will be upgraded at both experiments to meet HL-LHC conditions, extend coverage, and improve detector performance and trigger capabilities.

CMS Upgrade For the CMS detector, its current muon system consists of three different types of muons detectors. In the barrel region, drift tubes (DTs) are installed as well as resistive plate chambers (RPCs). In the endcaps, there are cathode strip chambers (CSCs) together with RPCs. At the HL-LHC, the existing muon detectors will be improved with upgraded electronics to enable 40 MHz readout (Ref. [219]). New muon detectors, namely gas electron multipliers (GEMs) and a new version of RPCs, will be added to the endcaps, covering the regions of $1.6 < |\eta| < 2.4$. Additional muon chambers, labeled MEo, will cover the very forward regions

of $2.4 < |\eta| < 2.8$, a region also covered by the upgraded inner tracker. The additional muon detectors are essential to achieve a high trigger efficiency at acceptable rate, especially in the forward region. The additional hits in the new endcap muon stations, combined with improved algorithms, permit efficient triggering on displaced muon tracks even in the harsh environment of the HL-LHC.

ATLAS Upgrade

4.1.1.4 Timing Detector

Precision timing can be provided by the aforementioned calorimetry upgrades. However, the tens of ps timing resolution in the calorimeters is only achievable for particles with energy above tens of GeV, and the calorimetry upgrades alone won't provide efficient precision timing information for minimum ionizing particles (MIPs). Therefore, global event timing with the ability to reconstruct the vertex time and exploit time information in charged particle reconstruction requires a dedicated MIP Timing Detector (MTD).

CMS Upgrade For the CMS experiment, the MTD will comprise a barrel and an endcap region composing a single layer device between the tracker and calorimeters, and cover $|\eta|$ up to ~ 3 . In the barrel, the proposal is to adapt the present Tracker Support Tube (TST) design by instrumenting the current location of the thermal screen with a thin, actively cooled, standalone detector, based on lutetium-yttrium orthosilicate crystals activated with cerium (LYSO:Ce) readout with SiPMs. The endcap region can be instrumented with a hermetic, single layer of MIP-sensitive silicon devices with high time resolution, with a pseudorapidity acceptance from about $|\eta| = 1.6$ to $|\eta| = 2.9$. The MTD is designed to provide timing resolution of a few tens of ps for charged tracks throughout the detector lifetime. The performance projection in Sec. 4.1.3 is evaluated with a 30 ps resolution for a p_T threshold of 0.7 GeV in the barrel and a p threshold of 0.7 GeV in the endcap, and covering the expected MTD fiducial region of $|\eta| < 3$.

ATLAS Upgrade

4.1.1.5 Trigger

The ATLAS and CMS experiments adopt a two-level trigger system, the hardware-based Level-1 trigger (L1) and the software-based high-level trigger (HLT).

CMS Upgrade For the CMS experiment, its L1 trigger currently only uses calorimeter and muon information. At HL-LHC, with the aforementioned tracker upgrade of p_T modules and stub finding

capabilities, tracker information will be included at L1(Ref. [220]). The L1 track trigger uses pattern recognition on stub information to achieve track finding at an output rate of 750kHz. The L1 tracking capability will be further complimented by the calorimeter and muon upgrades which provide more precise position and momentum resolution, calorimeter shower shape, and number of tracker and muon hits. The L1 Global Trigger (GT) will be upgraded with more sophisticated and effective topologically-based global trigger calculations, plus an additional intermediate Correlator Trigger (CT) to fully exploit the increased information in the trigger objects, such as matching tracking info with fine grain calo info, or fitting muon and track data together. The upgraded etector readout and DAQ systems will allow $12.5\mu s$ latency and L1 rate of 750 kHz, the latter may be substantially reduced by adding L1 tracking information matched to improved L1 Calo and Muon trigger objects.

ATLAS Upgrade

4.1.2 Upgrade Performance: Physics Objects

Signatures from long-lived particles are difficult to detect at collider experiments when standard reconstruction algorithms are usually designed for prompt physics objects. The high density environment at HL-LHC makes LLP searches even more challenging. The detector's ability to measure basic information such as position, energy, and time precisely, and to reconstruct physics objects, defines its experimental reach for displaced searches. This section reviews the ATLAS and CMS experiments' projected object-level performance at the HL-LHC, highlighting improvements and new features with the upgrades.

4.1.2.1 Tracking and Vertexing

CMS Performance With the aforementioned tracker and L1 track trigger upgrades, the CMS experiment will be able to do track finding at L1 as well as offline at HL-LHC. Both L1 and offline tracking performance are shown here.

All L1 tracking studies have been performed assuming 3 GeV stub p_T thresholds. Figure 4.1 presents the L1 tracking efficiency for prompt muons and electrons for $t\bar{t}$ events in a scenario with 200 pileup events on average. The tracking efficiency for muons exhibits a sharp turn-on at the 3 GeV stub p_T threshold, and saturates at approximately 98%. The tracking efficiency for electrons turns on more slowly and flattens out at 90%, mostly due to interaction with the detector material and consistent with the corresponding measurements of the stub finding efficiency. Figure 4.2 show the L1 tracking resolutions of the pT and zo parameters of muons with $p_T > 10$ GeV in $t\bar{t}$ events for various average pileup scenarios. The resolutions are defined in terms of an interval centred on

the residual distribution that contains 68% or 90% of the tracks. Loss in tracking efficiency due to truncation effects (where there is insufficient time to transfer all the stub data) is determined from hardware and emulation to be a few parts per mille when processing $t\bar{t}$ + 200 pileup samples. As expected, resolutions degrade at forward pseudorapidity due to a corresponding increase in multiple scattering. In general, L1 parameter resolutions are excellent, which will provide for robust trigger object matching and charged particle reconstruction in the L1 trigger.

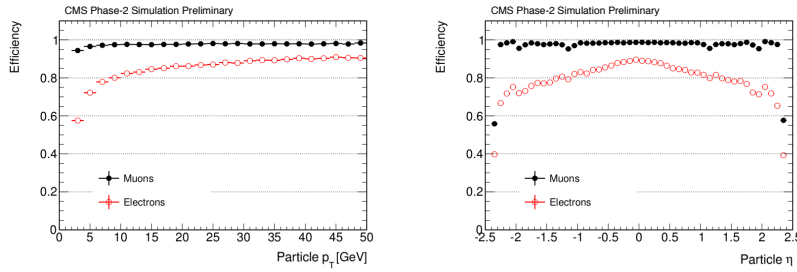


Figure 4.1: Left: L1 tracking efficiency versus generated particle p_T for $|\eta| < 2.4$. Right: L1 tracking efficiency versus η for $p_T > 3$ GeV. Results for muons (electrons) are shown as filled black (open red) circles, and are produced with $t\bar{t}$ events in a scenario with 200 pileup events on average.

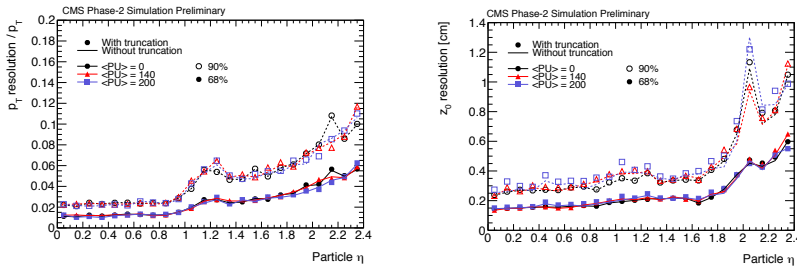


Figure 4.2: Relative p_T (left) and z_0 resolution versus pseudorapidity for muons in $t\bar{t}$ events with zero (black dots), 140 (red triangles), and 200 (blue squares) pileup events on average. Results are shown for scenarios in which truncation effects are (markers) or are not (lines) considered in the emulation of L1 track processing. The resolutions correspond to intervals in the track parameter distributions that encompass 68% (filled markers and solid lines) or 90% (open markers and dashed lines) of all tracks with $p_T > 3$ GeV.

Preliminary results on the offline tracking performance over the full acceptance of the CMS tracker are excellent with further improvements expected as the detector design and simulation algorithms are optimized. Figure 4.3 shows the resolution of the transverse momentum and the transverse impact parameter for single muons with $p_T = 10$ GeV as a function of the pseudorapidity both with the current detector and at the HL-LHC upgrade. The better hit resolution of the HL-LHC tracker and the reduction of the material budget result in a significantly improved p_T resolution. The transverse impact parameter resolution is also improved with respect to the current detector, ranging from below 10 mm in the central region to about 20 mm at the edge of the acceptance.

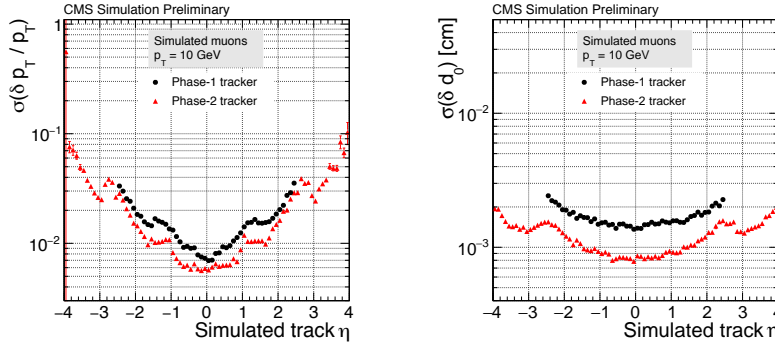


Figure 4.3: Relative resolution of the transverse momentum (left) and transverse impact parameter (right) as a function of the pseudorapidity for the current (black dots) and the upgraded (red triangles) CMS tracker, using single isolated muons with a transverse momentum of 10 GeV.

For $t\bar{t}$ events, the efficiency to identify the primary vertex correctly is $\sim 95\%$ with 140 pileup events, and $\sim 93\%$ with 200 pileup events. The vertex algorithm used is the same as the one used in Run 2 for a pileup of about 35, therefore it is not yet optimized for vertex reconstruction at very high pileup. Figure 4.4 shows the resolution of the vertex position in the x, y, and z coordinates as a function of the number of tracks associated to the vertex. The vertex position resolution is almost independent of the amount of pileup in the event and the longitudinal resolution is only 50% worse than the transverse one, as expected given the pixel dimensions of the inner tracker modules.

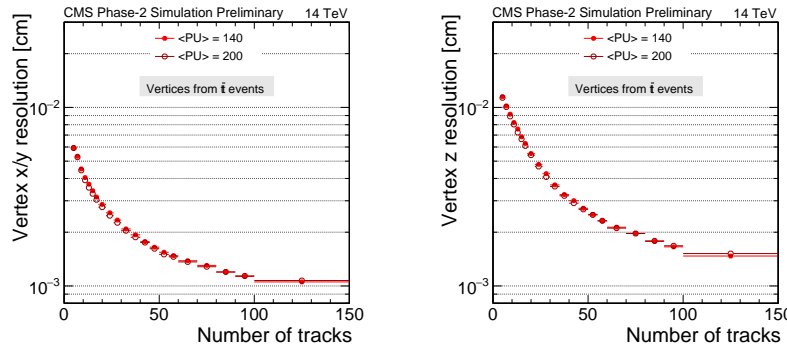


Figure 4.4: Vertex position resolution in x and y (left) and z (right) as a function of the number of tracks associated to the vertex, for $t\bar{t}$ events with 140 pileup events (full circles) and 200 pileup events (open circles).

Given that the CMS HLT tracking is based on the offline tracking code, a similar level of performance is expected. Because of HLT time constraints, a parallelization of the algorithms is already under development and will be applied also in the HLT track reconstruction at HL-LHC.

4.1.2.2 Leptons and Photon

CMS Performance At the L1 trigger level, the electron and photon trigger algorithms for HL-LHC will use information from the electromagnetic calorimeter as well as from the tracking detectors. The algorithm should preserve the ability to reconstruct electromagnetic clusters with p_T above a few GeV with high efficiency (95% or greater above 10 GeV) as well as achieve high spatial resolution which should be as close as possible to the offline reconstruction. Following the upgrade of both on-detector and off-detector electronics for the barrel calorimeters in HL-LHC, the EB will provide energy measurements with a granularity of (0.0174, 0.0174) in (η, ϕ) , as opposed to the current input to the L1 trigger consisting of trigger towers with a granularity of (0.087, 0.087). The much finer granularity and resulting improvement in position resolution of the electromagnetic trigger algorithms is critical in improving electron/ photon trigger efficiency and suppressing background at high pileup. Figure 4.5 shows the comparison between the L1 EG (e-gamma) trigger algorithm in current (black) based on trigger towers and the algorithm foreseen for HL-LHC (red), based on single crystal information.



Figure 4.5: CMS-TDR-017-002 Figure 9.19 Comparison between the Level-1 EG trigger algorithm in Phase-1 (black) and the algorithm foreseen for Phase-2 (grey), based on single crystal information. Left: position resolution, expressed in terms of DR with respect to the generated electron. Right: Level-1 EG trigger efficiency as a function of the transverse momentum of the generated electron. An electron gun sample, with flat p_T spectrum between 8 and 100 GeV and an average pileup level of 200, was used for both measurements.

The momentum resolution of the L1 muon trigger for muons coming from the primary vertex will be greatly improved by adding information from the L1 track trigger. The L1 track trigger can also be directly combined with trigger primitives at the first stage of the muon track finder electronics; this would mirror the offline reconstruction of “Tracker Muons” which improve the efficiency for very low p_T muons, especially in the barrel region.

Two classes of triggerable events from beyond-standard model physics require standalone muon trigger capabilities not covered by the Track Trigger system, namely for displaced muons and heavy stable charged particles (HSCP). To trigger on both prompt and

non-prompt muons effectively at L1, a standalone L1Muон generates two p_T measurements for each muon, prompt and non-prompt, which are matched with L1 tracks. If the track match is successful, the L1 track trigger p_T is used and a prompt candidate is formed. If the match is unsuccessful and the muon is not vetoed by L1 tracks, the non-prompt L1Mu p_T is used to form a displaced muon candidate. Figure 4.6 shows good performance for displaced muons with this method: reasonably high efficiency and a trigger rate for single muon trigger around 10 kHz at HL-LHC conditions. Further improvements to the algorithm are underway to accommodate high pile-up conditions. The upgrade of the RPC system will allow the trigger and identification of slowly moving particles by measuring their time of flight to each RPC station with a resolution of $O(1)$ ns. The speed of muon-like particles and the time (bunch crossing) of their origin will be computed with a fast algorithm to be implemented in the L1 trigger for HL-LHC. More details on the physics performance of displaced muon and HSCP searches are discussed in Section 4.1.3.

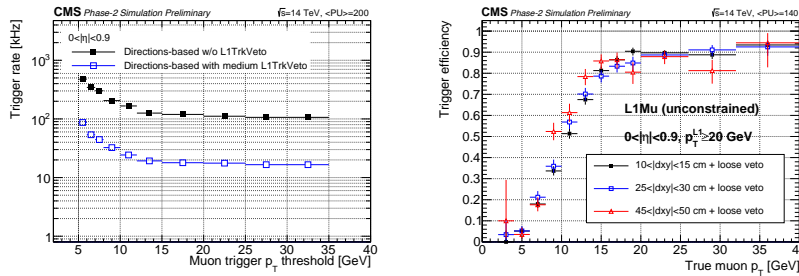


Figure 4.6: L1 Muon trigger rate (left) and efficiency (right) versus muon p_T threshold for the barrel displaced muon algorithm.

ATLAS Performance

4.1.2.3 Jets and Missing Energy

CMS Performance (TBA with HGCAL TDR approval)

ATLAS Performance

4.1.3 Upgrade Projection: LLP Searches

Searches for long-lived particles are well motivated by various classes of extensions of the Standard Model. Often, the cross section for such processes is expected to be very small. The HL-LHC will allow for the collection of much larger data sets needed to reach better sensitivity. The prospects are further strengthened with detector and trigger upgrades. This section discusses these potential improvements, and presents sensitivity projections on a number of benchmark LLP models with the aforementioned upgrades at HL-LHC.

4.1.3.1 Heavy Stable Charged Particles

A number of new physics scenarios give rise to heavy stable charged particles (HSCP) with long lifetimes that move slowly through the detector, heavily ionizing the sensor material as they pass through. In Split SUSY models, the supersymmetric particles stau ($\tilde{\tau}$) and gluino (\tilde{g}) can have such characteristic signatures.

Sensitivity projection with tracker upgrade Depending on their mass and charge of the new particles, HSCPs leave anomalously high energy loss through ionization (dE/dx) in the silicon sensors with respect to the typical energy loss for SM particles, as can be seen in Figure 4.7 (left). At the CMS experiment, the current strip tracker features analogue readout, and the pixel detector featured analogue readout at Phase-0 and features digital readout at Phase-1, allowing for excellent dE/dx measurements.

At the HL-LHC, the upgraded CMS inner pixel detector will continue providing dE/dx measurements, enabled by its Time over Threshold readout, while the Outer Tracker cannot provide such information, given that the readout is binary. To increase the sensitivity for signatures with anomalously high ionization loss, a second, programmable, threshold has been implemented in the Short Strip ASICs of the pixel-strip (PS) modules of the Outer Tracker, and a dedicated readout bit signals if a hit is above this second threshold.

Searches for HSCPs can thus be performed by measuring the energy loss in the inner pixel detector and by discriminating HSCPs from minimum ionizing particles based on the "HIP flag" in the Outer Tracker. The threshold of the minimum ionization needed to set the HIP flag is an adjustable parameter in the PS modules. A threshold corresponding to the charge per unit length of 1.4 MIPs, resulting from preliminary optimization studies, is used in the simulation, and the gain in sensitivity obtained by using the HIP flag is studied.

An estimator of the degree of compatibility of the track with the MIP hypothesis is defined to separate candidate HSCPs from tracks from SM background sources. The high resolution dE/dx measurements provided by the inner pixel modules are used for the computation of the dE/dx discriminator. The tracks in background events have a low number of high threshold clusters with HIP flag, compared to those observed for tracks in HSCP signal events and slow moving protons and kaons in minimum bias events.

Figure 4.7 (right) shows the performance of the discriminator by evaluating the signal versus background efficiency curves to identify tracks from signal events and reject those originating from backgrounds. The performance curves are evaluated for two different strategies for the discriminator: the dE/dx discriminator, which relies solely on the inner pixel modules (" dE/dx -only"), ignoring the HIP flags, and a recomputed discriminator which includes the HIP flags from the Outer Tracker PS modules (" $dE/dx+HIP$

flag"). The signal versus background efficiency performance curves demonstrate that for a background efficiency of 10^{-6} , analogous to the current analysis performance, the $dE/dx + \text{HIP}$ -based discriminator leads to an expected signal efficiency of 40%, around 4 to 8 times better than the dE/dx -only discriminator. In the dE/dx -only scenario, the efficiency for the HSCP signal is about 8 times smaller than that obtained in current data. The inclusion of the HIP flag for the PS modules of the Outer Tracker restores much of the efficiency, so that the same sensitivity as in Phase-1 will be realized with about four times the luminosity of Phase-1. The Phase-1 sensitivity will be surpassed with the full expected integrated luminosity of the HL-LHC. This study demonstrates the critical impact of the HIP flag in restoring the sensitivity of the CMS tracker for searches for highly ionizing particles.

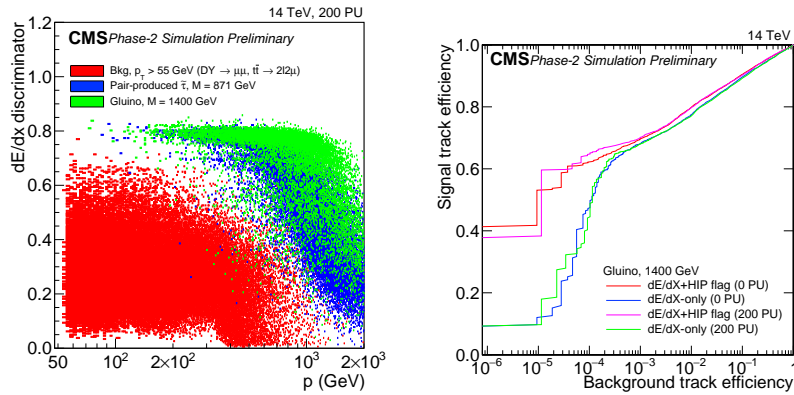


Figure 4.7: Left: distribution of the dE/dx discriminator versus track momentum (p_T) for tracks with high momentum ($p_T > 55$ GeV) in background events (red) and for candidate signal particles. Pair produced $\tilde{\tau}_s$ with a mass of 871 GeV (blue), and a gluino with a mass of 1400 GeV (green), are shown. Right: The performance of the dE/dx discriminator for selecting gluinos in events with 0 PU and 200 PU. The signal versus background efficiency performance curves for a discriminator making use of both the pixel information and the Outer Tracker HIP flag (red and magenta) demonstrate a better performance compared to a discriminator trained to exploit only the dE/dx information from the pixel modules (blue and green), for a background rejection of 10^{-6} .

HSCP trigger with muon upgrade The upgrade of the RPC system will allow the trigger and identification of slowly moving particles by measuring their time of flight to each RPC station with a resolution of $\mathcal{O}(1)$ ns. The speed of muon-like particles and the time (bunch crossing) of their origin will be computed with a fast algorithm to be implemented in the Level 1 trigger at HL-LHC.

The RPC detectors are synchronized to register muons moving at the speed of light with a local time equal to zero with respect to the collision event that produced the trigger. Slow-moving particles, as HSCPs, will arrive with a delay depending on their speed as shown in Fig 4.8. This time delay measured by each RPC layer crossed by the HSCP is exploited in order to trigger on and reconstruct such particles.

The principles of the proposed HSCP trigger algorithm are illus-

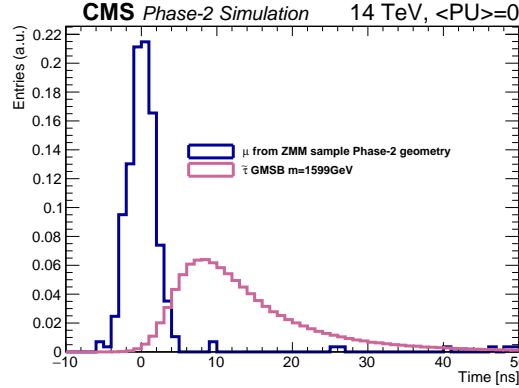


Figure 4.8: RPC hit time measurement distribution for muons from $Z \rightarrow \mu\mu$ events and for semi-stable $\tilde{\tau}$'s with $m \approx 1600$ GeV, produced in $pp \rightarrow \tilde{\tau}\tilde{\tau}$ processes.

trated in Fig 4.9. In this figure, the vertical axis is the time of signals in RPC chambers, as synchronized so that muons moving nearly at the speed of light from a particular collision are measured at the time of the collision. The horizontal axis is the distance from the collision point to the position of the RPC at which the time is measured. The diagram shows three successive bunch crossings, two of which contain muons represented at horizontal lines. The diagram also shows the RPC time measurements from two HSCPs having slopes different from zero due to their traveling significantly slower than the speed of light. The time delay Δt is related to the speed v of an HSCP via the following equation:

$$\Delta t = d \left(\frac{1}{v} - \frac{1}{c} \right), \quad (4.1)$$

where d is the distance between the IP and the point where an HSCP crosses an RPC. For RE4/1 chambers and $\beta = v/c = 0.2$, the delay time is > 6 BXs = 150 ns.

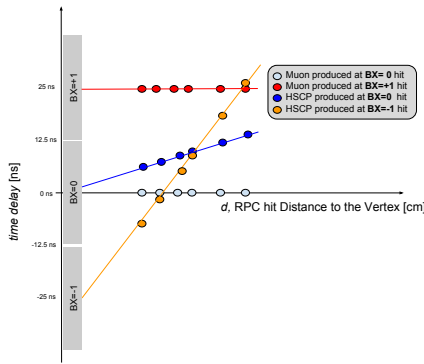


Figure 4.9: Diagram showing times measured at different RPC stations for particles originating at different BXs with different velocities. The x-axis represents the distances from IP to RPC detectors, while y-axis corresponds to time. Clock at all RPC stations is tuned so that particles moving with the speed of light are registered with the exact same “local” times. Hence, relativistic particles are represented by horizontal lines on this diagram.

A penetrating charge particle leaves a trail of hits in RPC chambers along its trajectory. The time of flight can be computed in each

RPC station with respect to a number of BX hypotheses. Should there be a common velocity solution, derived from Eq. (4.1), with $\beta < 0.6$, a trigger is formed. For $\beta > 0.6$, the delays are small and can be handled by the Phase-1 trigger. The performance of this algorithm has been studied in CMS full simulation. All the detector effects (electronics jitter, signal time propagation along strips) are taken into account. A particle speed measurement resolution is shown in Fig. 4.10 (right) for the case of 25 ns signal sampling time (Phase-1) and 1.56 ns sampling time provided with the upgraded RPC Link Board System.

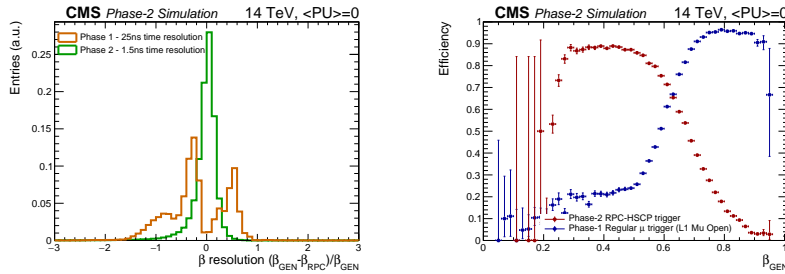


Figure 4.10: (Left) Resolution of a particle speed measurement at L1 trigger level with Phase-1 and upgraded RPC Link Board System. (Right) The efficiency as a function of β of the standard L1 muon trigger without any p_T threshold, and the RPC-HSCP Phase-2 trigger with 1.56 ns sampling time.

The efficiency of the RPC-HSCP algorithm as a function of β is studied and compared with the standard L1 muon trigger. The results are shown in Fig. 4.10 (right). The current CMS-HSCP Phase-1 trigger performs well down to $\beta \approx 0.75$. The upgraded RPC Link Board System will allow us to trigger, at the correct BX, HSCPs with velocities as low as $\beta \sim 0.25$.

Possible improvements for this trigger proposal in the β measurement could be achieved by matching the Tracker Track trigger to the HSCP muon trigger. The uncertainty coming from the propagation time along RPC strips can be reduced if the hit position is known along the local y coordinate, or the global η . This correction is not needed for the iRPCs thanks to the two-end strip readout for these new detectors.

4.1.3.2 Displaced Muons

Many BSM theories predict particle decays with displaced muon or muon pairs in its final state, such as dark SUSY and GMSB with smuons. These displaced muons usually have higher p_T and have been the focus of existing LLP searches. Their prospects at HL-LHC are discussed here. For models such as inelastic dark matter or dark showers that predict soft displaced muons in their final states, the reconstruction is more challenging and is discussed in Section 4.1.4.

Trigger and reconstruction Tracks from displaced muons have different properties depending on how much the muons are boosted. In case of a sufficiently boosted muon, the corresponding track

is roughly pointing back to the primary interaction leading to a transverse impact parameter which is small(er) but the decay may still occur at the outer edge of the tracker or even well outside the tracker volume. If the muon is not highly boosted, the corresponding track is not pointing back to the primary interaction vertex and we might even get a large impact parameter for a decay not far away from the primary interaction. For long-lived particles of a few hundred GeV mass, impact parameter ($|d_0|$) can reach up to approximately one meter (or longer) for sufficiently large lifetimes as shown in Fig. 4.11 (left).

Standard triggers and reconstruction algorithms that use the position of the primary vertex will not be very efficient in reconstructing tracks with large impact parameters. Consequently, to trigger on and reconstruct muons produced far away from the interaction vertex is challenging and requires dedicated trigger paths and reconstruction algorithms. As discussed in Section 4.1.2, Fig. 4.6 shows exemplarily the reconstruction capabilities of displaced muons on trigger level for the CMS detector at HL-LHC. In the meantime, a dedicated muon reconstruction algorithm was designed for non prompt muons that leave hits only in the muon system. This displaced stand-alone (DSA) algorithm is seeded by groups of track segments in the muon chambers. For each seed, a muon track is reconstructed with the same Kalman-filter technique as for the standard stand-alone (SA) muon reconstruction algorithm, but without constraining the interaction point. Figure 4.11 (right) shows the distribution of the number of hits in the Run 2 and HL-LHC detectors for displaced muons. The impact of the new stations is clearly visible. The charge misidentification probability is expected to further decrease with the additional hits.

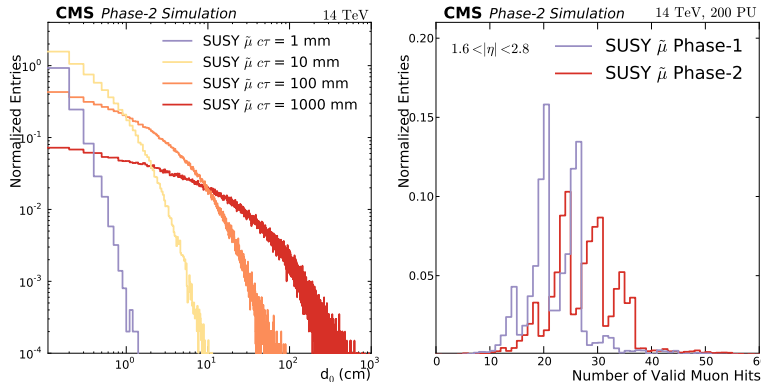


Figure 4.11: Left: The transverse imparameter, d_0 , for several simulated decay lengths, $c\tau$, before reconstruction. Right: Distribution of the minimum number of valid hits in the muon system for a SUSY $\tilde{\mu}$ ($M = 500 \text{ GeV}$ and $\tau = 1000 \text{ mm}$) for Run 2 (blue) and Phase-2 (red) detectors.

Sensitivity Projection To study the impact on physics sensitivity, a particular gauge-mediated SUSY breaking (GMSB) model is selected where the displaced signature consists of a dimuon final state plus gravitinos, which are escaping detection, emerging from

the decay of heavy sparticles (smuons). This signal serves as a proxy for any long-lived particle. The final state signature is then given by two displaced oppositely charged muons and significant missing transverse energy which can be characterized by a very clean final-state topology. Exemplarily long-lived particles with $c\tau = 10, 100, 1000$ mm and with several mass hypotheses (0.2, 0.5, 1 TeV).

The main background for this search comes from multi-jet production (QCD), $t\bar{t}$ production, and $Z/DY \rightarrow \ell\ell$ events where large impact parameters are (mis)reconstructed. Cosmic ray muons have been studied in Run 2 and are independent of the instantaneous luminosity. In the barrel they are efficiently rejected by the timing of the hits in the upper leg. Cosmic ray muons do not originate at the vertex and therefore pass the upper barrel sectors in reverse direction from outside in. The fraction of cosmic ray muons in the endcaps is negligible. Given the very low cross section of this process, it is essential to reduce the background efficiently. The best background discriminator is the impact parameter significance $d_0/\sigma(d_0) \geq 5$. Given the signal kinematics, the muons should move in roughly opposite directions and MET should be larger than 50 GeV. After this selection the signal efficiency is about 4–5% for $c\tau = 1000$ mm, nearly independent of the smuon mass, and $10^{-5} - 10^{-4}$ for QCD, $t\bar{t}$, and DY backgrounds.

Figure 4.12 shows expected exclusion limits for the GMSB model with the smuon being a (co-)NLSP for the predicted cross section as well as for a factor 100 larger cross section. The exclusion limits are shown as functions of smuon mass in Fig. 4.12 (left) and decay length in Fig. 4.12 (right).

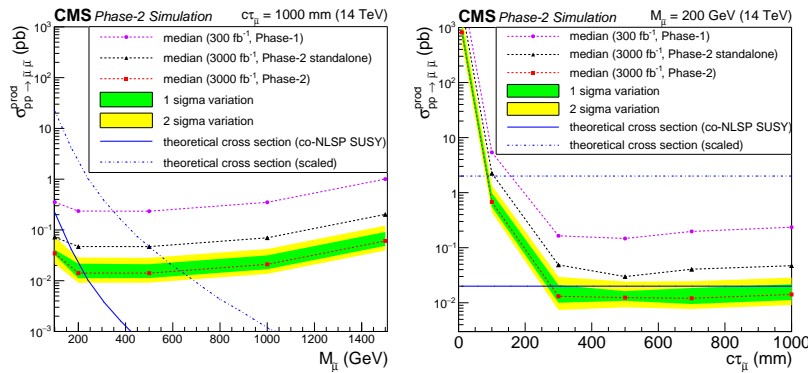


Figure 4.12: The 95% CL upper limits on $q\bar{q} \rightarrow \tilde{\mu}\tilde{\mu}$ for various mass hypotheses and $c\tau = 1$ m (left) and as a function of the decay length for $M = 200$ GeV (right). In both panels, the theoretical cross section for the specific model is represented by the blue solid line. For different SUSY breaking scales, $\tan\beta$ or otherwise modified parameters, the cross sections may be 100 times larger, reflected by the blue dash-dotted line. Green (yellow) shaded bands show the one (two) sigma range of variation of the expected 95% CL limits. Phase-2 results with an average 200 pileup events and an integrated luminosity of 3000 fb^{-1} are compared to results obtained with 300 fb^{-1} . The black line shows the sensitivity without the DSA algorithm, which reduces the reconstruction efficiency by a factor three.

The sensitivity depends on $c\tau$ because shorter decay lengths shift the signal closer to background. Figure 4.11 (right) shows the re-

sulting physics sensitivities in terms of production cross section for HL-LHC, normalized to 3000 fb^{-1} , for the dedicated reconstruction of displaced muons and for the standard reconstruction. Also shown is the expected sensitivity at the end of Phase-1. Systematic uncertainties for the Phase-1 scenario are taken from current Run 2 analyses: for HL-LHC they are guided by the assumptions of reduced systematics from Ref. [221]. Clearly, only the HL-LHC will allow this process to be studied. The expected exclusion limit is around 200 GeV for $c\tau = 1000 \text{ mm}$ with 3000 fb^{-1} . This also illustrates the importance of keeping lepton trigger thresholds at a few times 10 GeV, even in the environment of 200 pileup interactions.

In order to evaluate the discovery sensitivity of a search for the GMSB model the same input is used as in the limit calculation, now with the assumption that one would have such a signal in the data. The discovery sensitivity is shown as a function of smuon mass in Fig. 4.13 (left) and decay length in Fig. 4.13(right). The dependencies on those signal parameters are similar to the limit calculation. Analogous to the limit calculation, also the sensitivities are shown for the end of HL-LHC, normalized to 3000 fb^{-1} , for the dedicated reconstruction of displaced muons and for the standard reconstruction. Also shown is the expected sensitivity at the end of Phase-1. One can conclude that only the HL-LHC is sensitive to the discovery of a long-lived particle such as the smuon with a mass higher than 200 GeV. Another observation is the difference in discovery sensitivity for standard standalone reconstruction and dedicated displaced standalone reconstruction ranging from 1σ to 4σ .

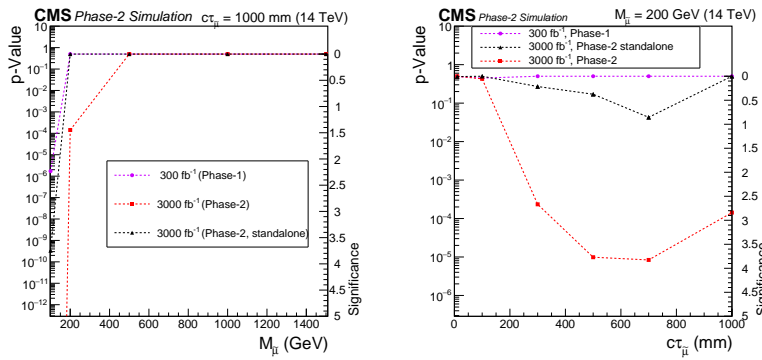


Figure 4.13: The discovery sensitivity on $q\bar{q} \rightarrow \tilde{\mu}\tilde{\mu}$ for various mass hypotheses and $c\tau = 1 \text{ m}$ (left) and as a function of the decay length for $M = 200 \text{ GeV}$ (right). Together with the discovery sensitivity the corresponding p-Value is shown. Phase-2 results with an average 200 pileup events and an integrated luminosity of 3000 fb^{-1} are compared to results obtained with 300 fb^{-1} . The black line shows the sensitivity without the DSA algorithm, which reduces the reconstruction efficiency by a factor three. NOT APPROVED!!!

4.1.3.3 Displaced Photons

A number of new physics scenarios suggest models with displaced photons in the final state. At the CMS experiment, with the scintillating crystal design of the ECAL that provides excellent resolution

but lacks pointing function, the photon arrival time in ECAL is the main observable used to distinguish signal from background in displaced photon searches.

One benchmark model for displaced photon search at collider is the GMSB model where the lightest neutralino ($\tilde{\chi}_0^1$) is the next-to-lightest supersymmetric particle, can be long-lived and decays to a photon and a gravitino (\tilde{G}), which is the LSP, as illustrated in Figure 4.14 (left). For a long-lived neutralino, the photon from the $\tilde{\chi}_0^1 \rightarrow \tilde{G} + \gamma$ decay is produced at the $\tilde{\chi}_0^1$ decay vertex, at some distance from the beam line, and reaches the detector at a later time than the prompt, relativistic particles produced at the interaction point. The time of arrival of the photon at the detector can be used to discriminate the signal from the background. The aforementioned upgrade to ECAL electronics in the barrel region, and the HGCAL upgrade in the endcaps, will improve photon timing resolution at HL-LHC by an order of magnitude to as little as ~ 30 ps for photons with p_T of tens of GeV or above, hence significantly improve the experimental reach of displaced photon searches.

Moreover, the proposed MIP Timing Detector (MTD) will be able to provide another dimension of information to reconstruct LLP decays. The time of flight of the photon inside the detector is the sum of the time of flight of the neutralino before its decay and the time of flight of the photon itself, until it reaches the detector. Since the neutralino is a massive particle the latter is clearly negligible with respect to the former. In order to be sensitive to short neutralino lifetimes of order 1 cm, the performance of the measurement of the photon time of flight is a crucial ingredient of the analysis. Therefore, the excellent resolution of the MTD apparatus can be exploited to determine with high accuracy the time of flight of the neutralino, and similarly the photon, also in case of a short lifetime.

An analysis has been performed at generator level in order to evaluate the sensitivity power of a search for displaced photons at CMS in the scenario where a 30 ps timing resolution is available from the MTD. The events were generated with Pythia8, exploring neutralino lifetimes ($c\tau$) explored in the range 0.1–300 cm. The values of the Λ scale parameter were considered in the range 100–500 TeV, which is relevant for this model to be consistent with the observation of a 125 GeV Higgs boson. After requiring the neutralino decaying within the CMS ECAL acceptance and the photon energy being above a “trigger-like” threshold, the generator-level photon time of flight was smeared according to the expected experimental resolutions. A cut off at a photon time greater than 3 s of the time resolution is applied and the “signal region” is assumed to be background free. The signal efficiency of such a requirement is computed and translated, assuming the theoretical cross sections provided in Ref [ref:GMSB], to an upper limit at 95

Figure 4.14(right) shows the analysis sensitivity in terms of the L scale (and therefore of the neutralino mass) and lifetime for three different assumptions on the timing resolution. The 300 ps resolu-

tion is representative of the time-of-flight resolution (TOF) for these events with current CMS detector performance]. The 180 ps resolution is representative of the TOF resolution of the upgraded CMS detector without the MTD, in which the TOF measurement will be dominated by the time spread of the luminous region. The vertex timing provided by the MTD detector will bring the TOF resolution to about 30 ps. As visible in the figure, a full scope upgrade of the CMS detector with photon and track timing will provide a dramatic increase in sensitivity at short lifetimes and high masses, already after the first 300fb^{-1} of integrated luminosity.

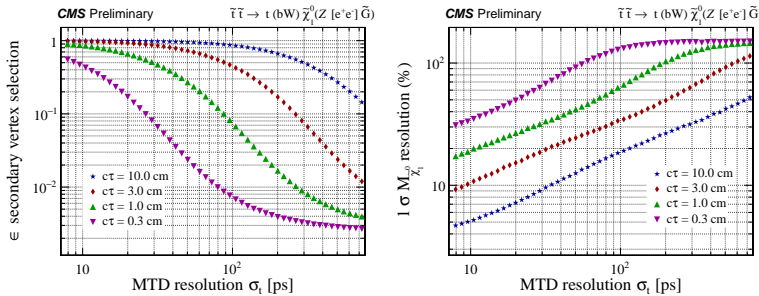


Figure 4.14: Left: Diagrams for a SUSY process that results in a diphoton final state through gluino production at the LHC. Right: Sensitivity to GMSB $\tilde{\chi}_0^1 \rightarrow \tilde{G} + \gamma$ signals expressed in terms of neutralino lifetimes for 300, 180 and 30 ps resolution, corresponding to the current detector, the HL-LHC detector with photon timing without MTD and with MTD, respectively.

4.1.3.4 LLP searches with precision timing

The MTD provides new, powerful information in searches for long-lived particles. A precision MIP timing detector allows one to assign timing for each reconstructed vertex and to measure the time of flight of LLPs between primary and secondary vertices. Using the measured displacement between primary and secondary vertices in space and time, the velocity of an LLP in the laboratory frame, $\vec{\beta}_{LAB}^p$ (and γ^p), can be measured. In such scenarios, the LLP can decay to fully-visible or partially-invisible systems. Using the measured energy and momentum of the visible portion of the decay, one can calculate its energy in the LLP rest frame and reconstruct the mass of the LLP, assuming that the mass of the invisible system is known.

In addition to the aforementioned GMSB displaced photon model, the benefits of precision timing with the MTD can be further demonstrated in SUSY scenarios where the LLP decay produces a Z boson, which then decays to an electron-positron pair. For example, in the GMSB scenario where the $\tilde{\chi}_0^1$ couples to the gravitino \tilde{G} via higher-dimension operators sensitive to the SUSY breaking scale, the $\tilde{\chi}_0^1$ may have a long lifetime. It is produced in top-squark pair production with $\tilde{t} \rightarrow t + \tilde{\chi}_0^1$, $\tilde{\chi}_0^1 \rightarrow Z + \tilde{G}$, $Z \rightarrow ee$.

Studies are performed to estimate the sensitivity of the search with the MTD. The events were generated with Pythia8. The masses of the top-squark and neutralino were set to 1000 GeV

and 700 GeV, respectively. Generator-level quantities were smeared according to the expected experimental resolutions. A position resolution of 12 mm in each of the three spatial directions was assumed for the primary vertex. The secondary vertex position for the electron-positron pair was reconstructed assuming 30 mm track resolution in the transverse direction. The momentum resolution for electrons was assumed to be 2%. And finally, the time resolution of charged tracks at the displaced vertex were assumed to be 30 ps.

The mass of the LLP was reconstructed assuming that the gravitino is massless. The fraction of events with separation between primary and secondary vertices exceeding 3s in both space and time as a function of the MTD resolution is shown in Figure 4.15 (left). The mass resolution, defined as half of the shortest mass interval that contains 68% of events with 3s displacement is shown in Figure 4.15(right), as a function of the MTD resolution.

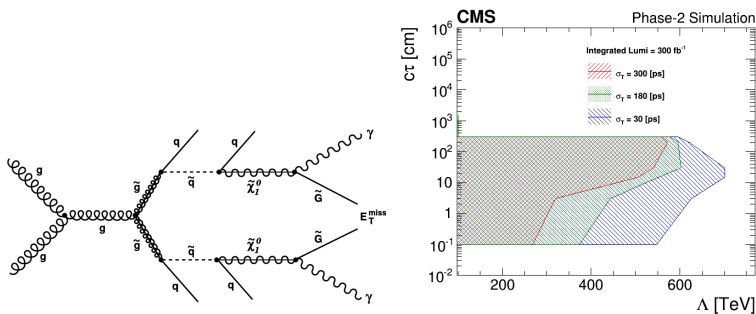


Figure 4.15: Efficiency (left) and mass resolution (right) as a function of the timing resolution of the MTD for reconstruction of the $\tilde{\chi}_0^1$ mass in the SUSY GMSB example of $\tilde{\chi}_0^1 \rightarrow \tilde{G} e^+ e^-$, with mass of $\tilde{\chi}_0^1 = 700$ GeV, considering events with a separation of primary and secondary vertices by more than 3s in both space and time.

A similar study is done with another SUSY scenario where the two lightest neutralinos and light chargino are higgsino-like. The light charginos and neutralinos are nearly mass degenerate and may become long-lived as a consequence of the heavy higgsinos. In both studies, the additional timing information from the MTD facilitates the reconstruction of the LLP mass, the resolution and efficiency of which are further improved with the excellent timing resolution of the MTD.

4.1.3.5 LLP searches with track trigger

As discussed in Section 4.1.1, a central feature of the CMS upgrade at HL-LHC is a new silicon outer tracker which allows track reconstruction for every LHC bunch crossing (40 MHz). The p_T selection for stubs (hit pairs in the p_T modules of the outer tracker) to be read out is determined by the bandwidth from the detector to the back end electronics, and is fixed at about 2 GeV. On the other hand, the choice of track finding algorithm and hardware is still being finalized, and there could be significant benefits to extend the L1 track trigger ability to off-pointing tracks.

To illustrate the case, a simple toy simulation (Ref. [222]) to study

rare Higgs decays into new particles with lifetime of order of a few mm is performed. This study considers all-hadronic final states with low H_T , taking SM Higgs decays into four jets as an example. Theoretical motivation to look for such decays is very strong, The goal is to probe very small branching fractions; in this note we assume $Br[h \rightarrow \phi\phi \rightarrow 4q] = 10^{-5}$. For prompt decays, the background is overwhelming, but if the ϕ has $c\tau$ of a few mm, the offline analysis has very low backgrounds. The problem is in getting such events on tape, in particular through L1. This toy study estimates how an off-pointing track reconstruction at L1 can help. To estimate the efficacy of the approach, the result projections are compared with the best alternatives in absence of off-pointing track trigger: using associated Higgs production with a W that provides a lepton trigger or considering L1 calorimeter jets with no associated prompt tracks.

This study is simulated with a toy tracker, which has six perfectly cylindrical double layers [**geom**] covering $|\eta| < 2.4$. For each layer, the allowed offset between the two measurements is below the one expected from 2 GeV prompt tracks. The sketch in Figure 4.16 (left) shows four tracks traversing a double layer: positively and negatively charged prompt 2 GeV tracks, and two off-pointing tracks. Dashed track would make a L1 trigger stub, and the dotted one would not.

Two extensions of track finder are considered. *Loose* tracks are only required to have a minimal number of stubs. *Tight* tracks are obtained by fitting the stubs they produced to a circle constrained to the beam line. The number of stubs on a tight track is the number of stubs deviating from that circular fit by less than 3 strips (300 microns). Tight tracks is a generous approximation for an algorithm that assumes prompt production when building a track and allows for non-zero impact parameter for track fit. For loose tracks, both track building and fitting assumes non-zero impact parameter. We only consider the transverse plane of the track finding since that's the plane in which the displacement is measured more precisely. We assume that the hits on a track are also linked in the rz , but do not rely on it for calculation of displacement.

The $h \rightarrow \phi\phi \rightarrow 4q$ events were generated using PYTHIA. Mass of ϕ is taken to be 30 GeV, and $Br[h \rightarrow \phi\phi \rightarrow 4q] = 10^{-5}$. A range of ϕ lifetimes is considered, from 1 mm to 5 m. Proper decay time was randomly generated for each ϕ and dilated according to its speed.

Figure 4.16 (right) shows the expected event yields for different triggers described above. Jet reconstruction parameters were slightly varied to make sure there are no large variations in efficiency. For track jets, one (solid lines) or two (dashed lines) tracks with five or more hits were required. For trackless jets, one track (solid line) or two tracks with total p_T below 10 GeV were allowed to point along the jet.

While the tight tracks offer substantial increase in sensitivity compared to Wh , trigger based on loose tracks yields more than

a factor of 5 more signal for $c\tau$ of a few mm. No-track jets, even with very optimistic 70 GeV threshold only become competitive at lifetimes of 50cm or more.

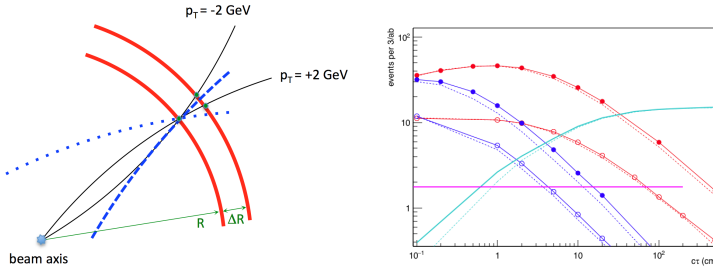


Figure 4.16: Left: Sketch of the toy stub formation in a doublet layer. Four tracks are passing through the same point in the inner layer. Only the tracks hitting the outer layer between the two green points would produce a L1 stub. The dashed track does, and the dotted does not. Right: Event yields for $\text{Br}[h \rightarrow \phi\phi \rightarrow 4q] = 10^{-5}$ as a function of ϕ proper lifetime. Red curves correspond to quad loose track jet trigger, blue - to quad tight track jet trigger. Open circles indicate track jets with p_T above 20 GeV, filled circles - displaced track jets above 10 GeV. Teal curve corresponds to the no-track 70 GeV di-jet trigger. Purple line shows the expected yield from Wh production triggered by a lepton from W .

The rare SM Higgs decays considered above is challenging, because of the small total H_T in the event. While Higgs-like signals may be accessible in associated production, some new physics signals may not, such as dark matter models where the mass splitting between chi_1 and chi_2 is small. Those will benefit a lot from the displaced track trigger.

4.1.4 New Ideas for Future Studies

TBA: coordinate with ATLAS & theory

4.1.4.1 New studies for HL-LHC

inelastic dark matter with displaced muon pairs: L1 track trigger; MTD

inelastic dark matter with displaced photons: ECAL/HGCAL
dark shower: L1 track trigger, MTD(?)

4.1.4.2 New detectors at future collider

4D pixel detector with timing

D.Curtin's crazy tracker idea: new tracking layer very close to beamline?

4.2 LHCb Upgrade

4.2.1 Introduction

The LHCb experiment is designed to detect the decay of long-lived particles: beauty and charmed mesons. As so, it is naturally suited for the search of BSM long-lived particles in a range of mass and

lifetime not too dissimilar. It is the only LHC experiment to be fully instrumented in the forward region $2 < \eta < 5$, where B and D decays are abundant and their decay length is enhanced thanks to the boost. In this region, detector occupancy is extremely high and therefore during LHC Run 1 and Run 2, the experiment has been run at reduced luminosity compared to ATLAS and CMS. However, an upgrade of the detector is foreseen to run at a five times larger luminosity ($2 \times 10^{33} \text{ cm}^{-2} \text{s}^{-1}$) in LHC Run 3 (starting in 2021) while maintaining or improving the current physics performance. This first upgrade phase (Phase-I) will entail a novel trigger paradigm where all sub-detectors are fast enough to be read out in real time and the first trigger level is done in software. This trigger scheme is extremely flexible and offers a great opportunity for searches of striking signatures like those of BSM long-lived particles. This upgrade comes earlier than the ATLAS and CMS upgrades planned for the HL-LHC phase (starting in 2026) and will be followed by a Phase-II upgrade (planned for 2031) to run at an even more challenging luminosity of $\sim 2 \times 10^{34} \text{ cm}^{-2} \text{s}^{-1}$.

Section 4.2.2 gives a brief overview of the (Phase I) upgraded-LHCb detector-design and the expected performance of sub-detectors. An overview of its capabilities in the context of LLP searches is given in Section 4.2.3 with a few example signatures. Finally, an overlook of the plans for the Phase-II upgrade and some thoughts on the opportunities given by putative additional detector features are reported in Section 4.2.4.

4.2.2 *LHCb detector and trigger upgrade for Run 3 (Phase I)*

In LHC Run 3, LHCb plans to take data at an instantaneous luminosity of $2 \times 10^{33} \text{ cm}^{-2} \text{s}^{-1}$, a factor five higher compared to the current one. The LHCb detector needs to be upgraded to cope with the higher radiation dose and most importantly to avoid the saturation of the trigger rate and exploit the higher luminosity. The main bottleneck in the current trigger is in the first stage, which reduces the accepted rate from 30 to 1 MHz directly at hardware level. For the upgrade, the hardware trigger will be removed and the full event will be read out at the bunch crossing rate of the LHC (40 MHz), with a very flexible software-based trigger.

	Current Conditions	Phase-I Conditions	Phase-II Conditions
\mathcal{L}	$4 \times 10^{32} \text{ cm}^{-2} \text{s}^{-1}$	$2 \times 10^{33} \text{ cm}^{-2} \text{s}^{-1}$	$2 \times 10^{34} \text{ cm}^{-2} \text{s}^{-1}$
$\int \mathcal{L}$	8 fb^{-1} by 2019	50 fb^{-1} by 2030	300 fb^{-1} by 203x
\sqrt{s}	13 TeV	14 TeV	14 TeV
μ	1.1	5.5	50

Table 4.1: LHCb current and upgraded operating conditions. Instantaneous luminosity \mathcal{L} , integrated luminosity $\int \mathcal{L}$, pp collision energy \sqrt{s} and average number of visible interactions μ are listed.

Table 4.1 summarises the current and upgraded conditions of the detector. To cope with the larger occupancy and higher rate of the upgraded detector, the electronics of all the sub-detectors have

to be upgraded and some sub-detectors fully replaced. This is the case for the whole tracking system which plays a crucial role in LLP searches.

The upgraded tracking system consists of the VErtex LOcator (VELO), surrounding the interaction point, the Upstream Tracker (UT), a tracking station placed before the magnet, and the Scintillating Fibers tracker (SciFi), three stations after the magnet. In the VELO [223], the current strips will be replaced by pixel detectors, with a custom developed ASIC (VeloPix) able to withstand a maximum hit rate of 900 Mhits/s/ASIC. The UT [224] is composed of four silicon micro-strip planes, with finer granularity and larger acceptance compared to the current tracker. Each station of the SciFi has four planes of 2.5 m long scintillating fibres read out by silicon photo-multipliers.

The upgrade components most important for LLP searches are probably the VELO, the tracking and the software trigger. In the following subsections a brief description of their design and capabilities is given.

4.2.2.1 Upgrade VELO

The VELO plays a fundamental role in LLP searches at LHCb: together with the large boost particles usually get in the forward direction, a very precise measurement of the LLP vertex position allows LHCb to access very low lifetimes that are often not accessible at ATLAS and CMS.

In upgrade conditions, the number of tracks and primary vertices will increase by about a factor five, making it much more difficult to identify displaced vertices close to the beam-line, left alone to do it in real time. The VELO was thus completely redesigned to cope with the new conditions, maintain high physics performance and allow real time readout for the software trigger. The new VELO has a pixel rather than strip geometry and its distance from the LHC beams is reduced from 8 to 5 mm. This allows to improve the vertex resolution (4.17) and to reduce the rate of unphysical (ghost) tracks.

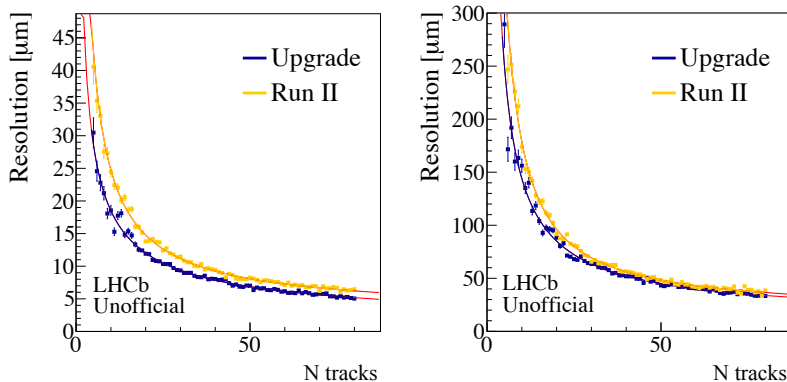


Figure 4.17: Resolution of the primary vertex as a function of number of tracks in the x (left) and z (right) direction. The same kind of improvement is also expected for secondary vertices (SV).

The pattern recognition efficiency is superior to the one of the current VELO evaluated in upgraded conditions. This can be seen for different observables. Particularly important for LLP searches is the efficiency as a function of the distance from the origin in z : for the upgraded VELO, the efficiency approaches 100% and is uniform in a window of 20 cm around the interaction point, thanks to the new configuration of the modules in the z direction and the shorter distance from the beam. After 20 cm in z the VELO acceptance degrades pretty fast, making that the upper limit for LLP decay lengths with vertices reconstructible in the VELO. A display of the upgrade VELO geometry and its acceptance in both forward and backward direction is given in Figure 4.19

Another important figure to evaluate the performance of the detector is the IP resolution, especially in LLP searches where it can be exploited to reduce the background due to fake tracks. With the upgrade the IP resolution significantly improves for low p_T tracks. For example, the IP resolution along x for tracks with p_T of $0.5 \text{ GeV}/c$ is $40 \mu\text{m}$ in the upgrade versus $70 \mu\text{m}$ in the current VELO. The replacement of strips with pixel sensors also makes the pattern recognition faster for the same multiplicity. This can be used in the trigger to find tracks and identify displaced vertices in the trigger, making it possible to soften or remove inefficient p_T requirements.

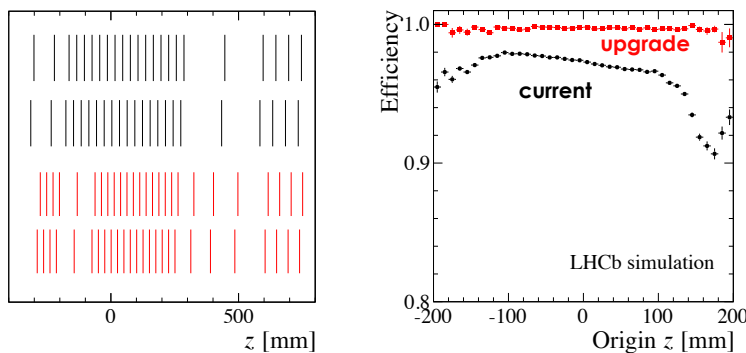


Figure 4.18: A comparison of the current and upgrade VELO z -layouts is shown on the left. The top layout (black) is the current VELO while the bottom layout (red) is the upgrade VELO. On the right the track reconstruction efficiency is shown as a function of the origin in z for the current (black) and upgrade (black) VELO in upgrade conditions.

Real tracks created in the VELO material can be a significant background to LLP searches (see more details in Appendix ??). The total material budget of the upgrade VELO is similar to the current one (about 20% radiation lengths) and is dominated by the Radio-Frequency foil separating the beam vacuum from the vacuum of the sensors. However, the average percentage of radiation length before the first measured point is significantly reduced in the upgrade VELO, passing from $4.6\%X_0$ in the current design to $1.7\%X_0$ in the upgrade VELO.

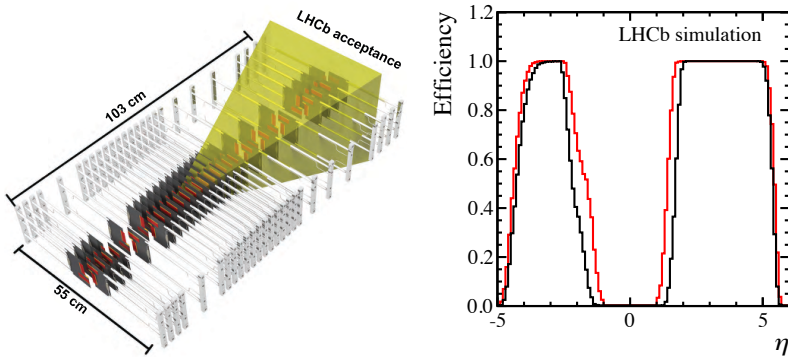


Figure 4.19: On the left is a display of the upgrade VELO geometry and a comparison with the LHCb spectrometer acceptance which is shaded in yellow. On the right the η acceptance of the upgrade VELO geometry is given both for forward and backward tracks. The fraction of tracks crossing three and four modules is given in red and black, respectively.

4.2.2.2 Upgraded trigger

The online event selection in the LHCb experiment during the 2010–2018 running period is performed by a trigger composed of a hardware level (Lo), and two software levels, High Level Trigger 1 (HLT1) and the High Level Trigger 2 (HLT2). The Lo reduces the rate from 30 MHz to 1 MHz, using information from the calorimeter and muon systems. Typical thresholds at the Lo are $p_T > 1.4 \text{ GeV}/c$ for muons and $E > 2.5 \text{ GeV}$ for electrons. The software trigger performs a partial event reconstruction at HLT1, reconstructing tracks and primary vertexes for any particle down to $p_T = 500 \text{ MeV}/c$, followed by complete event reconstruction at HLT2, reducing further the rate to 12.5 kHz (in Run 2).

Given the higher instantaneous luminosity foreseen after the Phase 1 upgrade, a new trigger system, able to fully exploit the LHC potentiality, has been designed.

The upgraded LHCb trigger consists of two paradigms, a triggerless readout and full software trigger. In addition, as already tested in Run 2, a real-time alignment and calibration will allow to achieve offline-quality reconstruction level already in the trigger and a higher signal purity of interesting decay channels. Figure 4.26 shows the current and the upgrade trigger scheme.

Triggerless readout and full software trigger With the LHCb trigger upgrade the 1 MHz readout limitation will be removed, allowing the full event rate to be processed in software. This will increase the efficiency for several final states which, already in Run 2, cannot benefit from the higher luminosity because of the Lo bottleneck. Figure 4.21 shows the saturation for not muonic final state with increasing luminosity. Moreover, a purely software trigger will not necessitate the tight p_T requirements currently applied at the hardware trigger level. Thanks to this, several physics program involving low- p_T particle, currently prevented because of the low Lo efficiency, will be possible.

Turbo stream Starting from Run 2, offline-quality alignment and calibration is applied between the HLT1 and the Hlt2 level. This made possible the design of a new dedicated trigger output, called Turbo Stream. The event record is written directly from the trigger and processed by the Tesla application [165]. Its output can be directly used for physics analysis, without the need of offline reconstruction. Several variation to Turbo have been introduced in the last few years. For the 2015 data taking, the first version of Turbo allowed only the exclusive triggered candidate to be saved, without keeping the rest of the event and discarding all sub-detectors information. While the event size was an order of magnitude smaller than for full stream data, any analysis relying on additional infos from the surrounding event could not use Turbo stream data. For this reason, in 2016, Turbo++ was implemented, where full event reconstruction was persisted. Finally, in 2017, a new intermediate solution between Turbo and Turbo++, called Turbo SP (Selective Persistence) was used. With Turbo SP both the trigger candidate and a subset of reconstructed event is saved. This extremely flexible solution allows the analyser to choose which objects to save, minimizing the size of the stored event. A sketch of the evolution of Turbo is showed in Figure 4.22. In view of a full software trigger in the Upgrade, Turbo becomes the only available solution. The reduced event size, would indeed allow to store candidate at high rate, fully exploiting the improvement due to the Lo removal.

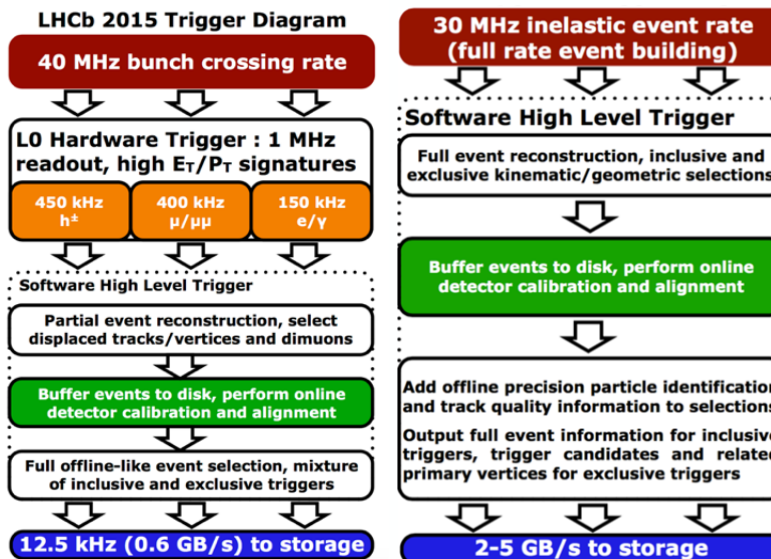


Figure 4.20: Scheme of the current (left) and of the upgraded LHCb trigger scheme (right).

4.2.3 Upgrade LHCb projections: LLP signatures

The much higher luminosity and improved capabilities of the upgraded LHCb detector is expected to largely improve the LHCb capabilities in LLP searches in LHC Run 3. In the following, the prospects for a few LLP signatures are given to showcase the up-

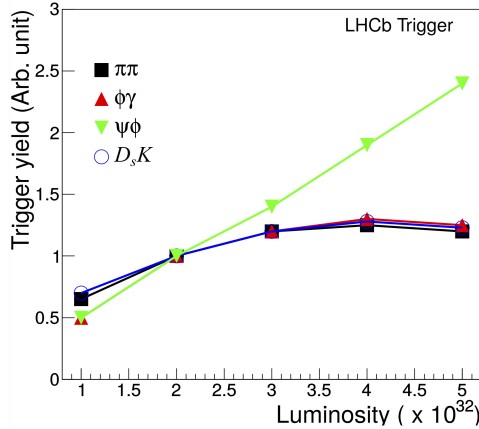


Figure 4.21: Trigger yield as a function of the luminosity. For not muonic channels, the saturation effect due to Lo bottleneck can be observed.

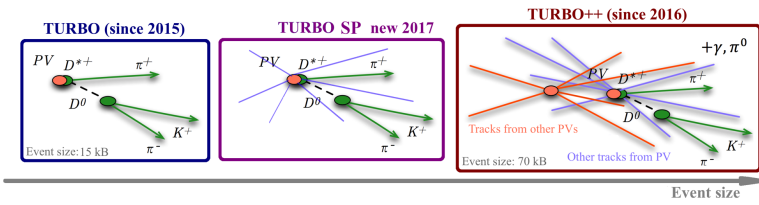


Figure 4.22: Sketch of the evolution of Turbo.

grade potential. However, the potential of the upgraded trigger-less readout has not been completely explored yet and its great flexibility could be exploited in several ways.

4.2.3.1 Displaced di-leptons

The upgraded LHCb experiment is expected to have exceptional sensitivity to low-mass displaced dilepton signatures thanks to mass resolution, excellent vertexing and the online selection allowed by the trigger-less readout.

The upgrade LHCb sensitivity to dileptons has been explored in the literature in the context of dark photon searches. Two complementary signatures have been considered: an inclusive search for $A' \rightarrow \mu\mu$ and a search for using radiative charm decays $D^{*0} \rightarrow D^0 A'(ee)$. The inclusive search [225] scans a very large region from the dimuon threshold $2m_\mu$ all the way up to the Z pole. The second proposed signature [226] exploits a tag of the radiative decay of the D^{*0} using its reconstructed invariant mass and a di-electron dark photon final state to probe a much lower mass range [$2m_e, 142$ MeV]. For both signatures, three non-overlapping search regions are defined according to different requirements on the A' flight distance:

- prompt resonant;
- displaced upstream of the first VELO module;
- displaced downstream of the first VELO module.

The prompt search is expected to probe mixing parameters ϵ^2 below 10^{-7} despite the large irreducible background from Drell-Yan and QCD. Since the search for displaced dark photons is not expected to exclude a physical parameter above the η mass, no attempt is made to probe that region.

An inclusive search has already been performed with Run 2 data [163]. This has been possible thanks to the high reconstruction and identification efficiency of soft di-muons at LHCb. These results demonstrated the unique sensitivity that can be reached at LHCb. The planned increase in luminosity and removal of the hardware-trigger stage in Run 3 should increase the number of expected $A' \rightarrow \mu\mu$ decays in the low-mass region by a factor of $\mathcal{O}(100 - 1000)$ compared to the 2016 data sample. The limits placed by the current data and the sensitivity expected with future LHC runs is shown in Figure 4.23.

On the other side, the exclusive search is much more challenging and not feasible prior to the upgrade, since the hardware trigger and the thicker RF foil degrade the sensitivity. This search highly relies on the online identification of e^-e^+ pairs, since over 5 trillions decays are expected in Run 3. The expected sensitivity probes unexplored regions of phase space at very low A' mass and mixing ϵ^2 which is usually the realm of beam-dump experiments.

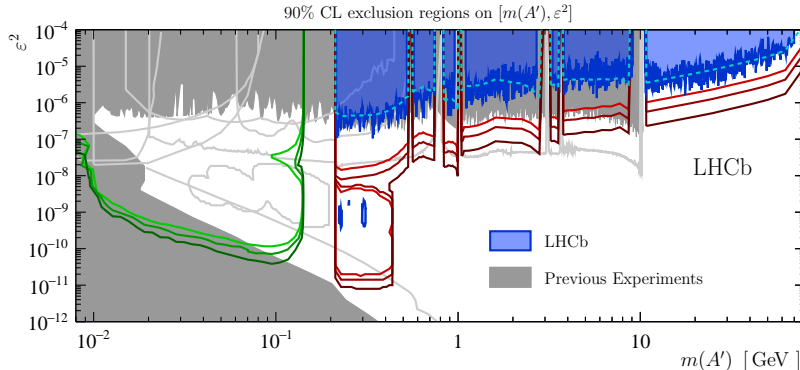


Figure 4.23: Current and expected limits in the dark photon parameter space mixing ϵ^2 versus A' mass. Blue-shaded limits are the current LHCb limits from [163] while grey-shaded ones are existing limits from other experiments. The dashed blue line represents the naive expected limit for the search that was performed with 13 TeV collisions [163]: it agrees fairly well with the observed limits. Limits from the proposed inclusive search with 15, 50 and 500 fb^{-1} are shown in progressively darker red. The expected sensitivity of $D^{*0} \rightarrow D^0 A'(ee)$ at low mass are shown in progressively darker green for 15, 50 and 300 fb^{-1} .

A displaced dimuon signature also appears in some hidden-valley scenarios where dark mesons have a large enough decay rate to leptons. The upgrade LHCb prospects for this kind of signature have been explored in [227] and are extremely promising. In the scenario explored in [227] dark mesons are produced with large multiplicities between 10 and 30 and selection criteria borrowed from the proposed dark photon search [225] in the region after the first VELO module. The expected reach for the proposed searches using Run 3 data from LHCb (15 fb^{-1}) and from ATLAS/CMS

(300 fb^{-1}) are shown in Figure 4.24. The model studied involves a $200 \text{ GeV}/c^2 U(1)'$ gauge boson Z_p decaying to a hidden-valley quark pair; showering and hadronization in the dark sector leads to a large multiplicity of hidden hadrons ω_V (with $m_{\omega_V} = 0.3 \text{ GeV}/c^2$) that can decay to dimuons. In this context the upgrade LHCb could have better sensitivity than other proposed searches at ATLAS and CMS.

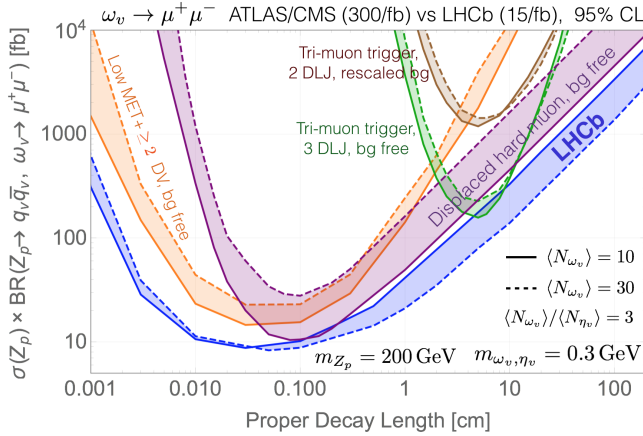


Figure 4.24: Projected bounds from various ATLAS/CMS searches and the LHCb search for the di-muon [227].

4.2.3.2 Displaced jets

Signatures with displaced jets are very common in the context of long-lived particle searches. LHCb has already started to explore its potential by using the data collected during Run 1 to search for the following signatures: a single [147] and a double [148] displaced di-jet and a single displaced high-multiplicity vertex including a high- p_T muon [167]. Starting with the former signature, already in Run 1 limits have been set on dark sector V-pions from Higgs decaying to quark-antiquark pairs.

In the upgrade LHCb, the background rejection for displaced jet searches is expected to improve thanks to the improved VELO resolution and the selection efficiency should be significantly higher thanks to the online displaced vertex identification. The main focus of LHCb will be to probe the region at very low lifetime where it has already probed to be most competitive (see discussion in EXPERIMENTAL COVERAGE CHAPTER). There, the background from QCD and material interactions is the main limiting factor and the improved vertex resolution of the upgrade VELO together with the lower material budget and the use of a detailed material map are expected to bring large improvements.

In some dark sector models the number of displaced vertices can be very large, even in the limited LHCb acceptance [215]. Typical displaced vertex searches would probably discard these events due to requirements on vertex isolation that are used to remove fake signatures, so a dedicated search strategy is needed. Furthermore, a dedicated software trigger looking for a large number of

displaced vertices in the VELO and very soft p_T requirements could in principle be very sensitive to this kind of models, but studies are needed to fully understand its potential and compare it to other experiments.

4.2.3.3 Displaced mesons

SM quark-antiquark pairs from the decay of a low mass particle can often hadronize in SM mesons that subsequently decay with known branching ratios. For example a dark-sector meson with a displaced decay to $c\bar{c}$ often produces two D mesons which in turn have a non-negligible lifetime. In this scenario, the authors of [227] have investigated the prospects of using more or less inclusive reconstruction of the two D mesons decays at the upgraded LHCb. A very similar approach could be used to target decays to $b\bar{b}$ that hadronize to B mesons since the latter is very likely to produce D mesons in its decay. Since LHCb is designed to reconstruct heavy flavour decays, it can be very competitive in this kind of searches as it was shown in [227]. Furthermore, this kind of search will greatly profit from the software trigger which is mainly designed to improve the efficiency of this kind of hadronic decays of heavy flavour mesons.

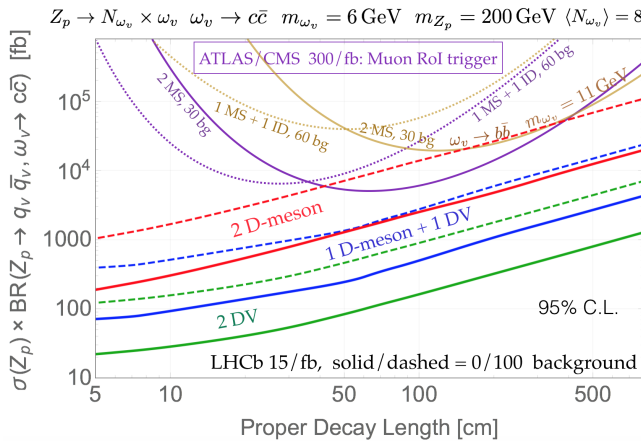


Figure 4.25: Projected bounds from various proposed searches for confining hidden valley models exploiting $c\bar{c}$ decays of hidden valley mesons ω_v taken from [227]. The sensitivities with various signatures at LHCb are shown: two displaced vertices (green), one reconstructed D meson and one DV (blue) and two reconstructed D mesons (red). Searches for this same particular model at ATLAS/CMS are shown not to be competitive (more details can be found in [227]).

4.2.4 After Phase-I upgrade: Phase-II and more

TO BE FILLED WITH SOME PROSPECTS AND NEW IDEAS

- downstream triggers for displacements larger than 20 cm
- removal of RF foil to reduce VELO material interaction background
- dedicated ASICs for downstream tracking embedded in DAQ

- Tracking chambers inside the magnet for low momentum particles (useful for soft pion from “disappearing” chargino track?)

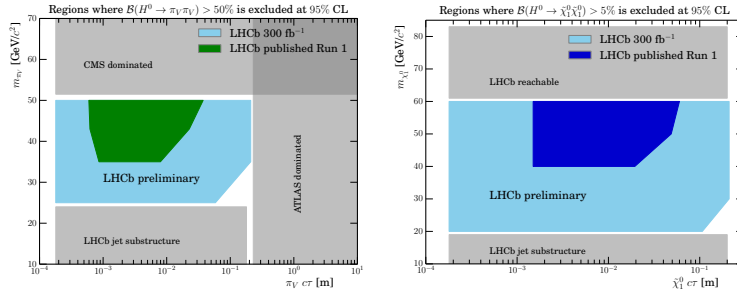


Figure 4.26: Naive projections of Run 1 results from searches of displaced jets at LHCb to the expected luminosity to be collected with the Phase-II upgraded detector. On the left is the projection of the search for a single displaced dijet [147] while on the right is the one for a single displaced vertex with a high- p_T muon [167].

4.3 Current and Proposed Dedicated LLP Detectors

Limit to 1-1.5 pages each, focus on projected sensitivity and complementarity

4.3.1 Moedal

4.3.2 MilliQan

4.3.3 MATHUSLA

4.3.4 CODEX-*b*

4.3.5 FASER

5

Reinterpretation and Recommendations for the Presentation of Search Results

5.1 Introduction

Models and scenarios with LLPs have seen an enormous rise in interest in recent years. They include supersymmetric scenarios with almost mass-degenerate lightest states [29, 31], highly split spectra [58, 228], very weakly interacting LSPs¹ like gravitinos or axinos [229, 230] or R -parity violation [25], as well as equivalent scenarios in other SM extensions (e.g., extra-dimensional models) with new SM gauge-charged particles. More recent ideas include models with feebly interacting dark matter [231] (supersymmetric or not), asymmetric dark matter [232], Hidden Valley [32] and other dark sector models—see the classification of existing well-motivated theories with LLPs in Chapter ?? of this Whitepaper.

All these models can feature a large variety of possible LLP signatures. In Hidden Valley models, for instance, new particles can either decay into invisible dark particles or back to the SM, thus possibly leading to a mix of long-lived and prompt signatures, with or without missing transverse energy (\cancel{E}_T). Furthermore, new theoretical frameworks are constantly emerging, often motivated by new approaches to the hierarchy problem or dark matter. It is therefore of great interest to our community to be able to (re-)interpret the LLP experimental results for new models, which may be brought up in the future.²

The re-interpretation can generically be done in two ways, either applying appropriate simplified-model results, or reproducing the experimental analysis in a Monte Carlo simulation. Clearly, the former is easier and faster, while the latter is more general but more difficult and much more time consuming. In the context of searches for prompt signatures with \cancel{E}_T , the use of simplified models has been shown to be a fruitful approach for both the experimental and theoretical communities [234, 235, 236, 237, 238, 239]. Dedicated tools [240, 241, 242] are publicly available and allow the user to re-interpret SUSY simplified-model results within the context of a full model. The coverage of a full model can, however, be severely limited by the kind of simplified-model results available,

¹ LSP: lightest supersymmetric particle; stable if R -parity is conserved.

² In this context we refer the reader also to the activities of the “Forum on the Interpretation of the LHC Results for BSM studies” [233], which brings together more than 100 theorists and experimentalists around this topic.

as discussed recently in [243] for the case of the phenomenological MSSM. Indeed, for some models the large number of relevant simplified-model topologies and their complexity can make the simplified-model approach inexpedient. In this case, a more complete and robust recasting procedure is necessary.

Again, for prompt signatures, a general recasting approach is available through several public tools, notably **CHECKMATE** [244, 245], **MADANALYSIS5** [246, 247], **RIVET** [248] (v2.5 onwards) and **Gambit’s COLLIDERBIT** [249]. These tools allow to reproduce experimental analyses by means of Monte Carlo event simulation coupled to an approximate emulation of detector effects.³ For the latter, **CHECKMATE** and **MADANALYSIS5** rely on **DELPHES3** [250], in some cases supplemented with appropriate tuning, while **RIVET** and **COLLIDERBIT** employ object smearing and analysis-specific reconstruction efficiencies. The ATLAS and CMS collaborations are helping these recasting efforts by providing more and more detailed information about their analyses and results; recently, in the case of the CMS SUSY group, even covariance matrices for the background correlation across signal regions in the framework of simplified likelihoods [251].

The situation is –so far– quite different for LLP searches. First, the presentation of results in terms of simplified models is still limited to few topologies and does not always include all the parameters required for a general purpose re-interpretation. Notice here that, compared to simplified models for prompt searches, simplified models for LLP searches always have at least one additional degree of freedom—the lifetime of the LLP. Second, general purpose recasting tools are not yet available. Recasting LLP searches outside the experimental collaborations is a difficult task, since they are very sensitive to the detector response, which in most cases cannot be easily emulated by a fast detector simulation. As a result, none of the available (public) tools can currently recast LLP searches, thus rendering the applicability of the experimental results extremely limited.

In order to allow for a more extensive re-interpretation or recasting of the experimental analyses, detailed information concerning the detector performance and object reconstruction is needed. These can in principle be provided in the format of efficiencies⁴ for selection and reconstruction of relevant objects, as demonstrated already by some pioneering experimental publications [252, 144]. One difficulty in this respect is that the information needed for recasting LLP searches is clearly analysis-dependent, which means an additional workload for the analysis groups to provide this information case by case.

The objective of this chapter is to discuss the presentation of the LLP search results with the aim that they can be re-used for interpretations beyond the models considered in the experimental publications. To this end, we first discuss in Section 5.2 the various options for presenting the LLP results, see Fig. 5.1, and compare

³ For completeness it should be noted that, while all these tools include a more or less extensive set of SUSY searches, many of the searches for other, “exotic” types of new physics cannot yet be reproduced outside the experimental collaborations. This concerns in particular searches relying on BDT or MVA techniques.

⁴ We employ the term “efficiency” in a broad sense. It can refer to reconstruction efficiencies, selection efficiencies, overall signal efficiencies, etc..

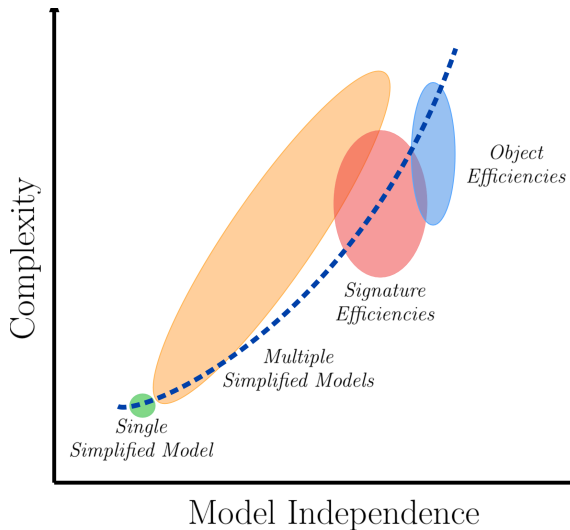


Figure 5.1: A qualitative overview of the possibilities for results presentation discussed in this chapter. The axes represent the complexity of information required by each format and the corresponding level of model independence.

their advantages and shortcomings. In Section 5.3 we discuss in more details how the simplified models in Chapter ?? can be used to re-interpret LLP searches. In Section 5.4, we present several attempts of recasting LLP searches, according to the LLP signature: heavy stable charged particles, disappearing tracks and displaced objects; for each case, the lessons learned are elaborated. Section 5.5 presents a first attempt to extend the public detector simulator DELPHES to deal with LLP searches, while Section 5.6 deals with reinterpretations performed within the experiments themselves, including the RECAST framework. In Section 5.7, we discuss complementary constraints on LLPs from re-interpreting prompt searches. We conclude in Section 5.8 with our recommendations for the presentation of LLP results.

5.2 Options for Presenting Experimental Results

A qualitative view of the various possibilities for presentation of search results is given in Fig. 5.1. We broadly classify these possibilities according to the type of information provided or type of efficiency. Each type refers to distinct signal objects, as illustrated in Fig. 5.2. As we can see, each possibility relies on distinct assumptions about the signal, resulting in different levels of model-dependence. Below we provide a brief discussion of the advantages and limitations of the various possibilities of presentation of LLP search results. We will gradually progress from the simplest case towards more complexity but also better re-usability.

Simplified Models: In most cases the simplified-model topology corresponds to single or pair production of the LLPs, though in principle simplified models for production through cascade decay of heavier states can also be envisaged. In any case, the simplified

model incorporates important assumptions on the LLP production, decay mode and quantum numbers. Simplified-model results can be presented at different levels of sophistication and re-usability:

- exclusion curves in, e.g., a mass-vs-mass or mass-vs-lifetime plane, are highly model dependent and can rarely be used for re-interpretation;
- cross-section upper limits⁵ can be applied to a larger variety of models in which the same LLP production and decay mode occurs through a rescaling of the cross section times branching ratio factor;
- simplified-model efficiencies allow to go one step further: they make it possible to combine different topology contributions to the same signal region and compute an approximate likelihood using the number of expected and observed events.

The main advantages of simplified models are a parametrization in terms of few physical parameters and a unified language and format applicable to a wide range of searches. Also, when re-using simplified-model results one avoids detector simulation uncertainties. The disadvantages are that the simplified-model result cannot be applied to other LLP production or decay modes, resulting in too conservative limits if the LLP signal is composed from multiple topologies. This can be considerably relevant if the LLP is a color singlet, but there are several heavier color-charged states which can be produced and decay to the LLP. In principle this can be overcome if efficiencies are provided for a sufficiently large number of simplified models (including cascade decays), as a function of the simplified-model parameters, which should include the LLP lifetime. These efficiencies can then be combined in order to compute the corresponding constraints to complex models, where multiple topologies are present.⁶ We stress, however, that in order for this combination to be possible, signal efficiencies and not cross-section upper limits must be provided. The major drawback of this approach is that in order for the results to be applicable to a broad class of models, the number of required simplified models and their complexity can easily become very large. For achieving a high level of model independence, it is therefore desirable that the experimental analysis can be recast with Monte Carlo event simulation. Two ways of presenting results are useful to this end: *signature efficiencies* and *object efficiencies*.

Signature efficiencies are efficiencies for the reconstruction of the main LLP signature (single charged track, displaced vertex, disappearing track, ...) as a function of the LLP kinematical parameters and the lifetime. Signal efficiencies require the assumption of a specific LLP decay, but are highly model independent, since they make no assumption on the LLP production mode. In addition, they are fully model-independent for stable particles (within the detector dimensions), since in this case no assumptions about

⁵ For the sake of re-usability, cross section upper limits in absolute terms are much preferred over limits on the signal strength.

⁶ These points are illustrated by the re-interpretation of the CMS search for heavy stable charged particles [252] discussed in Section 5.3: for the specific model considered in [46], constraints obtained using only a single simplified model (direct production of $\tilde{\tau}$ s in this case) can underestimate the bounds on the LLP mass by almost a factor of two.

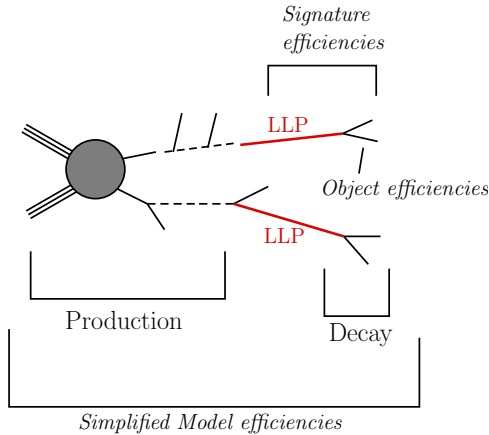


Figure 5.2: Possibilities for the presentation of results: simplified-model efficiencies assuming a specific topology of LLP production and decay, signature efficiencies assuming only a specific LLP decay, and object efficiencies which are independent of the specific decay mode.

the LLP decay mode are required. In many cases, however, the reconstruction efficiencies depend on multiple variables, such as the LLP p_T , its transverse decay position, impact parameter, etc. As illustrated in section 5.4.7, these efficiencies could be very useful for recasting LLP searches, but often they are not provided by the experimental collaborations. Many recasting efforts consist in extracting these efficiencies from the provided information, but can result in large uncertainties.

Object efficiencies are efficiencies for the reconstruction of the physics objects relevant for building the LLP signature. They can clearly be applied to a wide range of LLP decay and production modes, since no specific assumptions about these are required. For instance, a displaced lepton reconstruction efficiency can be provided as a function of the lepton p_T and its production position. As discussed in Section 5.4.2, these efficiencies can be used to recast LLP searches to an acceptable accuracy ($\sim 20\%$). Furthermore, as illustrated in Section 5.4.7, knowledge of object efficiencies are essential for a general purpose recasting of the search. Within this approach the model dependence is minimal and can be restricted to a few general assumptions about the nature of the LLP. Also, object efficiencies could be included in fast detector simulators, thus providing a way of recasting LLP searches on the same footing as prompt searches. The main difficulty with providing such object efficiencies is the potentially large number of parameters required for their parametrization.

5.3 Reinterpretation using Simplified Models

One of the possibilities for extending the experimental results from LLP searches to a large variety of scenarios is through the use of simplified model topologies. Simplified models (or simplified model spectra, SMS) have been widely used for the interpreta-

tion of prompt and LLP searches. As discussed in Chapter ??, a large number of SMS topologies are possible for the distinct LLP signatures, which can be grouped by the LLP production mode, decay and lifetime. These SMS topologies aim to capture the main physical properties of the LLP signal and can then be used to constrain other scenarios containing similar topologies. The use of simplified model results to constrain full models has been shown to be possible [240, 242, 253, 254, 42, 243], even though it has its shortcomings [243]. Also within the context of LLP searches, the use of simplified model results for re-interpretation can be a good alternative, e.g., when a recasting based on a Monte Carlo simulation is difficult or computationally too expensive. In this Section we will briefly review how SMS results can be used to re-interpret searches for full models as well as the particular challenges presented by LLP searches. A concrete example of re-interpretation using simplified models is given in Sec. 5.3.2, based on the results of Ref. [46].

5.3.1 From Simplified to Full Models

The interpretation of experimental results using simplified models typically correspond to upper limits on the production cross-section or signal efficiencies for a specific SMS topology (production and decay channel). These results are provided as a function of the simplified model parameters, which have been largely taken to be the masses of the BSM particles appearing in the topology. For LLP topologies, however, a new parameter must be considered: the LLP lifetime (see Ch. ??). With the exception of searches for stable particles, the lifetime is one of the main parameters affecting the topology efficiency and upper limit.

Once signal efficiencies⁷ (ϵ) are provided for one or more SMS topologies, these can be used, under some approximations, to quickly compute the number of expected signal events (S) for a full model:

$$S = \mathcal{L} \times \left(\sum_{\text{SMS}} \sigma_{\text{SMS}} \times BR_{\text{SMS}} \times \epsilon_{\text{SMS}} \right), \quad (5.1)$$

where \mathcal{L} is the luminosity for the respective search and the sum runs over simplified model topologies. Since the production cross-section (σ_{SMS}) and branching ratios (BR_{SMS}) for each topology can be quickly computed for any full model, the simplified model signal efficiencies (ϵ_{SMS}) can be directly used to obtain the signal yield.

This procedure does not rely on any Monte Carlo simulation or recasting of LLP searches and can be easily applied to a wide variety of models, if ϵ_{SMS} is known. The main limitation of this approach comes from the limited (although growing) number of SMS results available. Since ϵ_{SMS} is typically known only for very few simplified models, the sum in eq. 5.1 is limited to the number of available topologies, resulting in an underestimation of S .

For prompt SUSY searches a systematic approach for re-interpreting

⁷ For simplicity we will refer to the signal acceptance times efficiency as “signal efficiency”. This efficiency is a function of the simplified model parameters, including the LLP lifetime.

simplified model results based on the procedure outlined above has been developed in Refs. [240, 242]. Furthermore, using the large number of available SUSY SMS results, public tools are available for constraining full models using these results [242, 241]. Although no public tools are currently available for models with long-lived particles, the same procedure can also be applied to LLP SMS results. This has been shown in Ref. [46], where, using simplified model topologies, the 8 TeV CMS results for heavy stable charged particles (HSCPs) have been used to constrain regions of the CMSSM parameter space. In the next section we review some of the results found in Ref. [46]. Although these have been obtained within the context of HSCPs, the main results can be generalized to other LLP signatures and demonstrate some of the advantages and shortcomings of re-interpretations using LLP simplified models.

5.3.2 Reinterpretation using HSCP Simplified Models

The CMS search for HSCPs in Ref. [252] provided signal efficiencies for the simplified model topology: $pp \rightarrow \tilde{\tau}\tilde{\tau}$ as a function of the stau mass. The stau is assumed to be stable (at detector scales), thus producing a highly ionizing track, which can be used to search for this scenario. Since the stau lifetime (τ) is assumed to be $\gg 10$ ns, the signal efficiencies do not depend on τ , thus simplifying the SMS parameter space, which reduces to the stau mass.⁸ The relevant selection efficiencies required for a general purpose Monte Carlo recasting of the HSCP search have also been provided by the CMS analysis (see Sec. 5.4.1 for details).

The efficiencies for the stau simplified model can be used to constrain a full BSM scenario which contains HSCPs. In Ref. [46] the region of the CMSSM parameter space with $m_{\tilde{\tau}} - m_{\tilde{\chi}_1^0} < m_{\tau}$ has been considered, since it provides a possible solution to the Lithium problem [255, 256]. Due to the small mass difference, the stau is long-lived and decays outside the detector, thus generating a HSCP signal. In Fig. 5.3 we show the constraint on the CMSSM parameter space obtained using only the simplified model provided by CMS (direct stau production). Since the simplified model only contains one parameter it translates to a limit on the stau mass ($m_{\tilde{\tau}} < 260$ GeV), as shown by the blue region in the Figure. In this CMSSM scenario, however, direct production of staus only contribute to a small fraction of the total HSCP signal, since staus are typically produced from cascade decays of heavier SUSY states, such as squarks and gluinos. Furthermore, there are several possible topologies which contain a stau and the LSP ($\tilde{\chi}_1^0$) in the final state, thus resulting in a mixed missing energy-HSCP signature. Therefore using only the CMS constraints for the direct stau production simplified model largely underestimate the exclusion potential of the CMS search.

In order to improve the constraints shown in Fig. 5.3, one must have efficiencies for several SMS topologies. Fortunately a Monte

⁸ We point out that it is still possible to apply these simplified model results to models with smaller LLP lifetimes if we include the suppression factor from the LLP decay length distribution, as discussed in Sec. 5.4.1.2.

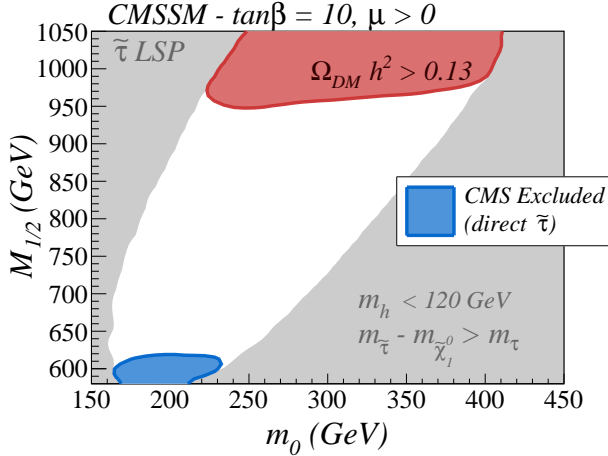


Figure 5.3: Region of the CMSSM parameter space with long-lived NLSP staus. The light gray regions are excluded by the requirements $m_{\tilde{\tau}} \gtrsim m_{\tilde{\chi}_1^0}$ and $120 \text{ GeV} \leq m_h \leq 130 \text{ GeV}$. The top red region is excluded by the upper limit on the neutralino relic density, while the lower blue region is excluded by the CMS constraints on direct production of long-lived staus. For more details see Ref. [46].

Carlo recasting of the 8 TeV CMS search is possible (see Sec. 5.4.1 for details) and can be used to compute simplified model efficiencies. In Ref. [46] seven additional simplified models (containing cascade decays) were considered and their efficiencies computed as a function of the masses appearing in the topology. A summary of the topologies considered are shown in Table 5.1. It is important to point out that it is not necessary to specify the Standard Model final states appearing in the simplified models, since the HSCP search is inclusive and the efficiencies do not depend on the additional event activity. Using this extended database of simplified model efficiencies and eq. 5.1 we can compute a more inclusive signal yield for each point of the CMSSM parameter space and improve the constraints on the model. The results are shown in Fig. 5.4, where we see a drastic improvement in the region excluded by the constraints on HSCPs, as expected. For this specific scenario (with $\tan \beta = 10$), all the parameter space is excluded either by the CMS or dark matter constraints [46].

SMS topology
$pp \rightarrow X X$
$pp \rightarrow Y_1 Y_1, Y_1 \rightarrow SM X$
$pp \rightarrow Y_1 Y_1, Y_1 \rightarrow SM Y_2, Y_2 \rightarrow SM X$
$pp \rightarrow Y_1 Y_2, Y_1 \rightarrow SM Y_2, Y_2 \rightarrow SM X$
$pp \rightarrow Y Y, Y \rightarrow SM SM X$
$pp \rightarrow inv X,$
$pp \rightarrow Y_1 Y_2, Y_1 \rightarrow SM inv, Y_2 \rightarrow SM X$
$pp \rightarrow Y_1 Y_2, Y_1 \rightarrow SM inv, Y_2 \rightarrow Y_3 SM, Y_3 \rightarrow SM X$

Table 5.1: Definitions of the HSCP simplified models considered in this Section. X represents the HSCP, Y_i represent intermediate BSM particles, SM represents any Standard Model particle and inv represents an invisible final state, such as the neutralino.

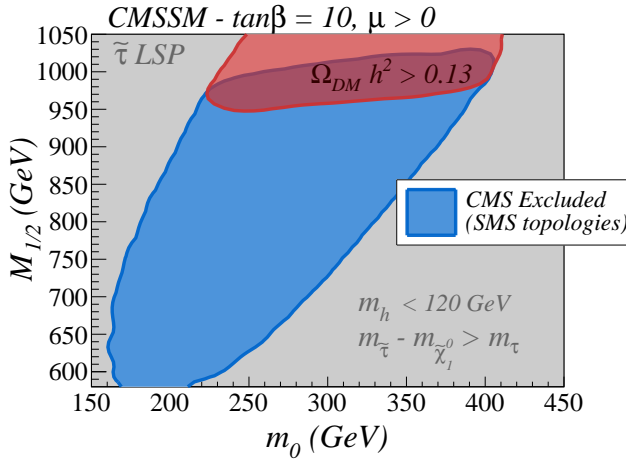


Figure 5.4: Same as Fig. 5.4, but using all the simplified models listed in Table 5.1.

Fig. 5.4 illustrates the feasibility of using simplified model efficiencies to constrain full models. This approach has the advantage of being computationally inexpensive (once the efficiencies are known) and can be used to quickly test a large number of model points. However the approach relies on a few approximations and is never fully inclusive, since the number of available SMS topologies is always limited. Hence it is relevant to verify how close the simplified model re-interpretation comes to the full recasting using a Monte Carlo simulation. In Ref. [46] it was shown that, within the CMSSM scenario discussed above and using eight simplified model topologies, the SMS results reproduce the full simulation within 20% or better. Since this error is of the order of the uncertainties in recasting, the use of simplified models becomes a viable alternative to full recasting. The SMS re-interpretation can become even more relevant for the cases where a Monte Carlo recasting is not possible.

Lessons learned

The example discussed in Sec. 5.3.2 illustrates how simplified models for LLPs can be used as a re-interpretation tool. One important point which becomes clear once we compare Figs. 5.3 and 5.4 is the importance of a sufficiently inclusive database of simplified model efficiencies. This can be provided by the experimental collaborations or generated by theory groups if a full recasting is available. Furthermore, since LLP searches can be very inclusive, the simplified models considered can also be defined inclusively, as discussed above. In this way a few number of simplified models can cover a large number of event topologies, thus increasing the SMS coverage of full models.

5.4 Recasting Examples for Specific Searches

Here we provide examples of recasting specific experimental searches for several LLP signatures: heavy stable charge particles, displaced leptons, displaced jets, displaced lepton-jets, non-

pointing photons, disappearing tracks and displaced vertices. These recasting attempts have been made outside the experimental collaborations, making use of the public information provided by the experimental note or publication. The aim here is to point out the challenges faced when recasting LLP searches and also to highlight the cases where the experimental information provided is straightforward and useful for recasting.

5.4.1 Heavy Stable Charged Particles

Searches for heavy stable charge particles (HSCPs) are based on the signature of highly ionizing tracks and/or an anomalous time-of-flight between the particle's production at the interaction point and its arrival in the muon detector [257]. Both signatures are sensitive to the particle's velocity and exploit the production of HSCPs in the non-ultrarelativistic regime, allowing for a powerful discrimination against the Standard Model background. HSCP searches assume particles long-lived enough to traverse the entire detector. They have been performed at the 7 [258, 259], 8 [187, 189] and 13 TeV LHC [260, 188] and interpreted for HSCPs that are purely electrically charged or colored, the latter of which hadronize to form R -hadrons [261]. Typically, the HSCP signature yields high sensitivities providing a very strong background rejection while still allowing for large signal efficiencies. As a consequence, search strategies for new physics models with HSCPs typically do not benefit from more model-dependent selection criteria, like requiring additional particles in the event [44]. The corresponding searches can, hence, be performed in a mostly inclusive manner concentrating on the HSCP candidate itself. This fact opens up the possibility to provide a widely applicable recasting based on signature efficiencies. This approach has been followed by the CMS Collaboration [252], which has provided probabilities for HSCP candidates to pass the on- and off-line selection criteria for the 8 TeV LHC run as a function of the relevant kinematical parameters.

In this section we describe the recasting of the 8 TeV CMS search for HSCPs and discuss its validation and applicability. Furthermore, we comment on the attempt to extrapolate the 8 TeV signature efficiencies to the corresponding 13 TeV analysis, for which the corresponding efficiencies have not been provided by CMS.

5.4.1.1 Recasting using signature efficiencies

In Ref. [252] efficiencies for the reconstruction and selection of HSCP candidates are provided in the form of on- and off-line probabilities, $P_{\text{on}}(\mathbf{k})$ and $P_{\text{off}}(\mathbf{k})$. These are given as a function of the truth-level kinematics velocity (β), pseudo-rapidity (η) and transverse momentum (p_T) of isolated HSCP candidates, so the vector \mathbf{k} is defined as: $\mathbf{k} = (\beta, \eta, p_T)$. The on and off-line probabilities must be applied to isolated HSCP candidates, which are required to

fulfill

$$\left(\sum_i^{\text{charged}} p_T^i \right) < 50 \text{ GeV}, \quad \left(\sum_i^{\text{visible}} \frac{E^i}{|\boldsymbol{p}|} \right) < 0.3, \quad (5.2)$$

where the sums include all charged and visible particles, respectively, within a radius of $\Delta R = \sqrt{\Delta\eta^2 + \Delta\phi^2} < 0.3$ around the HSCP candidate track, p_T^i denotes their transverse momenta and E^i their energy. Muons are not counted as visible particles and the HSCP itself is not included in either sum.

If an event contains one or more HSCPs satisfying the above isolation criteria, the efficiency for the event to pass the analysis selection is given by:

$$\epsilon = \epsilon_{\text{on}} \times \epsilon_{\text{off}}. \quad (5.3)$$

For an event with one HSCP candidate $\epsilon_{\text{on/off}}$ is directly given by the signature efficiencies $P_{\text{on/off}}(\mathbf{k})$. While for an event with two candidates it reads [252]

$$\epsilon_{\text{on/off}} = P_{\text{on/off}}(\mathbf{k}^1) + P_{\text{on/off}}(\mathbf{k}^2) - P_{\text{on/off}}(\mathbf{k}^1)P_{\text{on/off}}(\mathbf{k}^2), \quad (5.4)$$

where $\mathbf{k}^{1,2}$ are the kinematical vectors of the two HSCPs in the given event. Therefore the on- and off-line probabilities combined with the isolation criteria allows for the complete recasting of the HSCP search using only truth level events generated by a Monte Carlo simulator.

The recasting of the 8 TeV search was performed in Ref. [46], where the procedure described above was used. Events were simulated using PYTHIA 6 [262] and the total signal efficiency for a given model was then computed using:

$$\epsilon = \frac{1}{N} \sum_{i=1}^N \epsilon_i.$$

where the sum runs over all the (N) generated events and ϵ_i is the efficiency for each event computed using eq. 5.3. Since the probabilities $P_{\text{on/off}}(\mathbf{k})$ are given for four distinct cuts on the reconstructed HSCP mass (m_{rec}), these were considered as four different signal regions. The number of observed events and the expected background for which of these cuts are reported in Ref. [252].

5.4.1.2 Validation and applicability

A validation of the method described above was done in Ref. [46] using the same gauge-mediated supersymmetry breaking (GMSB) model considered by CMS [252]. This supersymmetric model features a gravitino and a long-lived stau as the lightest and next-to-lightest supersymmetric particle, respectively. Since the stau only decays outside the detector volume, all cascade decays of the produced sparticles terminate in the lightest stau, which provides the HSCP signature. Figure 5.5 (left) shows the comparison of the resulting signal efficiency obtained by the recasting and the full CMS

detector simulation. The signal efficiencies agree within 3% providing an excellent approximation. The differences are of the order of the statistical uncertainties from the Monte Carlo simulation of the signal. In Fig. 5.5 (right) we also show the 95% CL upper limits on the inclusive production cross sections, which, again, agree (within $\sim 3\%$) with the ones obtained by the full simulation in Ref. [252]. Note that both limits are based on the discrete mass cuts on m_{rec} mentioned above. In the full CMS analysis [187] an event-based mass cut is used, resulting in slightly stronger constraints for some HSCP masses.

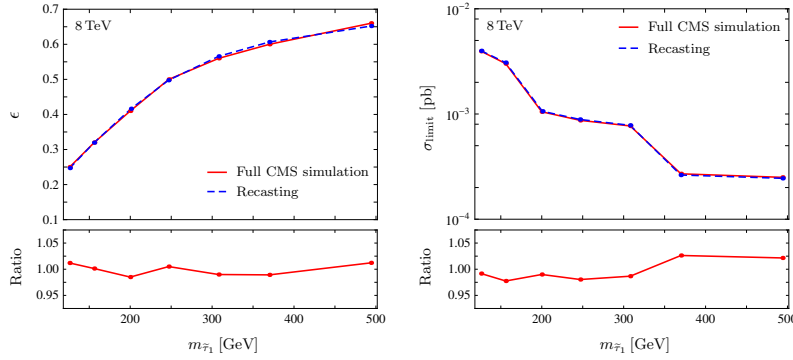


Figure 5.5: **Left:** Resulting signal efficiency ϵ . **Right:** 95% CL cross section upper limit for the GMSB model as the function of the stau mass. We compare the CMS analysis [252] from the full detector simulation (red solid lines) with the recasting using signature efficiencies (blue dashed lines). In the lower frames we show the respective ratios $\epsilon^{\text{Full}}/\epsilon^{\text{Recast}}$, $\sigma_{\text{limit}}^{\text{Full}}/\sigma_{\text{limit}}^{\text{Recast}}$. Taken from [46].

Due to the inclusive nature of the search, the above recasting provides a widely applicable and highly reliable way to reinterpret the HSCP search for arbitrary models containing detector-stable HSCPs. Accordingly it has been used in a variety of phenomenological studies. For instance, it has been used for reinterpretations in supersymmetric models [164, 263, 264] and non-supersymmetric models of very weakly interacting dark matter [265, 84]. In [84] the recasting has been used to reinterpret the HSCP search for finite lifetimes by convoluting the signature efficiency with the fraction of HSCPs that decay after traversing the relevant parts of the detector. The recasting has also been used for a reinterpretation in terms of simplified models, as discussed in Sec. 5.3.2.

5.4.1.3 Extrapolation to 13 TeV

While the CMS search for HSCPs at 8 TeV has provided the signature efficiencies discussed above, the same is not true for the 13 TeV analysis [188]. Therefore a straightforward recasting of the run 2 search is not possible. Nonetheless, since the 8 TeV CMS search has proven to be extremely useful in constraining models with long-lived charged particles, it would be desirable to recast the 13 TeV analysis as well. In the following we discuss an attempt [266] to obtain a similar recasting for the respective HSCP search at 13 TeV. Our aim is to extrapolate the public 8 TeV efficiencies for the 13 TeV run by introducing a correction function F that accounts for the

differences between both runs:

$$P_{\text{off}}^{13 \text{ TeV}}(\mathbf{k}) = F(\beta) \times P_{\text{off}}^{8 \text{ TeV}}(\mathbf{k}), \quad (5.5)$$

where we have assumed that the correction function is mainly dependent on the HSCP velocity. If $F(\beta)$ is sufficient to account for the difference between both runs and can be computed, we can directly obtain $P_{\text{off}}^{13 \text{ TeV}}$ and, using the procedure described in Sec. 5.4.1.1, recast the 13 TeV analysis.

In order to compute the correction function $F(\beta)$ we use the total signal efficiencies reported by the 13 TeV CMS analysis [188] for direct production of long lived staus. Since the signal efficiencies have been provided for six distinct values of the stau mass, we perform a fit of F to the efficiencies reported. We chose to parametrize the correction function $F(\beta)$ by eight parameters (C_i). Using MADGRAPH5_AMC@NLO [135] and PYTHIA 6 [262] we obtain generator level events for each of the stau mass points at 13 TeV. Then, comparing the total signal efficiencies obtained for a given set C_i to the efficiencies reported in Ref. [188], we can determine the best-fit values for the C_i parameters and consequently the best-fit for the correction function ($F_{\text{best-fit}}$). The result of the best-fit function and its 1σ uncertainty is shown in Fig. 5.6. The deviation of F from 1 implies a decrease or increase of the respective detector and signal efficiency between the 8 and 13 TeV analyses. The Figure also shows that the function is loosely constrained for low values of β .

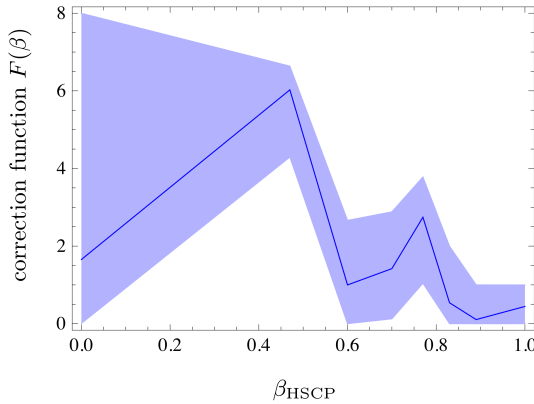


Figure 5.6: Best-fit correction function $F(\beta)$ and its $\pm 1\sigma$ band.

In order to verify the validity of the extrapolation to 13 TeV, we use $F_{\text{best-fit}}$ and eq. 5.5 to compute the total signal efficiencies for the same six benchmark points used in the fit. A comparison between the results obtained through recasting and the efficiencies reported by CMS is shown by the second and third columns in Table 5.2. The results reproduces the CMS values well within the expected uncertainties, thus validating the fitting procedure. Furthermore, the inclusion of the correction function significantly improves the agreement with respect to the direct extrapolation of the 8 TeV efficiencies ($F = 1$), as shown by the forth column in Table 5.2.

The high level of agreement obtained with $F_{\text{best-fit}}$ for the direct stau benchmark points is expected, since these points were used in

m_{HSCP} [GeV]	direct production		
	$\epsilon(\text{CMS})$	$\epsilon(F_{\text{best-fit}})$	$\epsilon(F = 1)$
200	0.235	0.232	0.259
308	0.294	0.298	0.346
494	0.387	0.384	0.452
651	0.450	0.448	0.503
1029	0.497	0.501	0.466
1599	0.428	0.429	0.225

Table 5.2: Efficiencies for the 13 TeV LHC for the six benchmark masses in the direct stau production scenario reported by CMS (second column) and obtained through recasting using $F_{\text{best-fit}}$ and without the inclusion of the correction function ($F = 1$).

order to fit the correction function. Therefore an independent test of the above fit must be performed in order to properly validate the recasting of the 13 TeV analysis. Fortunately CMS has also reported efficiencies for a second scenario, the GMSB model with long lived staus. This scenario not only contains direct stau production, but also includes production through cascade decays of heavier sparticles. Since the GMSB model produces distinct event topologies, it provides a good test for the validity of the recasting procedure.

The results for the six GMSB benchmark points considered in Ref. [188] are shown in Table 5.3. As we can see, they deviate from the CMS values by up to 20% for large stau masses, where our estimate undershoots the CMS efficiencies. Although the overall agreement is improved by the correction function, the result is not entirely satisfactory, given that the uncertainties for the 8 TeV recasting were under 5% (see Fig. 5.5). The observed difference might arise from several shortcomings in our description. In particular, we assume F to only depend on β whereas the full probability maps are parametrized in the three kinematic variables β, η and p_T . However assuming a dependence of all three kinematic variables is clearly not feasible given the very limited amount of information provided by the 13 TeV CMS analysis. Therefore we conclude that it is not possible to extrapolate the 8 TeV efficiencies in a straightforward way without additional information from the experimental collaboration.

m_{HSCP} [GeV]	GMSB		
	$\epsilon(\text{CMS})$	$\epsilon(F_{\text{best-fit}})$	$\epsilon(F = 1)$
200	0.276	0.297	0.279
308	0.429	0.401	0.423
494	0.569	0.494	0.556
651	0.628	0.524	0.580
1029	0.665	0.538	0.493
1599	0.481	0.442	0.228

Table 5.3: Efficiencies for the 13 TeV LHC for the six GMSB model benchmark points reported by CMS (second column) and obtained through recasting using $F_{\text{best-fit}}$ and without the inclusion of the correction function ($F = 1$).

Lessons learned

The prominent signature of HSCPs allows for a mostly inclusive search strategy concentrating on the HSCP track itself. Hence, searches for HSCPs can be recasted by the use of signature efficiencies in a widely applicable and highly reliable way. This possibility has been followed by the CMS Collaboration providing signature efficiency maps for the 8 TeV LHC. The validation reveals an ex-

cellent performance. The recasting has been successfully used in the literature. The signature efficiencies for 8 TeV can also be used to estimate the ones for the 13 TeV run by applying a multiplicative correction function. While such an extrapolation introduces some level of approximation a better knowledge of the underlying changes between both runs might reduce the uncertainties.

5.4.2 Displaced Leptons

Searching for displaced leptons by requiring these to have large impact parameters with respect to the primary vertex is a very clean strategy, and these searches are usually very straightforward to recast. The CMS displaced $e\mu$ search [267] demands two oppositely charged, different flavour (e, μ) leptons with large impact parameters and it is fairly straightforward to recast. The biggest difficulty in doing so is locating all of the relevant information, as it is not all provided within the main document. The “standard” isolation requirements used in the search can be found in an earlier version of the search [268]. The necessary cuts on the displaced decay position (v_T, v_Z) as well as the invaluable selection (as a function of p_T), reconstruction (as a function of impact parameter, d_0) and trigger efficiencies can be found on an additional website [269] containing auxiliary information for recasting. Although all of this information is excellent and greatly facilitates recasting the search, the fact that the additional material is not referenced in the document makes rounding up the information challenging.

Cut Summary of CMS displaced $e\mu$	
Preselection	
1 OS $e^\pm \mu^\mp$ pair	
$d_\ell > 100 \mu\text{m}$	
$p_{T,\ell} > 25 \text{ GeV}, \eta_\ell < 2.5$	
Reject $1.44 < \eta_e < 1.56$	
$I_{\Delta R < 0.3}^{calo,e} < 0.10, I_{\Delta R < 0.4}^{calo,\mu} < 0.12$	
$\Delta R_{\ell j} > 0.5 \forall \text{jets with } p_T > 10 \text{ GeV}$	
$\Delta R_{e\mu} > 0.5$	
$v_{T,\ell} < 4 \text{ cm}, v_{Z,\ell} < 30 \text{ cm}$	
Veto additional leptons	

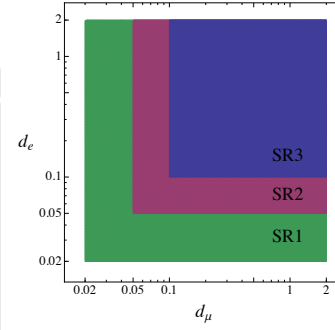


Table 5.4: Left: Preselection cuts in [267] (see also [268, 269]). Right: the transverse impact parameter bins that define the exclusive signal regions. Table and figure taken from [164].

The benchmark model used in this search is the direct pair production of stops that decay through small lepton-flavor-universal RPV $\lambda'_{ijk} L_i Q_j D_k^c$ couplings ($\lambda'_{133} = \lambda'_{233} = \lambda'_{333}$) to yield displaced $\tilde{t} \rightarrow eb, \mu b$, and τb decays. The signal is simple to generate, the only challenge is in handling the displacement properly. The most identifying preselection requirement of this search is that the transverse impact parameter, d_0 , is required to be larger than $100 \mu\text{m}$ for both the electron and muon. The impact parameter is not the point

where the parent object (e.g., τ or b) decays, i.e., the v mentioned above, but the distance to the point of closest approach for the lepton's track relative to the center of the beampipe. Backgrounds in this search from $Z \rightarrow \tau\tau$ or heavy flavor tend to result in leptons that are nearly collinear with the parent due to the small mass-to-momentum ratio, and yield a small impact parameter even for decays well on the lifetime tail of the parent. Events are binned across three exclusive signal regions: SR₃, where both leptons have transverse impact parameters d_e and d_μ between 0.1 and 2.0 cm; SR₂, with d_e and d_μ between 0.05 and 2.0 cm, but not satisfying the requirement of SR₃; and SR₁, with d_e and d_μ between 0.02 and 2.0 cm, but not within SR₂ or SR₃. All selection requirements are summarized in Table 5.4.

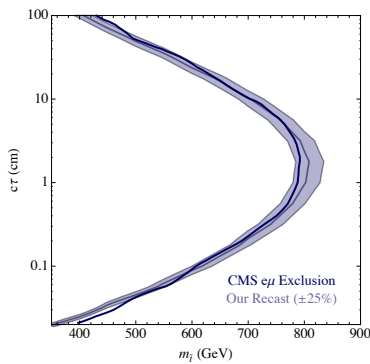


Figure 5.7: Validation of the CMS displaced $e\mu$ search [267] for the displaced supersymmetry benchmark model [270]. Figure taken from [164].

In Figure 5.7, we present the validation of the CMS displaced $e\mu$ search [267] from the study performed in [164]. For this search, we show the recommended 25% modeling uncertainty. The recast agrees very well with the results from the CMS displaced $e\mu$ search in the region of highest sensitivity, $300 \mu\text{m} \lesssim c\tau \lesssim 50 \text{ cm}$, but exhibits a moderate deviation on the tails. As this extremely low efficiency region is overly sensitive to the tails of the distribution, it may be the case that the sensitivity is slightly underestimated for lifetimes near 1 m or 100 μm , but this discrepancy typically has no qualitative impact on any application of the results.

5.4.2.1 Extrapolation to 13 TeV

We now show another reinterpretation example of the CMS displaced $e\mu$ in order to highlight the comparison between 8 [267] and 13 TeV [114] analyses. We compare in Figure 5.8 our reproduction of expected signal events with the published validation material for the 8 TeV version, and the partially-available validation material for the 13 TeV search. Information on efficiency maps from the 8 TeV analysis was needed to obtain an extrapolation to 13 TeV, as the 13 TeV maps are not yet public. As we can see, the 8 TeV recast for the CMS displaced lepton search [267] agrees very well in the region of highest sensitivity. The 13 TeV recasting, however, underestimates

the CMS values by a factor of two or more. This is likely due to the fact that the lepton efficiencies can not be directly extrapolated from 8 to 13 TeV, as assumed in Figure 5.8. Also, with the absence of a cutflow table, it is impossible to verify where the mismatch arises: if it is due to mis-modelling of the signal region cuts or indeed due to changes in the efficiencies.

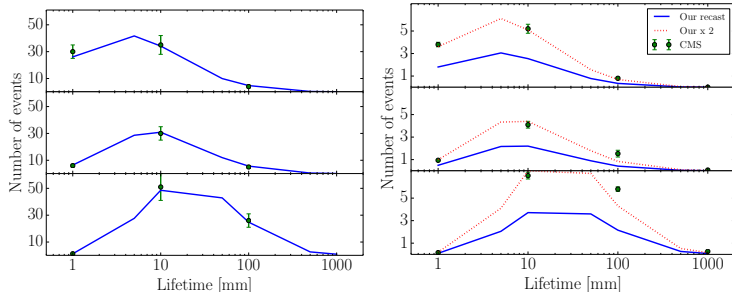


Figure 5.8: Number of expected events in the signal regions defined based on d_0 . The green points refer to the expected signal published by the analysis. **Left:** Validation for 8 TeV analysis. Production cross section assumed NLO+NLL value 85.6 fb for $M_{\tilde{t}_1} = 500$ GeV, BR = 0.33 in each ℓ -channel. **Right:** Validation for 13 TeV analysis. Production cross section assumed NLO+NLL value 67.0 fb for $M_{\tilde{t}_1} = 700$ GeV. The 13 TeV numbers are made using efficiency maps published for the 8 TeV search, as the 13 TeV maps are not yet public. Figures taken from [271].

Lessons learned

The selection and trigger efficiencies provided by CMS are very useful for recasting the 8 TeV CMS search for displaced leptons [267] and allow for a very good level of agreement. The main challenge, however, consisted in collecting all the available information, which was not provided by the main document in Ref. [267]. Furthermore, the corresponding information for the 13 TeV search is not publicly available and an extrapolation of the 8 TeV efficiencies was shown to be inadequate.

5.4.3 Displaced Jets

Searches for displaced jets are less straightforward to reinterpret than displaced leptons. Interest in accurate reinterpretation is increasing, as many new physics models are sensitive to this particular signature. The work in [5] explores long-lived particle (LLP) signatures for certain weak-scale models of baryogenesis [3, 272, 5], where the CMS search for displaced dijets [273] was reinterpreted.

This search uses a multivariate discriminant composed of observables that are challenging to model in Monte Carlo (MC), such as the track vertex multiplicity and the root-mean-square of a cluster track multiplicity variable. The reinterpretation approach in Ref. [5] was to construct track information at truth level based on the output of a parton shower program (such as PYTHIA 8), and then use the truth-level information to construct the various vertex, cluster, and track-level observables for each event. As it is difficult to adequately account for inefficiencies of track and vertex reconstruction, the efficiency of passing the cuts with truth-level

observables was considered and then it was normalized to the results from CMS. To do so, we simulated identical signal models to those with efficiencies reported by the CMS collaboration, assumed that the MC truth-level reconstruction gave an adequate description of kinematics but *not* track and vertex reconstruction, and so computed a ratio of truth-level efficiencies to those reported by CMS. Then we use these efficiency ratios to re-scale the truth-level results of other models, leading to a reinterpretation of the CMS search for different models beyond the ones they considered. The details can be found in Ref. [5].

To validate this approach, truth-level quantities for the models constrained in Ref. [273] were computed and compared to the numbers and distributions reported in Ref. [273]. For example, comparisons of the distributions of the observables going into the multivariate discriminant, as well as the output of the multivariate discriminant could be performed. While the truth-level distributions disagreed with those of CMS for individual observables, the actual multivariate discriminant output agreed with that of CMS at better than 25%. The ratio of truth-level efficiencies to CMS efficiencies are also compared for different LLP masses and kinematics, and these typically agree with one another at the factor-of-two level [5]. This suggests that this reinterpretation of the CMS results in terms of cross-section limits is likely accurate to the factor-of-two level.

Lessons learned

We find that a rather naïve truth-level reconstruction of the event could give a reinterpretation of cross-section limits to agree within a factor of two, provided the efficiencies were normalized to the experimental values using an overlapping set of signal models. One of the major obstructions to improving on the accuracy of the estimate was the model-dependence observed among the ratios of efficiencies. For instance, it was found that highly boosted models showed a much lower relative reconstruction rate in data vs. truth-level MC. Since pair production of LLPs was considered near threshold, this degradation in the performance of highly boosted LLPs is not particularly troubling. However, it does suggest that characterizing the effects of the particle boost are important for reinterpretation.

In addition, with a larger and more diverse set of signal benchmarks available, the prospects for the reinterpretation of search results are better. The reasons are twofold:

- Increasing the number of presented signal models by the collaboration allows for more cross-checks between MC and the results in data. This allows for more sophisticated tuning of models;
- Having a more diverse set of benchmark signal models means that it is easier to dis-entangle various kinematic effects on the efficiency (such as the LLP mass, boost, etc.) and find a signal

benchmark that most closely matches the model for which one wants to derive a limit.

5.4.4 Displaced Lepton-Jets

GC: Will include recast later, Michael agreed to contribute to this, awaiting for input.

5.4.5 Non-pointing Photons

The search for non-pointing photons produced in association with missing transverse energy (\cancel{E}_T) [182] plays an important role in probing beyond-the-SM (BSM) particles that decay to a SM photon and an invisible particle through a highly suppressed coupling. Beside the gauge-mediated supersymmetry breaking (GMSB) models [274], which were the main motivation for the non-pointing photon search, this type of signal can also appear in many hidden sector models. For example, in the dipole-mediated DM model (the Dark Penguin) [81], the production of two heavier dark fermions $pp \rightarrow Z^*/\gamma^* \rightarrow \chi_h \bar{\chi}_h$ is followed by the decays $\chi_h \rightarrow \chi_l + \gamma$. If the flavor structures of the DM mass and coupling are aligned, χ_h can be long-lived and give rise to non-pointing photons. Another example is provided by the dark shower scenario [275, 276] that explains the galactic center gamma-ray excess. In this model, many hidden pions can be produced in the same LHC event. Some of these have displaced decays to a pair of SM photons, while others decay outside of the detector, yielding \cancel{E}_T . Notice that in this case the topology of the events is different from the previous examples, as the non-pointing photons and \cancel{E}_T originate from separate particles.

In this note we describe a method to recast the bounds of Ref. [182] to a BSM scenario that is different from the GMSB model, using the Dark Penguin signal [81] as example.

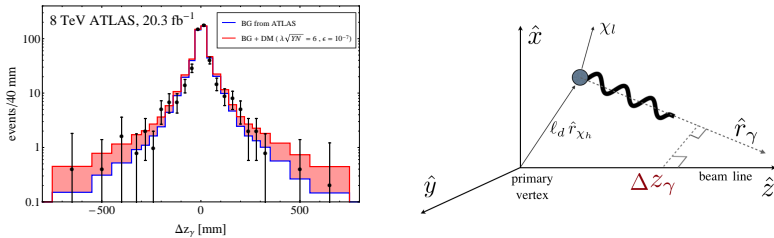


Figure 5.9: **Left:** the Δz_γ distribution of the non-pointing photon signals measured by ATLAS. The background reported by ATLAS (blue histogram) was obtained from a data-driven analysis, using diphoton events with $\cancel{E}_T < 20$ GeV. Also shown, stacked on top of the background (red histogram), is the signal distribution from the dipole-mediated DM scenario with $(m_{\chi_h}, m_{\chi_l}, M) = (300, 10, 300)$ GeV, $\lambda \sqrt{N}Y = 6$, and $\epsilon = 10^{-7}$. See Ref. [81] for more details. **Right:** the geometry of the displaced signals.

5.4.5.1 Calculation of the signal efficiency for the non-pointing photon search

We follow the non-pointing photon analysis in Ref. [182], performed by the ATLAS collaboration on about 20 fb^{-1} of 8 TeV data. In Ref. [182] delayed photons were also considered, but here we focus only on the measurement of the Δz_γ of non-pointing photons (see Fig. 5.9). For DM signals given by the long-lived $\chi_h \rightarrow \chi_l \gamma$ decay, Δz_γ can be related to the χ_h decay length ℓ_d in the lab frame:

$$\Delta z_\gamma = \ell_d \left(\hat{r}_{\chi_h,z} - \frac{\hat{r}_{\chi_h,T} \cdot \hat{r}_{\gamma,T}}{1 - (\hat{r}_{\gamma,z})^2} \hat{r}_{\gamma,z} \right) = \ell_d \left[\cos \theta_{\chi_h} - \cos(\phi_{\chi_h} - \phi_\gamma) \cot \theta_\gamma \sin \theta_{\chi_h} \right] \quad (5.6)$$

where $\hat{r}_{T,z}$ represent the transverse and longitudinal components of the unit vector \hat{r} , respectively, as shown in Fig. 5.9. To obtain the Δz_γ distribution of the DM decay, we first simulate the prompt process, $p p \rightarrow \chi_h \bar{\chi}_h, \chi_h \rightarrow \chi_l \gamma, \bar{\chi}_h \rightarrow \bar{\chi}_l \gamma$ in MadGraph5, then we apply the cuts performed in the ATLAS analysis, and finally reweight the events using the dark penguin form factors. Then we calculate the proper lifetime of χ_h and boost it to the lab frame using the momenta of each parton-level event. The angular information of the photon and χ_h allow us to calculate Δz_γ in Eq. (5.6) as a function of the decay length. Using this, each simulated MC event contributes to the differential cross section in Δz_γ as

$$\frac{d\sigma_{\text{displaced}}}{d\Delta z_\gamma} = \sigma_{\text{prompt}} \frac{dP}{d\Delta z_\gamma} = \sigma_{\text{prompt}} \frac{|\mu|}{2} e^{-\mu \Delta z_\gamma}, \quad (5.7)$$

where the μ characterizing the probability distribution $dP/d\Delta z_\gamma$ of the decay is defined as

$$\mu \equiv \frac{\Gamma_{\chi_h} m_{\chi_h}}{p_{\chi_h}} \left(\hat{r}_{\chi_h,z} - \frac{\hat{r}_{\chi_h,T} \cdot \hat{r}_{\gamma,T}}{1 - (\hat{r}_{\gamma,z})^2} \hat{r}_{\gamma,z} \right)^{-1}. \quad (5.8)$$

Summing the distributions derived from all the simulated events we obtain the differential cross section in Δz_γ , see Fig. 5.9.

The ATLAS search requires at least two loose photons with $|\eta| < 2.37$ and $E_T > 50 \text{ GeV}$. At least one photon is required to be in the barrel region $|\eta| < 1.37$. To avoid collisions due to satellite bunches, both photons are required to have an arrival time at the ECAL t_γ smaller than 4 ns, with zero defined as the expected time of arrival for a prompt photon from the primary vertex. We approximate t_γ with the time of flight of the χ_h , requiring it to be smaller than 4 ns. In our estimation we do not include the detailed isolation cuts on the photon. We also neglect the effect of the displaced decay on the angular acceptance of the photons, simply imposing the requirements on $|\eta|$ at the level of the prompt event. The signal region also requires $E_T > 75 \text{ GeV}$. Finally, to simplify the discussion we assume that every event has a reconstructed primary vertex in the geometrical center of the detector.

For events where only one photon satisfies $|\eta| < 1.37$ (i.e. it is in the barrel calorimeter), this photon is used for the measurement

of Δz_γ . For events where both photons are in the barrel, the photon with larger t_γ is used. We approximate this timing condition by taking the photon emitted by the more boosted χ_h , in which case the average decay is more delayed. In Fig. 5.9 the generated Δz_γ signal distribution is shown, on top of the expected background. The latter is taken from Fig. 4 of the ATLAS paper [182]. Because we are focusing on the non-pointing photon signals, to set constraints on the DM couplings in [81] we remove events with $|\Delta z_\gamma| < 30$ mm. In our exploratory analysis we only consider the statistical uncertainty on the background, neglecting the effect of systematics.

Lessons learned

The ATLAS paper gives detailed descriptions of the cuts and background analysis, which makes an approximate estimation of the signal efficiency quite straightforward.

The background analysis in Ref. [182] is based on a data-driven study, for which events passing the diphoton selection with $\cancel{E}_T < 20$ GeV are used as control region sample. It is challenging for theorists to simulate the background for different energy cuts. Especially for the \cancel{E}_T cut that plays a vital role in the DM and Hidden Valley searches.

In order to obtain a more precise result it would be useful if the ATLAS collaboration could provide the reconstruction efficiency of non-pointing photons as function of Δz_γ , or of the angle between the photon and the surface of the ECAL, a variable that may be relevant to the efficiency. The paper does provide a table of signal acceptance times efficiency for the GMSB SPS8 model, but it is not easy to apply those results to different new physics models.

It would also be very useful to have a table of background events for different cuts on \cancel{E}_T . For instance, for the Dark Penguin the typical \cancel{E}_T from the decay of $\chi_h \bar{\chi}_h$ with electroweak-scale m_{χ_h} can easily be higher than 100 GeV. By contrast, in the dark shower scenario where soft hidden pions decay to two SM photons, the \cancel{E}_T originating from additional late-decaying pions can be much lower than the 75 GeV cut used in the ATLAS analysis. Knowing the background and systematic uncertainty for different \cancel{E}_T cuts would be very important to constrain different models.

5.4.6 Disappearing Tracks

ZL: Awaiting input from Rakhi Mahbubani

5.4.7 Displaced Vertices

Displaced vertex searches differ from displaced jets and displaced leptons ones in the fact that actual reconstruction of a secondary vertex using track information is made. The lifetime of the LLP should allow it to decay either in the inner trackers or muon spectrometer of the LHC detectors, where vertexing is possible [144,

[113](#), [143](#), [152](#), [156](#), [167](#), [147](#)]. These searches have an extremely low background, as there are no irreducible contributions from the SM, making them sensitive to very small signals of new physics.

In this section we make the distinction when reinterpretation of displaced searches makes use of truth information to identify displaced decays and where an attempt to reconstruct them from displaced tracks is performed (with an approximate detector response).

5.4.7.1 Truth Level Displaced Vertices

The work in [5] reinterpreted the 8 TeV ATLAS search for a displaced muon and a multi-track vertex ($DV+\mu$) [\[277\]](#), where long-lived particle signatures for certain weak-scale models of baryogenesis [\[3, 272, 5\]](#) were explored. For reinterpreting this search, a similar procedure described in the displaced jets section [5.4.3](#) of constructing ratios of truth-level vs. ATLAS efficiencies for the ATLAS multi-track vertex analysis [\[277\]](#) was performed, with similar results for the validation being correct within approximately a factor of two.

This $DV+\mu$ analysis has since been superseded by [\[113\]](#), where a displaced vertex is looked for at 8 TeV in association with either a muon, electrons, jets and missing transverse momenta. Recently, an updated ATLAS paper [\[144\]](#), which looks for multi-track displaced vertices at 13 TeV in association with large missing transverse momenta, was made public. This search now includes a prescription using parametrized efficiencies as a function of vertex radial distance, number of tracks and mass. Their prescription can be applied to vertices and events passing certain particle level acceptance requirements using the truth MC event record.

Here we validate the prescription with parametrized selection efficiencies in [\[144\]](#)⁹. The results of this search are interpreted by ATLAS in a split SUSY simplified model with a long-lived gluino that hadronizes forming an R -hadron before decaying, $\tilde{g} \rightarrow q\bar{q}\tilde{\chi}_1^0$. Event samples are generated with Pythia 8.2 [\[138\]](#). We use truth level missing transverse momenta and we identify the truth R -hadron decay position and decay products, as the ATLAS collaboration provides selection efficiencies that can be directly applied to this truth level quantities. These efficiencies can be found in the auxiliary material in [\[278\]](#), and are given at the event-level as a function of the truth missing transverse momenta and displaced vertex radial distance, and at the vertex level parametrized as function of vertex invariant mass and number of tracks, and are given for different detector regions, encapsulating also the effect of the material veto cut.

The selection of events used for the signal region requires:

- truth level missing transverse momenta > 200 GeV.
- one trackless jet with $p_T > 70$ GeV, or two trackless jets with $p_T > 25$ GeV. A trackless jet is defined as a jet with $\sum_{tracks} p_T < 5$

⁹ This prescription is also validated in Ref. [\[271\]](#).

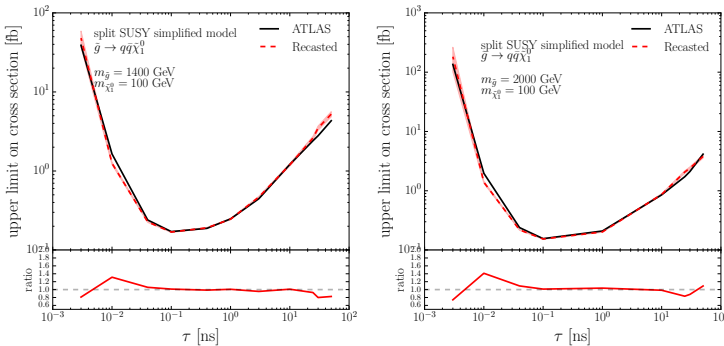


Figure 5.10: Comparison of our recast and ATLAS [144] on the upper limit in the gluino production cross section against its proper lifetime [271].

GeV.

In addition, events must have at least one displaced vertex with:

- transverse distance between the IP and the decay position > 4 mm.
- the decay position must lie in the fiducial region $r_{DV} < 300$ mm and $|z_{DV}| < 300$ mm.
- the number of selected decay products must be at least 5, where selected decay products are charged and stable, with $p_T > 1$ GeV and $|d_0| > 2$ mm.
- the invariant mass of the truth vertex must be larger than 10 GeV, and is constructed assuming all decay products have the mass of the pion.

Applying these cuts and efficiencies, we get event-level efficiencies for two of the benchmarks, where the gluino mass is 1400 GeV or 2000 TeV (and the neutralino mass is fixed to 100 GeV). Based on the efficiencies obtained and the estimated number of background vertices, we can extract 95% CL upper limits on the total visible cross section for the two gluino masses. For reference, assuming 100% efficiency, we get an upper limit of 0.091 fb. The curves in Figure 5.10 show our recasting results compared to ATLAS. The level of agreement is very good, within 20% for most of the lifetime values. We also point out that the recasting limits agree well even for regions where the efficiency is very low ($\tau > 10$ ns and $\tau < 10^{-2}$ ns).

5.4.7.2 Displaced Vertex Reconstruction

Before parametrized efficiencies applicable for truth-level displaced vertices were made public, attempts to recast displaced vertex searches were made by performing their reconstruction from charged tracks only, with an approximate detector response. In Ref. [279] the ATLAS DV+jets multitrack analysis [113] was recasted. Reinterpretation was performed using generator-level

events and the detector fiducial region was reproduced as well as possible. The jets are clustered according to the anti-kt prescription in the analysis with momentum smearing (this is validated by reproducing the jets+MET exclusion curve of prompt searches). The selection of events used for the signal region (and the approximations to real detector simulation) were as follows:

DV jets	4 or 5 or 6 jets with $ \eta < 2.8$ and $p_T > 90, 65, 55$ GeV, each
DV reconstruction*	DV made from tracks with $p_T > 1$ GeV, $ \eta < 2.5$ and $ d_0 > 2$ mm. Vertices within 1 mm are merged. Note: a tracking efficiency needed here; we assume a functional form given by equation 5.9
DV fiducial	DV within $4 \text{ mm} < r_{\text{DV}} < 300 \text{ mm}$ and $ z_{\text{DV}} < 300 \text{ mm}$
DV material*	No DV in regions near beampipe or within pixel layers. Discard tracks with $r_{\text{DV}}/\text{mm} \in \{[25, 38], [45, 60], [85, 95], [120, 130]\}$.
N_{trk}	DV track multiplicity ≥ 5
m_{DV}	DV mass > 10 GeV

Table 5.5: Implementation of cuts applied in the ATLAS multitrack DV + jets search, from Ref. [113]. * These are approximations to the experimental analysis in the absence of the full detector simulation.

A tracking efficiency of the form

$$\varepsilon_{\text{trk}} = 0.5 \times \left(1 - \exp\left(\frac{-p_T}{4.0 \text{ GeV}}\right)\right) \times \exp\left(\frac{-z_{\text{DV}}}{270 \text{ mm}}\right) \times \max(-0.0022 \times \frac{r_{\text{DV}}}{1 \text{ mm}} + 0.8, 0), \quad (5.9)$$

is used, where r_{DV} and z_{DV} are the transverse and longitudinal distance of the track's production vertex (same as displaced vertex origin when using truth-level generator information). This functional form is designed to take into account the size of the detector (linear dependence on r_{DV} , exponential on z_{DV}), as well as a turn-on like feature dependent on the p_T of the track. It reproduces the overall behavior of efficiency falling off with vertex displacement. The parameters were determined by fitting the efficiency curve (with lifetime dependence), for three benchmarks in the analyses. We find that fitting only one benchmark does not correctly reproduce the efficiency curve for any of the others. This is most likely due to insufficient dimensionality of the efficiency map. We expect that a full tracking efficiency parametrisation depends not only on r_{DV} , z_{DV} and p_T , but also transverse and longitudinal impact parameters (d_0, z_0), and on charge and pseudorapidity of the track. Furthermore, we expect a vertex efficiency that depends on the topology of the event and the nature of the particles forming the vertex. The fit for the event efficiencies from this tracking function can be seen in Figure 5.11.

Lessons learned

With a larger and more diverse set of signal benchmarks the

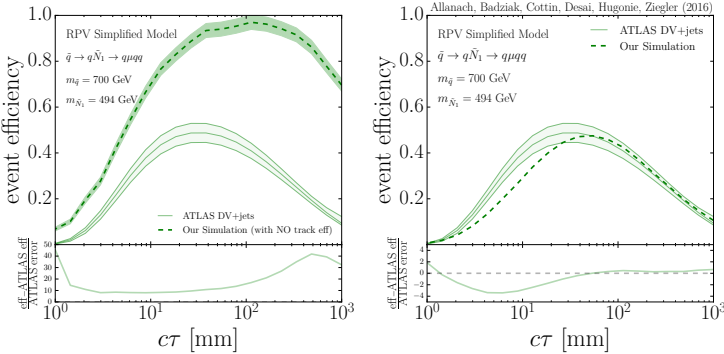


Figure 5.11: Validation of the DV + jets search for the ATLAS benchmark of a simplified RPV model with a 700 GeV squark decaying to a neutralino, $\tilde{q} \rightarrow q(\tilde{N}_1 \rightarrow \mu\bar{\nu})$. **Left:** without any tracking efficiency. **Right:** with a tracking efficiency function given by equation 5.9, taken from Ref [279].

prospects for reinterpretation are better. For example, the ATLAS analysis examined in [277] only showed limits for three signal model benchmark points for which efficiencies were shown, making it challenging to find a benchmark whose kinematics matched the desired signal models for the reinterpretation in Ref. [5]. Because the efficiencies and limits were shown for either a high-mass, low-boost LLP or a low-mass, high-boost LLP, this made it more challenging to reinterpret the results for other types of kinematics.

The new parametrized efficiencies presented by ATLAS in [278] are extremely useful. They constitute an optimal efficiency map for recasting these type of analyses, as they can be applied in a straightforward way to truth level quantities. Before this information was public, efficiency tables (for vertex-level efficiency) in terms of r_{DV} where only available for few channels and for a single benchmark. It was not clear how to translate it to other channels, and also for parent particles of a different mass. Even more, a functional parametrization for track efficiency was needed (as shown in [279]) to be able to reproduce the experimental results. Finding this kind of parametrization is not easy, as it needs to be validated across different benchmarks. This had the difficulty that fitting only one benchmark did not correctly reproduce the event-level efficiency curve for any of the others.

5.5 Handling long-lived particles in DELPHES-based detector simulations

5.5.1 Long-lived particle simulation in DELPHES 3.4.1

The DELPHES package [250] allows for the generic simulation of the response of a typical detector used in high-energy physics experiments. It is widely used for simulating the effects of the ATLAS and CMS detectors or the hypothetical detectors that could be used for the future FCC and CLIC projects. The architecture of DELPHES is composed of distinct and specialized modules that interact with

each other. The detector is described by the user through an input card, where the modules to be used in the simulation are sequentially enumerated and their input parameters are specified.

The detector simulation relies on a mix of parametric and algorithmic modules. More precisely, tracking is simulated through efficiency and smearing functions that are applied to the properties of the electrically-charged stable particles. The particles are then propagated to the calorimeters and dedicated modules simulate the energy deposits in the electromagnetic and hadronic calorimeters. The output of such step consists in a list of calorimetric towers. Moreover, **DELPHES** includes a particle-flow like algorithm that combines tracking and calorimetric data in order to improve the identification of the final-state objects and the resolution on their reconstructed momenta.

Jet clustering is performed via an internal call to the **FASTJET** package [280] which takes as input the list of calorimeter towers or, alternatively, the particle-flow candidates and outputs jet objects. Lepton and photon isolation is then handled through a specific isolation module. Finally, **DELPHES** takes care of removing the double-counting of objects that could be simultaneously identified as element of different collections. The final output is stored in a **ROOT** file.

In addition, **DELPHES** allows for the simulation of pile-up effects by superimposing minimum-bias events attached to displaced interaction vertices to the hard scattering event. Procedures mimicking pileup removal can then be configured in the input card. The subtraction of the charged particles belonging to pile-up vertices is performed at the tracker level. Neutral particles are removed by applying the jet area method [281] supplied within the **FASTJET** package. More advanced methods are also available in **DELPHES**, such as the **PUPPI** [282] or **SOFTKILLER** [283] techniques, and they can easily be added to the input card. The loss of performance originating from pile-up, in particular relative to the isolation, is automatically accounted for.

The official **DELPHES** package (version 3.4.1) with the default detector cards needs to be adapted for the proper handling of long-lived particles (LLP). By default, the decay products of a long-lived particle enter the simulation as if the corresponding decay would have occurred within the tracker volume. However, the user has the possibility to define a volume in which the particle can decay and still be detected outside the tracker volume. This is achieved in practice by making use of the **RadiusMax** parameter of the **ParticlePropagator** module, that is by default set to the tracker radius stored in the **Radius** parameter. When setting the **Radius** and **RadiusMax** parameters to different values, the particles decaying outside the tracker volume, but inside the ‘decay volume’ of radius **RadiusMax**, are included in the collection of stable particles stored in the output **Root** file. They can in this way be used for an offline, more correct, treatment.

Moreover, several modules that are not used in the default ATLAS and CMS cards could serve for a better simulation of the long-lived particles in **DELPHES**. For instance, the `TrackSmearing` module allows the user to smear the track momentum according to the impact parameter in the transverse plane (*i.e.*, the d_0 parameter) and in the longitudinal plane (*i.e.*, the d_z parameter).

By default, the detector simulation in **DELPHES** totally ignores the presence of any long-lived particle. While this is convenient for neutral particles like a neutralino which could be considered as invisible from the detector standpoint, a charged particle leaves tracks in the tracker and would interact with the calorimeters if its lifetime is large enough. In this case, if the long-lived particle decays inside the tracker, its trajectory is properly propagated to the calorimeters and the displaced vertex is correctly accounted for. However, if the long-lived particle decays outside the tracker, its decay products are ignored in **DELPHES**, unless the `RadiusMax` parameter has been specified to be larger than the tracker `Radius` parameter. In this case the decay products can be found in the `Delphes/stableParticles` output collection and treated with adequate smearing functions and efficiency directly from the **DELPHES** output.

Finally, disappearing tracks are simply treated as missing energy in **DELPHES**. Emerging tracks or tracks containing kinks are not treated appropriately, in the sense that the parameterizations required for a proper description of such signatures has not been implemented yet. Also, **DELPHES** does not include any trigger simulation, and the latter is in general complex in the case of long-lived particles.

5.5.2 Displaced tracks with the MADANALYSIS 5 tune of **DELPHES**

The so-called **DELPHES-LLP** package can be installed from the version v1.6 of **MADANALYSIS 5** [284, 246] and contains improvements of **DELPHES** specific to long-lived particles. It consequently opens the door for phenomenological investigations of long-lived particles and the recasting of related LHC analyses. More information is available on the web page:

<https://madanalysis.irmp.ucl.ac.be/wiki/MA5LongLivedParticle>

This new package was designed to handle neutral long-lived particles that decay into leptons within the tracker volume. Realistic efficiencies are applied to the displaced tracks and several parameters specific to this kind of analyses have been made available within **MADANALYSIS 5**. An extension to the case of neutral long-lived particles decaying into muons outside the tracker volume can be easily implemented, the muons being thus reconstructed only through their hits in the muon chambers. The simulation of the displaced leptons is performed through efficiencies and resolution functions to be specified by the user. Furthermore, another extension allowing to handle long-lived charged particles that decay into leptons could be implemented.

The **DELPHES**-LLP package contains a new module called **MA5EfficiencyD0** that allows for the definition of a track reconstruction efficiency parameterized as a function of the d_0 and d_z parameters (named `d0` and `dz` in the **DELPHES** input card). The default efficiency function, specified via a `DelphesFormula` is taken from the 8 TeV tracking performance of CMS [267],

<https://twiki.cern.ch/twiki/bin/view/CMSPublic/DisplacedSusyParametrisationStudyForUser>,

```
set EfficiencyFormula {
  (d0<=20) * (-5.06107e-7 * d0**6 + 0.0000272756 * d0**5 - 0.00049321 * d0**4
    + 0.00287189 * d0**3 + 0.00522007 * d0**2 - 0.0917957 * d0 + 0.924921) +
  (d0> 20) * (0.00)
}
```

In addition, the data-format of **DELPHES** has been extended so that the **Muon** and **Electron** classes now include the transverse (d_0) and longitudinal (d_z) impact parameters relative to the closest approach point (encoded in the `d0` and `dz` variables), the coordinates of the closest approach point (x_d, y_d, z_d) (encoded in the `xd`, `yd` and `zd` variables) and the four-vector of the vertex from which the lepton is originating from (t_p, x_p, y_p, z_p) (encoded within the `tp`, `xp`, `yp` and `zp` variables), the latter quantity being evaluated from Monte Carlo information.

Region	$c\tau_{\tilde{t}}$ [cm]	MA5	CMS	Difference [%]
SR-1	0.1	3.89	3.8	2
	1	4.44	5.2	15
	10	0.697	0.8	15
	100	0.0610	0.009	> 100%
SR-2	0.1	0.924	0.94	2
	1	3.87	4.1	5
	10	0.854	1.0	15
	100	0.0662	0.03	~ 100%
SR-3	0.1	0.139	0.16	15
	1	6.19	7.0	10
	10	4.45	5.8	25
	100	0.497	0.27	85

Table 5.6: Number of events populating the three signal regions (SR-1, SR-2 and SR-3) of the CMS-EXO-16-022 analysis for different stop decay lengths ($c\tau_{\tilde{t}}$). We compare the CMS and **MADANALYSIS 5** (MA5) results in the second and third column of the table, respectively, and the difference taken relatively to CMS is shown in the last column.

Consequently, the data-format of **MADANALYSIS 5** has been extended, so that the **Muon** and **Electron** classes now contains the `d0()` and `dz()` methods allowing to access the value of the d_0 and d_z parameters, the `closestPoint()` method that returns the coordinates of the closest approach point (through the `X()`, `Y()` and `Z()` daughter methods) and the `vertexProd()` method that returns coordinates of the displaced vertex from which the lepton originates from (through the `X()`, `Y()` and `Z()` daughter methods). An

analysis example can be found in the public analysis database of **MADANALYSIS 5**,

<http://madanalysis.irmp.ucl.ac.be/wiki/PublicAnalysisDatabase>

where information about the re-implementation in **MADANALYSIS 5** of the CMS-EXO-16-022 [285] analysis of 2.6 fb^{-1} of 13 TeV LHC data is available. This is a search for long-lived particles decaying into electrons and muons, where signal events are selected by requiring the presence of either an electron or a muon whose transverse impact parameter lies between $200 \mu\text{m}$ and 10 cm . For a given benchmark signal where a pair of long-lived stops is produced through usual QCD interactions and where each stop further decays into a displaced b -jet and a displaced lepton. In Table 5.5.2, we present the number of events surviving the selection of the three different signal regions of the CMS analysis. Our event generation has been performed with **PYTHIA 8** [127] and for the benchmark scenario SPS 1a. We observe that a good agreement is obtained, except in the case of a long stop lifetimes, $c\tau \gtrsim 1\text{m}$. This is however the region in which no public information on the CMS reconstruction efficiencies is available.

The **MADANALYSIS 5** tune of **DELPHES** has neither been designed for disappearing (or appearing) tracks nor for track kinks. Concerning the disappearing (or appearing) tracks, the only missing experimental ingredients are the track reconstruction efficiency and resolution as a function of the number of missing hits in the (inner) outer layers of the tracker. There is to this date no public material on the tracking performance description related to track kinks.

5.5.3 What about other LLP signatures?

In this section, we briefly discuss how **DELPHES** could be improved for a better handling of LLP signatures.

5.5.3.1 Displaced jets

Displaced jets are jets that are reconstructed either from standalone calorimeter information, or from the particle-flow input with a minimum requirement on the multiplicity of tracks with high transverse displacement (see Ref. [152]). Conceptually, such jets can be handled in **DELPHES** provided that the displaced tracks are properly parameterized. As described above, a module designed to smear the full set of track properties, including their transverse and longitudinal displacement, exists (*i.e.*, the `TrackSmearing` module). In addition, efficiencies based on displacement parameters have already been implemented in **MADANALYSIS 5** (see above) and a module that performs the matching of an existing jet collection with a track collection based on track displacements is very similar to the already existing `TrackCountingBTagging` module. Minor modifications to this module are hence needed to be able to select tracks based on an absolute displacement instead of the impact parame-

ter significance. Finally, in order to be able to perform a displaced jet selection, one would need a (not-yet existing) module that performs jet clustering on the basis of the secondary vertices based and the displaced tracks matched with these jets. Alternatively, a module that includes a vertex reconstruction efficiency and a module including a vertex position smearing could be implemented.

5.5.3.2 *Displaced vertices*

The missing modules described in Section 5.5.3.1 could perfectly serve the purpose of a displaced vertex analysis. Provided that tracking efficiencies and resolutions are available as a function of the full set of tracking parameters (d_0 , d_z , p_T , ϕ , and θ) and, eventually, of the Monte Carlo truth vertex position, a simple vertexing algorithm can be implemented in DELPHES.

5.5.3.3 *Discussion: DELPHES versus a specific parametric simulation*

In a fully parametric simulation of the detector, the detector effects are encoded in terms of efficiencies and resolution functions. Such type of simulation is typically very fast, but is likely to suffer from a lack of accuracy in the modeling of complex observables such as jet properties and missing energy. The DELPHES simulation is an admixture of such a parametric simulation, and of an algorithmic one. This is slower, but has the clear advantage of correctly treating in particular the reconstruction of the jets and the missing energy.

In order to be able to answer whether DELPHES should be used, instead of a fully parametric simulation, to perform the recasting of long-lived particle analyses, further studies are needed. In the meantime, the following guidelines could be used. If the signal selection is based only on displaced tracks, a simple parametric simulation should in principle be sufficient. This simulation could encapsulate the track reconstruction efficiency and resolution, including pile-up effects. DELPHES could then optionally be used to mix the resulting "reconstructed" tracks with the additional tracks originating from the pile-up vertices. On the other hand, if the analysis under consideration additionally uses calorimetric information (*i.e.*, jets or missing energy), DELPHES should be preferred to a fully parametric framework. However, a precise quantification of these effects cannot be assessed without detailed comparative studies between the two approaches. Finally, it should be pointed out that neither of these techniques can be used to correctly simulate the instrumental background.

5.6 *Recasting Inside the Experimental Collaborations*

Reinterpretations performed within the experiments themselves present unique advantages and disadvantages. They allow for thorough and consistent treatment of detector effects and geometry, object reconstruction, and systematic uncertainties in a way which

is impossible through external recasting. Groups can share resources and easily communicate all necessary details. On the other hand, they are of course limited to the model(s) chosen for reinterpretation. In the ideal situation, reinterpretation(s) which provide meaningful results can be performed with minimal overhead to a given analysis.

5.6.1 The RECAST Framework

GC: Lukas agreed to prepare written contribution, awaiting input

5.7 Reinterpretation with Prompt Analysis

Depending on the lifetime, a part of the LLP decays will always happen outside the detector, leading to a \cancel{E}_T signature if the LLP is electrically and color neutral. Likewise, some part of the LLP decays will always appear “promptly”. Prompt searches with and without \cancel{E}_T can therefore provide additional, corroborating constraints on models with LLPs. Therefore, it is important to understand the sensitivity of prompt searches to displaced objects.

Reinterpreting prompt searches in the context of LLPs is, however, quite nontrivial, because not all prompt searches make explicit requirements on the primary vertex. Moreover, it is not documented how reconstruction efficiencies drop as a function of small displacement. Thus, the reinterpretation of prompt searches in the context of LLPs is currently best done within the collaborations themselves.

5.7.1 An Experiment-Internal Example

An example of an experiment-internal reinterpretation can be found in a CMS search for an RPV SUSY model where pair-production of stops each proceed through an R-parity violating decay to a b quark and a lepton. A dedicated long-lived search for this model exists in the $e - \mu$ channel [114]. This search includes selection criteria which require the transverse impact parameter to the interaction point be greater than $10\mu\text{m}$. This maximizes sensitivity to the long-lived model and greatly reduces standard model backgrounds. It also necessarily highly reduces the sensitivity of the search at low stop lifetime. The exclusion curve in the stop lifetime ($c\tau$) vs. top squark mass is shown in the left frame of Figure 5.12.

A reinterpretation was performed by a search for pair-production of second generation leptoquarks (LQs) [286]. In this model, massive leptoquarks are pair-produced. Each of these bosons then decay to a muon and c quark, leading to a final state with two muons and two jets from c quarks. In the prompt limit of the RPV SUSY model with a final state of two muons and two jets from b quarks, the kinematics of the LQs is nearly identical. In the LQ search, no selection is made on jet flavor. The LQ search uses final selections which are optimized to the event kinematics for each LQ mass

hypothesis, but the search in general strives to remain as model-independent as possible. In this case, the reinterpretation was simply performed using the original LQ analysis, and replacing the signal samples with the long-lived RPV samples, only taking into account the reduced branching fraction to the two muons, two jets final state. The expected and observed exclusion curves of the reinterpretation are shown in the right frame of Figure 5.12, with the observed limit of the dedicated search overlaid in red.

The reinterpretation gives large improvement for lifetimes $\leq 1\text{mm}$, and as expected, contributes little in the large lifetime limit. This type of reinterpretation is valuable not only because it extends coverage of a given model, but also because it helps guide the analysts performing the dedicated search to focus their efforts in areas which are truly uncovered.

Reinterpretations like this one, which provide meaningful results without placing a large burden on analysis teams, should be highly encouraged.

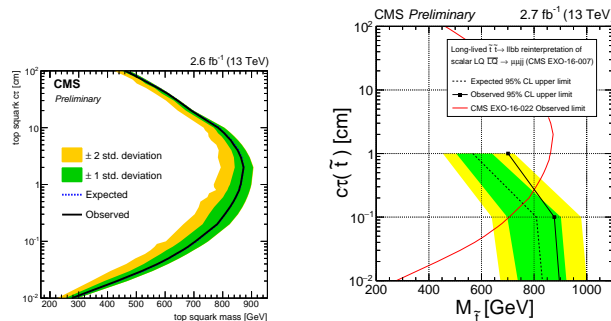


Figure 5.12: **Left:** Expected and observed 95% confidence level limits in the $c\tau$ - $M_{\tilde{t}}$ plane from the displaced lepton search [114] for pair-production of long-lived stops decaying to b quarks and leptons. **Right:** Exclusion in the $c\tau$ - $M_{\tilde{t}}$ plane from the prompt reinterpretation of pair-production of long-lived stops decaying to b quarks and leptons [286]. Exclusion from the dedicated long-lived search in Ref. [114] is overlaid with a solid red line [287].

5.8 Our Proposals for the Presentation of Results

Here we summarize the recommendations for the presentation of long-lived particles search results. These recommendations follow from the detailed examples presented in Sections 5.3 and 5.4.

Our primary recommendation is that the experiments provide as detailed information as possible to make a generic recasting possible. We therefore encourage the experiments to:

- A.1. Provide LLP reconstruction and selection efficiencies at the signature or object level. Although the parametrization of efficiencies is strongly analysis dependent, it is of advantage if they are given as a function of model independent variables (such as function of displaced vertex p_T , η , etc.), so they do not rely on a specific LLP decay or production mode;

- A.2. Present results for at least two distinct benchmark models, with distinct event topologies, since it greatly helps validating the recasting. For clarity, the input cards for the benchmark points should also be provided;
- A.3. Present cut-flow tables, for both the signal benchmarks and the background, since these are very useful for validating the recasting;
- A.4. When an analysis is superseded, differences and commonalities with previous versions of the same analysis should be made clear, especially if the amount of information presented in both analysis differs. The understanding to which extent the information presented in an old version can be used directly in a later version greatly helps the recasting procedure;
- A.5. Provide all this material in numerical form, preferably on HEPdata, or on the collaboration wiki page.

We realize that the above requires an enormous amount of time and effort by the collaborations and may not be always feasible to full extent. However, good examples of presentations are already available, such as the parametrized efficiencies provided by the ATLAS 13 TeV displaced vertex [144] (see auxiliary material on [278]) and the CMS 8 TeV heavy stable charged particle [252] analyses.

When object- or signature-level efficiency maps are not feasible, providing efficiencies for a large, diverse array of simplified models can be useful for re-interpretation. With respect to simplified-model results we recommend that the experiments:

- B.1. Provide signal efficiencies (acceptance times efficiency) for simplified models and not only upper limits or exclusion curves;
- B.2. Present efficiency maps as a function of the relevant simplified model parameters, such as the LLP mass and lifetime, with sufficient coverage of the simplified model parameter space. While for direct production of LLPs the parameter space is 2-dimensional (LLP mass and lifetime), simplified models with cascade decays have a higher dimensional parameter space. In these cases we strongly recommend efficiencies to be provided for a significant range of *all* the parameters;
- B.3. Release the efficiencies in digital format (on HEPdata or on the collaboration wiki page), going beyond the 2-dimensional parameterization suitable for paper plots whenever necessary;
- B.4. Consider a range of simplified models which aim to encompass:
 - (a) Different multiplicities of final-state particles, to allow ready re-interpretation of the limits for both 2-body and 3-body decays, which are qualitatively different;
 - (b) Different LLP boosts (for example, provide efficiencies and limits for distinct parent particle masses, which decay to the LLP);

Although extensive, the above recommendations for the choice of simplified models allow for a thorough comparison between the

range of validity of the LLP analyses and a detailed test of recasting methods. Furthermore, when a Monte Carlo based recasting is not available, one can use the “nearest” simplified model or a combination of them to estimate the constraints on the theory of interest. Finally, if a large enough spectrum of simplified models is covered, this can be useful for fast testing of complex models which feature a large variety of signatures, and quickly finding the interesting region in a model scan before going to more precise but computationally more expensive Monte Carlo simulation.

We hope that our recommendations, in particular points A.1–A.5, will serve as a guide for best practice and help establish a reliable and robust re-interpretation of LLP searches. The added value for the experiments, and the whole HEP community, will be a fast and more precise feedback on the implications of the LLP results for a broad range of theoretical scenarios.

6

Frontiers: Dark Showers and Quirky Signatures

A short section (3-5 pages?) outlining how dark showers don't easily fall into existing simplified models or experimental search programs. Give a few examples of specific models (emerging jets model, 1-2 others) as well as some concrete experimental methods being used now. This should motivate and lead into the work of the Dark Showers WG, although if they have concrete results by the time the white paper goes out we can include those.

6.1 Dark Showers

6.2 Quirks

7

Conclusions

Conclude and finish.

Acknowledgements:

A

Appendix: Discussion of Backgrounds for LLP Searches

A.1 Introduction

A.2 Known long-lived particles

Weak decays of SM particles normally have displaced vertices at the boosts typically encountered at the LHC. The searches for signature at low enough LLP mass and lifetime suffer from large backgrounds due to displaced SM decays. One simple example is found in the search for long-lived dark photons [163] decaying to $\mu^+ \mu^-$, which drastically loses sensitivity when getting too close to the $K_S \rightarrow \pi^+ \pi^-$ invariant mass despite the very low $\pi \rightarrow \mu$ mis-ID.

Decays of b-hadrons give displacements of few millimetres and can be indistinguishable from a LLP with mass few tens of GeV decaying to a pair of jets. Requiring a large track multiplicity of the displaced vertex and performing a mass fit to the dijet invariant mass can help to significantly reduce the effect of this background (see for example [152, 147]. Backgrounds from heavy flavours are typically more abundant in the forward region (e.g. if the signature searched is a LLP from a SM Higgs decay). However, the LHCb forward detector, being designed to study these SM decays, typically is also capable of rejecting them more effectively.

A.3 Real particles generated in the detector

Interactions of particles produced in the pp collision with nuclei of the detector material can give displaced vertices and fake a LLP signal. Vertices from these interactions will be positioned in the detector material volume and are therefore effectively vetoed by using detailed material maps.

LHC detectors have developed tools internal to the collaborations to define a material volume to be vetoed. Maps from ATLAS and CMS obtained with data collected in 2010 can be found in [Aaboud:2016poq] and [CMS:2010nua] and are valid for the Run 1 configuration. More recent maps for the Run 2 detectors configurations can be found in [144] and [CMSmaterial] for ATLAS and CMS, respectively.

LHCb recently developed a precise material map of the Vertex

Locator (VELL) using beam-gas collisions. This type of collisions is mostly free from long-lived heavy flavour background and allows to cover precisely the whole VELO geometry, not only the region close to the interaction point. This map was used to veto photon conversions to dimuons, which is the main background affecting displaced dark photon searches at low mass [163]. As a rule of thumb, LHCb material interaction background is dominant for vertices at a distance from the beam axis larger than 6 mm (where the VELO material begins). Below 6 mm the background is dominated by heavy flavour decays [225].

The LLP community is interested in using public tools for material maps of LHC experiments to improve the reliability of sensitivity studies to signatures with displaced vertices. The availability of such tools in fast parametric simulations such as Delphes [250] could be very interesting.

A.4 Real particles generated outside the detector

There are several types of real particles generated outside the detector that could be sources of background in a LLP search.

A.4.1 Cosmic muons

For example, cosmic rays from the atmosphere could enter the detector as cosmic-ray muons. These cosmic-ray muons could be reconstructed as displaced muons in the muon system or as displaced jets in the calorimeters. If cosmic-ray muons are reconstructed in the muon systems, they will typically appear as two back-to-back muons with ϕ values near $\pm\pi/2$. The rate of cosmic muons in the detector is about 500 Hz at L1, but depending on the HLT path and the offline selection used, the rate of cosmic-ray muons entering a given LLP analysis is generally much less.

Cosmic-ray muons are typically an important background source to consider for displaced signatures, especially those with large displacements [Chatrchyan:2012dxa, Khachatryan:2010uf, Aad:2012zn, 202, 201]. Cosmic-ray muons are generally only an issue for CMS and ATLAS analyses, but not for LHCb analyses, since LHCb has only forward coverage.

For many analyses, cosmic-ray muons can be rejected with a simple veto on back-to-back dimuons. However, in some analyses, this veto is not optimal for the signal acceptance or it is insufficient. Another often-used way to minimize the contribution from cosmic-ray muons is requiring high-momentum muons and/or high-energy jets, since cosmic-ray muons have a falling p_T spectrum. In addition, if a search primarily looks for inner-tracker or calorimeter objects, cosmic-ray-muon events can be rejected by requiring little muon system activity [Chatrchyan:2012dxa, Khachatryan:2010uf, 202].

If the cosmic-ray muon background is significant for an analysis,

it can be estimated using data from dedicated cosmic data-taking runs or from empty bunches in pp collision runs [[Chatrchyan:2012dxa](#), [Khachatryan:2010uf](#), [202](#)]. Cosmic-ray-muon simulations can be made, but in many LLP analyses, a data-driven approach is favoured. Timing information in the calorimeters or the muon systems can be used to discriminate the signal from cosmic-ray muons, sometimes in conjunction with impact parameter variables.

A.4.2 Beam halo

Another type of real particle generated outside the detector that could be a significant source of background for LLP searches is beam halo. Beam halo is produced when protons from the LHC beam scatter off the LHC collimators and produce debris, which can appear in the detector. Beam halo can create energy deposits in the calorimeters or hits in the muon system, both of which would be largely in the beam direction. These energy deposits or muon system hits would appear earlier than if they had been made from particles coming from the collision (see [FIXME:](#)). Beam halo is usually not modelled in MC simulation, since it is highly dependent on the beam parameters.

Beam halo is most relevant for searches for displaced signatures without tracks in the inner tracker and for searches for decays in non-collision bunches (stopped particles) [[Chatrchyan:2012dxa](#), [Khachatryan:2010uf](#), [202](#)].

The contribution from beam halo can often be reduced by requiring high-momentum or high-energy reconstructed objects. One can also decrease the number of beam halo events by requiring central objects or vetoing forward muon system activity, since beam halo is usually in the very forward direction [[Chatrchyan:2012dxa](#), [Khachatryan:2010uf](#), [202](#)]. For inner tracker-based signatures, events from beam halo are rejected by requiring a minimum number of early hits.

Beam halo background can be estimated by using data control regions near $\phi = 0$ and π . One could also identify cells with a low number or zero tracks that are assigned an early time.

A.4.3 Cavern radiation

There could also be radiation from the cavern walls, which might be a significant background in a LLP search. Cavern radiation is usually not modelled in MC simulation.

Cavern radiation is most relevant for searches looking in non-collision data, that is, stopped-particle searches, and for searches using muon system information to form tracks and vertices.

Cavern radiation can be estimated from data by collecting events triggered by random triggers when there are no collisions. It can also be estimated by overlaying a cavern radiation simulation with minimum-bias events from data.

A.5 *Fake particle signatures*

Another type of background for LLP searches is that from signatures that mimic real particles in the detector, but are in fact fake. By this, we mean the contribution from spurious detector noise. Noise appears differently depending on the detector, but in general, it is characterized by a single and concentrated energy deposit or hit that does not correspond in time or space to any other energy deposits or hits in the detector. Noise is usually difficult to model with MC simulation.

Calorimeter detector noise is most relevant for searches looking in non-collision bunches and low-energy collisions [[Chatrchyan:2012dxa](#), [Khachatryan:2010uf](#), [202](#)]. Muon system noise is most relevant for searches that are also highly affected by cosmic-ray muons.

Calorimeter noise can be rejected by vetoing single and concentrated energy deposits [[Chatrchyan:2012dxa](#), [Khachatryan:2010uf](#), [202](#)]. Muon system noise can be rejected by requiring high-quality muon tracks.

Noise in both the calorimeters and the muon systems could be estimated by looking at dedicated cosmic data-taking runs and then applying some selection criteria to reject cosmic-ray muons. The remaining events would most likely be noise.

A.6 *Algorithmically induced fakes*

For searches that aim to reconstruct the decay vertex of a long-lived particle, and especially for long-lived particles decaying in the proximity of the interaction region, algorithmically induced fakes and/or instrumental backgrounds can be of importance.

A.6.1 *Random/merged vertices*

This type of background is especially important in the high-track-density environment close to the interaction region and arises from two main sources: two or more individual tracks crossing each other and getting reconstructed as a displaced vertex as well as two close-by low-mass vertices reconstructed as one high-mass displaced vertex (such a final merging/cleaning step is often part of vertexing algorithms to reduce fakes in standard vertexing).

The former source is mostly suppressed by requirements originally targeting the removal of meta-stable SM particles: a minimum $|d_0|$ for tracks and a minimum distance between primary and a given displaced vertex.

The latter source is obviously harder to suppress, though can be estimated by randomly merging vertices from distinct events. By studying number of reconstructed ‘merged’ high-mass vertices as a function of distance between the two low-multiplicity low-mass vertices that got ‘merged’ both with vertices from the same event as well as from different events and scaling them accordingly,

an estimate for this background can be derived. This method has been successfully used the a recent ATLAS analysis searching for displaced vertices [144].

A.6.2 *Randomly crossing tracks*

Typically of more relevance than merged vertices is the background stemming from low-mass vertices crossed by unrelated tracks, resulting in the reconstruction of a high-mass vertex. The mass of the reconstructed displaced vertex is especially increased when the random track crosses the vertex in a direction that is perpendicular to the distance vector pointing from the primary vertex to the displaced one.

As demonstrated in detail in Ref. [144], this background can be estimated by constructing vertices (n -track) from lower-multiplicity ones ($n-1$ -track) by adding pseudo-tracks, drawn randomly from data-driven track templates derived for various radial detector regions. The normalisation of the prediction is performed by comparing the $n-1$ -track-based constructed vertices with the actual n -track vertices in all radial detector regions.

A.7 *Summary*

Bibliography

- [1] A. Bouquet and P. Salati, *R Parity Breaking and Cosmological Consequences*, Nucl. Phys. **B284** (1987) 557.
- [2] B. A. Campbell et al., *Cosmological baryon asymmetry constraints on extensions of the standard model*, Phys. Lett. **B256** (1991) 484–490.
- [3] Y. Cui and R. Sundrum, *Baryogenesis for weakly interacting massive particles*, Phys. Rev. **D87.11** (2013) 116013, arXiv: [1212.2973 \[hep-ph\]](#).
- [4] K. Barry, P. W. Graham, and S. Rajendran, *Displaced vertices from R-parity violation and baryogenesis*, Phys. Rev. **D89.5** (2014) 054003, arXiv: [1310.3853 \[hep-ph\]](#).
- [5] Y. Cui and B. Shuve, *Probing Baryogenesis with Displaced Vertices at the LHC*, JHEP **02** (2015) 049, arXiv: [1409.6729 \[hep-ph\]](#).
- [6] S. Ipek and J. March-Russell, *Baryogenesis via Particle-Antiparticle Oscillations*, Phys. Rev. **D93.12** (2016) 123528, arXiv: [1604.00009 \[hep-ph\]](#).
- [7] M. Baumgart et al., *Non-Abelian Dark Sectors and Their Collider Signatures*, JHEP **04** (2009) 014, arXiv: [0901.0283 \[hep-ph\]](#).
- [8] D. E. Kaplan, M. A. Luty, and K. M. Zurek, *Asymmetric Dark Matter*, Phys. Rev. **D79** (2009) 115016, arXiv: [0901.4117 \[hep-ph\]](#).
- [9] Y. F. Chan et al., *LHC Signatures of a Minimal Supersymmetric Hidden Valley*, JHEP **05** (2012) 155, arXiv: [1112.2705 \[hep-ph\]](#).
- [10] K. R. Dienes and B. Thomas, *Dynamical Dark Matter: I. Theoretical Overview*, Phys. Rev. **D85** (2012) 083523, arXiv: [1106.4546 \[hep-ph\]](#).
- [11] K. R. Dienes, S. Su, and B. Thomas, *Distinguishing Dynamical Dark Matter at the LHC*, Phys. Rev. **D86** (2012) 054008, arXiv: [1204.4183 \[hep-ph\]](#).
- [12] I.-W. Kim and K. M. Zurek, *Flavor and Collider Signatures of Asymmetric Dark Matter*, Phys. Rev. **D89.3** (2014) 035008, arXiv: [1310.2617 \[hep-ph\]](#).

- [13] J. C. Helo, M. Hirsch, and S. Kovalenko, *Heavy neutrino searches at the LHC with displaced vertices*, Phys. Rev. **D89** (2014), [Erratum: Phys. Rev.D93,no.9,099902(2016)] 073005, arXiv: [1312.2900 \[hep-ph\]](#).
- [14] S. Antusch, E. Cazzato, and O. Fischer, *Displaced vertex searches for sterile neutrinos at future lepton colliders*, JHEP **12** (2016) 007, arXiv: [1604.02420 \[hep-ph\]](#).
- [15] M. L. Graesser, *Broadening the Higgs boson with right-handed neutrinos and a higher dimension operator at the electroweak scale*, Phys. Rev. **D76** (2007) 075006, arXiv: [0704.0438 \[hep-ph\]](#).
- [16] M. L. Graesser, *Experimental Constraints on Higgs Boson Decays to TeV-scale Right-Handed Neutrinos* (2007), arXiv: [0705.2190 \[hep-ph\]](#).
- [17] E. Izaguirre and B. Shuve, *Multilepton and Lepton Jet Probes of Sub-Weak-Scale Right-Handed Neutrinos*, Phys. Rev. **D91.9** (2015) 093010, arXiv: [1504.02470 \[hep-ph\]](#).
- [18] A. Maiezza, M. Nemevek, and F. Nesti, *Lepton Number Violation in Higgs Decay at LHC*, Phys. Rev. Lett. **115** (2015) 081802, arXiv: [1503.06834 \[hep-ph\]](#).
- [19] B. Batell, M. Pospelov, and B. Shuve, *Shedding Light on Neutrino Masses with Dark Forces*, JHEP **08** (2016) 052, arXiv: [1604.06099 \[hep-ph\]](#).
- [20] G. F. Giudice and R. Rattazzi, *Theories with gauge mediated supersymmetry breaking*, Phys. Rept. **322** (1999) 419–499, arXiv: [hep-ph/9801271 \[hep-ph\]](#).
- [21] G. Burdman et al., *Folded supersymmetry and the LEP paradox*, JHEP **02** (2007) 009, arXiv: [hep-ph/0609152 \[hep-ph\]](#).
- [22] H. Cai, H.-C. Cheng, and J. Terning, *A Quirky Little Higgs Model*, JHEP **05** (2009) 045, arXiv: [0812.0843 \[hep-ph\]](#).
- [23] Z. Chacko, H.-S. Goh, and R. Harnik, *The Twin Higgs: Natural electroweak breaking from mirror symmetry*, Phys. Rev. Lett. **96** (2006) 231802, arXiv: [hep-ph/0506256 \[hep-ph\]](#).
- [24] J. Fan, M. Reece, and J. T. Ruderman, *Stealth Supersymmetry*, JHEP **11** (2011) 012, arXiv: [1105.5135 \[hep-ph\]](#).
- [25] R. Barbier et al., *R-parity violating supersymmetry*, Phys. Rept. **420** (2005) 1–202, arXiv: [hep-ph/0406039 \[hep-ph\]](#).
- [26] C. Csaki, E. Kuflik, and T. Volansky, *Dynamical R-Parity Violation*, Phys. Rev. Lett. **112** (2014) 131801, arXiv: [1309.5957 \[hep-ph\]](#).
- [27] A. Arvanitaki et al., *Mini-Split*, JHEP **02** (2013) 126, arXiv: [1210.0555 \[hep-ph\]](#).
- [28] N. Arkani-Hamed et al., *Simply Unnatural Supersymmetry* (2012), arXiv: [1212.6971 \[hep-ph\]](#).

- [29] C. H. Chen, M. Drees, and J. F. Gunion, *Searching for invisible and almost invisible particles at e+ e- colliders*, Phys. Rev. Lett. **76** (1996) 2002–2005, arXiv: [hep-ph/9512230 \[hep-ph\]](#).
- [30] S. D. Thomas and J. D. Wells, *Phenomenology of Massive Vectorlike Doublet Leptons*, Phys. Rev. Lett. **81** (1998) 34–37, arXiv: [hep-ph/9804359 \[hep-ph\]](#).
- [31] J. L. Feng et al., *Discovering supersymmetry at the Tevatron in wino LSP scenarios*, Phys. Rev. Lett. **83** (1999) 1731–1734, arXiv: [hep-ph/9904250 \[hep-ph\]](#).
- [32] M. J. Strassler and K. M. Zurek, *Echoes of a hidden valley at hadron colliders*, Phys. Lett. **B651** (2007) 374–379, arXiv: [hep-ph/0604261 \[hep-ph\]](#).
- [33] M. J. Strassler and K. M. Zurek, *Discovering the Higgs through highly-displaced vertices*, Phys. Lett. **B661** (2008) 263–267, arXiv: [hep-ph/0605193 \[hep-ph\]](#).
- [34] M. J. Strassler, *Possible effects of a hidden valley on supersymmetric phenomenology* (2006), arXiv: [hep-ph/0607160 \[hep-ph\]](#).
- [35] T. Han et al., *Phenomenology of hidden valleys at hadron colliders*, JHEP **07** (2008) 008, arXiv: [0712.2041 \[hep-ph\]](#).
- [36] M. J. Strassler, *Why Unparticle Models with Mass Gaps are Examples of Hidden Valleys* (2008), arXiv: [0801.0629 \[hep-ph\]](#).
- [37] M. J. Strassler, *On the Phenomenology of Hidden Valleys with Heavy Flavor* (2008), arXiv: [0806.2385 \[hep-ph\]](#).
- [38] D. Alves, *Simplified Models for LHC New Physics Searches*, J. Phys. **G39** (2012), ed. by N. Arkani-Hamed et al. 105005, arXiv: [1105.2838 \[hep-ph\]](#).
- [39] J. Abdallah et al., *Simplified Models for Dark Matter Searches at the LHC*, Phys. Dark Univ. **9-10** (2015) 8–23, arXiv: [1506.03116 \[hep-ph\]](#).
- [40] L. Edelhäuser, M. Krämer, and J. Sonneveld, *Simplified models for same-spin new physics scenarios*, JHEP **04** (2015) 146, arXiv: [1501.03942 \[hep-ph\]](#).
- [41] L. Edelhäuser et al., *Constraining supersymmetry at the LHC with simplified models for squark production*, JHEP **12** (2014) 022, arXiv: [1410.0965 \[hep-ph\]](#).
- [42] C. Arina et al., *Constraints on sneutrino dark matter from LHC Run 1*, JHEP **05** (2015) 142, arXiv: [1503.02960 \[hep-ph\]](#).
- [43] S. Kraml et al., *Scalar versus fermionic top partner interpretations of $t\bar{t} + E_T^{\text{miss}}$ searches at the LHC*, JHEP **11** (2016) 107, arXiv: [1607.02050 \[hep-ph\]](#).
- [44] J. Heisig and J. Kersten, *Long-lived staus from strong production in a simplified model approach*, Phys. Rev. **D86** (2012) 055020, arXiv: [1203.1581 \[hep-ph\]](#).

- [45] Z. Liu and B. Tweedie, *The Fate of Long-Lived Superparticles with Hadronic Decays after LHC Run 1*, JHEP **06** (2015) 042, arXiv: [1503.05923 \[hep-ph\]](#).
- [46] J. Heisig, A. Lessa, and L. Quertenmont, *Simplified Models for Exotic BSM Searches*, JHEP **12** (2015) 087, arXiv: [1509.00473 \[hep-ph\]](#).
- [47] V. V. Khoze, A. D. Plascencia, and K. Sakurai, *Simplified models of dark matter with a long-lived co-annihilation partner*, JHEP **06** (2017) 041, arXiv: [1702.00750 \[hep-ph\]](#).
- [48] R. Mahbubani, P. Schwaller, and J. Zurita, *Closing the window for compressed Dark Sectors with disappearing charged tracks*, JHEP **06** (2017) 119, arXiv: [1703.05327 \[hep-ph\]](#).
- [49] O. Buchmueller et al., *Simplified Models for Displaced Dark Matter Signatures*, JHEP **09** (2017) 076, arXiv: [1704.06515 \[hep-ph\]](#).
- [50] A. Haas et al., *Looking for milli-charged particles with a new experiment at the LHC*, Phys. Lett. **B746** (2015) 117–120, arXiv: [1410.6816 \[hep-ph\]](#).
- [51] J. P. Chou, D. Curtin, and H. J. Lubatti, *New Detectors to Explore the Lifetime Frontier*, Phys. Lett. **B767** (2017) 29–36, arXiv: [1606.06298 \[hep-ph\]](#).
- [52] V. V. Gligorov et al., *Searching for Long-lived Particles: A Compact Detector for Exotics at LHCb* (2017), arXiv: [1708.09395 \[hep-ph\]](#).
- [53] J. Feng et al., *FASER: ForwArd Search ExpeRiment at the LHC* (2017), arXiv: [1708.09389 \[hep-ph\]](#).
- [54] R. Essig et al., *Heavy Flavor Simplified Models at the LHC*, JHEP **01** (2012) 074, arXiv: [1110.6443 \[hep-ph\]](#).
- [55] C. Brust et al., *SUSY, the Third Generation and the LHC*, JHEP **03** (2012) 103, arXiv: [1110.6670 \[hep-ph\]](#).
- [56] M. Papucci, J. T. Ruderman, and A. Weiler, *Natural SUSY Endures*, JHEP **09** (2012) 035, arXiv: [1110.6926 \[hep-ph\]](#).
- [57] S. Dimopoulos et al., *Experimental signatures of low-energy gauge mediated supersymmetry breaking*, Phys. Rev. Lett. **76** (1996) 3494–3497, arXiv: [hep-ph/9601367 \[hep-ph\]](#).
- [58] N. Arkani-Hamed and S. Dimopoulos, *Supersymmetric unification without low energy supersymmetry and signatures for fine-tuning at the LHC*, JHEP **06** (2005) 073, arXiv: [hep-th/0405159 \[hep-th\]](#).
- [59] M. Byrne, *Universal extra dimensions and charged LKPs*, Phys. Lett. **B583** (2004) 309–314, arXiv: [hep-ph/0311160 \[hep-ph\]](#).
- [60] V. Khachatryan et al., *Precise determination of the mass of the Higgs boson and tests of compatibility of its couplings with the standard model predictions using proton collisions at 7 and 8 TeV*, Eur. Phys. J. **C75-5** (2015) 212, arXiv: [1412.8662 \[hep-ex\]](#).

- [61] G. Aad et al., *Constraints on new phenomena via Higgs boson couplings and invisible decays with the ATLAS detector*, JHEP **11** (2015) 206, arXiv: [1509.00672 \[hep-ex\]](#).
- [62] D. Curtin et al., *Exotic decays of the 125 GeV Higgs boson*, Phys. Rev. **D90**.7 (2014) 075004, arXiv: [1312.4992 \[hep-ph\]](#).
- [63] N. Craig et al., *Naturalness in the Dark at the LHC*, JHEP **07** (2015) 105, arXiv: [1501.05310 \[hep-ph\]](#).
- [64] V. Silveira and A. Zee, *SCALAR PHANTOMS*, Phys. Lett. **161B** (1985) 136–140.
- [65] P. Langacker, *The Physics of Heavy Z' Gauge Bosons*, Rev. Mod. Phys. **81** (2009) 1199–1228, arXiv: [0801.1345 \[hep-ph\]](#).
- [66] B. Holdom, *Two $U(1)$'s and Epsilon Charge Shifts*, Phys. Lett. **166B** (1986) 196–198.
- [67] J. L. Feng, M. Kaplinghat, and H.-B. Yu, *Halo Shape and Relic Density Exclusions of Sommerfeld-Enhanced Dark Matter Explanations of Cosmic Ray Excesses*, Phys. Rev. Lett. **104** (2010) 151301, arXiv: [0911.0422 \[hep-ph\]](#).
- [68] M. R. Buckley and P. J. Fox, *Dark Matter Self-Interactions and Light Force Carriers*, Phys. Rev. **D81** (2010) 083522, arXiv: [0911.3898 \[hep-ph\]](#).
- [69] S. Tulin, H.-B. Yu, and K. M. Zurek, *Resonant Dark Forces and Small Scale Structure*, Phys. Rev. Lett. **110**.11 (2013) 111301, arXiv: [1210.0900 \[hep-ph\]](#).
- [70] C. Boehm and P. Fayet, *Scalar dark matter candidates*, Nucl. Phys. **B683** (2004) 219–263, arXiv: [hep-ph/0305261 \[hep-ph\]](#).
- [71] C. Boehm, P. Fayet, and J. Silk, *Light and heavy dark matter particles*, Phys. Rev. **D69** (2004) 101302, arXiv: [hep-ph/0311143 \[hep-ph\]](#).
- [72] M. Pospelov, A. Ritz, and M. B. Voloshin, *Secluded WIMP Dark Matter*, Phys. Lett. **B662** (2008) 53–61, arXiv: [0711.4866 \[hep-ph\]](#).
- [73] N. Arkani-Hamed and N. Weiner, *LHC Signals for a SuperUnified Theory of Dark Matter*, JHEP **12** (2008) 104, arXiv: [0810.0714 \[hep-ph\]](#).
- [74] N. Arkani-Hamed et al., *A Theory of Dark Matter*, Phys. Rev. **D79** (2009) 015014, arXiv: [0810.0713 \[hep-ph\]](#).
- [75] Y. Hochberg, E. Kuflik, and H. Murayama, *SIMP Spectroscopy*, JHEP **05** (2016) 090, arXiv: [1512.07917 \[hep-ph\]](#).
- [76] D. Tucker-Smith and N. Weiner, *Inelastic dark matter*, Phys. Rev. **D64** (2001) 043502, arXiv: [hep-ph/0101138 \[hep-ph\]](#).
- [77] K. Griest and D. Seckel, *Three exceptions in the calculation of relic abundances*, Phys. Rev. **D43** (1991) 3191–3203.
- [78] M. J. Baker et al., *The Coannihilation Codex*, JHEP **12** (2015) 120, arXiv: [1510.03434 \[hep-ph\]](#).

- [79] A. Falkowski et al., *Hidden Higgs Decaying to Lepton Jets*, JHEP **05** (2010) 077, arXiv: [1002.2952 \[hep-ph\]](#).
- [80] Y. Bai and T. M. P. Tait, *Inelastic Dark Matter at the LHC*, Phys. Lett. **B710** (2012) 335–338, arXiv: [1109.4144 \[hep-ph\]](#).
- [81] R. Primulando, E. Salvioni, and Y. Tsai, *The Dark Penguin Shines Light at Colliders*, JHEP **07** (2015) 031, arXiv: [1503.04204 \[hep-ph\]](#).
- [82] Y. Bai, J. Bourbeau, and T. Lin, *Dark matter searches with a mono-Z[?] jet*, JHEP **06** (2015) 205, arXiv: [1504.01395 \[hep-ph\]](#).
- [83] E. Izaguirre, G. Krnjaic, and B. Shuve, *Discovering Inelastic Thermal-Relic Dark Matter at Colliders*, Phys. Rev. **D93.6** (2016) 063523, arXiv: [1508.03050 \[hep-ph\]](#).
- [84] M. Garny et al., *Coannihilation without chemical equilibrium*, Phys. Rev. **D96.10** (2017) 103521, arXiv: [1705.09292 \[hep-ph\]](#).
- [85] A. Davoli et al., *Displaced Vertices from Pseudo-Dirac Dark Matter*, JHEP **11** (2017) 025, arXiv: [1706.08985 \[hep-ph\]](#).
- [86] P. Minkowski, $\mu \rightarrow e\gamma$ at a Rate of One Out of 10^9 Muon Decays? Phys. Lett. **67B** (1977) 421–428.
- [87] T. Yanagida, *HORIZONTAL SYMMETRY AND MASSES OF NEUTRINOS*, Conf. Proc. **C7902131** (1979) 95–99.
- [88] R. N. Mohapatra and G. Senjanovic, *Neutrino Mass and Spontaneous Parity Violation*, Phys. Rev. Lett. **44** (1980) 912.
- [89] S. L. Glashow, *The Future of Elementary Particle Physics*, NATO Sci. Ser. B **61** (1980) 687.
- [90] R. N. Mohapatra and J. W. F. Valle, *Neutrino Mass and Baryon Number Nonconservation in Superstring Models*, Phys. Rev. **D34** (1986) 1642.
- [91] W.-Y. Keung and G. Senjanovic, *Majorana Neutrinos and the Production of the Right-handed Charged Gauge Boson*, Phys. Rev. Lett. **50** (1983) 1427.
- [92] A. Ferrari et al., *Sensitivity study for new gauge bosons and right-handed Majorana neutrinos in pp collisions at s = 14-TeV*, Phys. Rev. **D62** (2000) 013001.
- [93] L. Basso et al., *Phenomenology of the minimal B-L extension of the Standard model: Z' and neutrinos*, Phys. Rev. **D80** (2009) 055030, arXiv: [0812.4313 \[hep-ph\]](#).
- [94] P. Fileviez Perez, T. Han, and T. Li, *Testability of Type I Seesaw at the CERN LHC: Revealing the Existence of the B-L Symmetry*, Phys. Rev. **D80** (2009) 073015, arXiv: [0907.4186 \[hep-ph\]](#).
- [95] M. Nemevsek et al., *First Limits on Left-Right Symmetry Scale from LHC Data*, Phys. Rev. **D83** (2011) 115014, arXiv: [1103.1627 \[hep-ph\]](#).

- [96] M. Nemev  ek, F. Nesti, and J. C. Vasquez, *Majorana Higgses at colliders*, JHEP **04** (2017) 114, arXiv: [1612.06840 \[hep-ph\]](#).
- [97] T. Asaka, S. Blanchet, and M. Shaposhnikov, *The nuMSM, dark matter and neutrino masses*, Phys. Lett. **B631** (2005) 151–156, arXiv: [hep-ph/0503065 \[hep-ph\]](#).
- [98] T. Asaka and M. Shaposhnikov, *The nuMSM, dark matter and baryon asymmetry of the universe*, Phys. Lett. **B620** (2005) 17–26, arXiv: [hep-ph/0505013 \[hep-ph\]](#).
- [99] J. C. Pati and A. Salam, *Lepton Number as the Fourth Color*, Phys. Rev. **D10** (1974), [Erratum: Phys. Rev.D11,703(1975)] 275–289.
- [100] R. N. Mohapatra and J. C. Pati, *A Natural Left-Right Symmetry*, Phys. Rev. **D11** (1975) 2558.
- [101] G. Senjanovic and R. N. Mohapatra, *Exact Left-Right Symmetry and Spontaneous Violation of Parity*, Phys. Rev. **D12** (1975) 1502.
- [102] G. Senjanovic, *Spontaneous Breakdown of Parity in a Class of Gauge Theories*, Nucl. Phys. **B153** (1979) 334–364.
- [103] E. Accomando et al., *Novel SM-like Higgs decay into displaced heavy neutrino pairs in $U(1)?$ models*, JHEP **04** (2017) 081, arXiv: [1612.05977 \[hep-ph\]](#).
- [104] A. Das, Y. Gao, and T. Kamon, *Heavy Neutrino Search via the Higgs boson at the LHC* (2017), arXiv: [1704.00881 \[hep-ph\]](#).
- [105] A. Caputo et al., *The seesaw portal in testable models of neutrino masses*, JHEP **06** (2017) 112, arXiv: [1704.08721 \[hep-ph\]](#).
- [106] V. Khachatryan et al., *Search for narrow resonances in dilepton mass spectra in proton-proton collisions at $\sqrt{s} = 13$ TeV and combination with 8 TeV data*, Phys. Lett. **B768** (2017) 57–80, arXiv: [1609.05391 \[hep-ex\]](#).
- [107] A. M. Sirunyan et al., *Search for dijet resonances in proton?proton collisions at $\sqrt{s} = 13$ TeV and constraints on dark matter and other models*, Phys. Lett. **B769** (2017), [Erratum: Phys. Lett.B772,882(2017)] 520–542, arXiv: [1611.03568 \[hep-ex\]](#).
- [108] M. Aaboud et al., *Search for new phenomena in dijet events using 37 fb^{-1} of pp collision data collected at $\sqrt{s} = 13$ TeV with the ATLAS detector*, Phys. Rev. **D96.5** (2017) 052004, arXiv: [1703.09127 \[hep-ex\]](#).
- [109] A. M. Sirunyan et al., *Search for Low Mass Vector Resonances Decaying to Quark-Antiquark Pairs in Proton-Proton Collisions at $\sqrt{s} = 13$ TeV*, Phys. Rev. Lett. **119.11** (2017) 111802, arXiv: [1705.10532 \[hep-ex\]](#).
- [110] M. Aaboud et al., *Search for new high-mass phenomena in the dilepton final state using 36 fb^{-1} of proton-proton collision data at $\sqrt{s} = 13$ TeV with the ATLAS detector*, JHEP **10** (2017) 182, arXiv: [1707.02424 \[hep-ex\]](#).

- [111] M. Aaboud et al., *Search for $W' \rightarrow tb$ decays in the hadronic final state using pp collisions at $\sqrt{s} = 13$ TeV with the ATLAS detector* (2018), arXiv: [1801.07893 \[hep-ex\]](#).
- [112] M. Aaboud et al., *Search for light resonances decaying to boosted quark pairs and produced in association with a photon or a jet in proton-proton collisions at $\sqrt{s} = 13$ TeV with the ATLAS detector* (2018), arXiv: [1801.08769 \[hep-ex\]](#).
- [113] G. Aad et al., *Search for massive, long-lived particles using multitrack displaced vertices or displaced lepton pairs in pp collisions at $\sqrt{s} = 8$ TeV with the ATLAS detector*, Phys. Rev. **D92.7** (2015) 072004, arXiv: [1504.05162 \[hep-ex\]](#).
- [114] *Search for displaced leptons in the e-mu channel*, tech. rep. CMS-PAS-EXO-16-022, Geneva: CERN, 2016.
- [115] P. Bhupal Dev, R. N. Mohapatra, and Y. Zhang, *Displaced photon signal from a possible light scalar in minimal left-right seesaw model*, Phys. Rev. **D95.11** (2017) 115001, arXiv: [1612.09587 \[hep-ph\]](#).
- [116] N. Weiner and I. Yavin, *How Dark Are Majorana WIMPs? Signals from MiDM and Rayleigh Dark Matter*, Phys. Rev. **D86** (2012) 075021, arXiv: [1206.2910 \[hep-ph\]](#).
- [117] S. Dimopoulos, S. D. Thomas, and J. D. Wells, *Sparticle spectroscopy and electroweak symmetry breaking with gauge mediated supersymmetry breaking*, Nucl. Phys. **B488** (1997) 39–91, arXiv: [hep-ph/9609434 \[hep-ph\]](#).
- [118] G. Abbiendi et al., *Search for stable and longlived massive charged particles in $e^+ e^-$ collisions at $s^{**}(1/2) = 130$ -GeV to 209-GeV*, Phys. Lett. **B572** (2003) 8–20, arXiv: [hep-ex/0305031 \[hep-ex\]](#).
- [119] B. Bajc and G. Senjanovic, *Seesaw at LHC*, JHEP **08** (2007) 014, arXiv: [hep-ph/0612029 \[hep-ph\]](#).
- [120] B. Bajc, M. Nemevsek, and G. Senjanovic, *Probing seesaw at LHC*, Phys. Rev. **D76** (2007) 055011, arXiv: [hep-ph/0703080 \[hep-ph\]](#).
- [121] R. Franceschini, T. Hambye, and A. Strumia, *Type-III see-saw at LHC*, Phys. Rev. **D78** (2008) 033002, arXiv: [0805.1613 \[hep-ph\]](#).
- [122] A. Arhrib et al., *Collider Signatures for Heavy Lepton Triplet in Type I+III Seesaw*, Phys. Rev. **D82** (2010) 053004, arXiv: [0904.2390 \[hep-ph\]](#).
- [123] G. Aad et al., *Search for magnetic monopoles and stable particles with high electric charges in 8 TeV pp collisions with the ATLAS detector*, Phys. Rev. **D93.5** (2016) 052009, arXiv: [1509.08059 \[hep-ex\]](#).
- [124] V. Khachatryan et al., *Search for long-lived charged particles in proton-proton collisions at $\sqrt{s} = 13\text{??TeV}$* , Phys. Rev. **D94.11** (2016) 112004, arXiv: [1609.08382 \[hep-ex\]](#).

- [125] V. Khachatryan et al., *Search for disappearing tracks in proton-proton collisions at $\sqrt{s} = 8$ TeV*, JHEP **01** (2015) 096, arXiv: [1411.6006 \[hep-ex\]](#).
- [126] M. Aaboud et al., *Search for long-lived charginos based on a disappearing-track signature in pp collisions at $\sqrt{s} = 13$ TeV with the ATLAS detector* (2017), arXiv: [1712.02118 \[hep-ex\]](#).
- [127] T. Sjostrand, S. Mrenna, and P. Z. Skands, *A Brief Introduction to PYTHIA 8.1*, Comput. Phys. Commun. **178** (2008) 852–867, arXiv: [0710.3820 \[hep-ph\]](#).
- [128] F. Buccella, G. R. Farrar, and A. Pugliese, *R BARYON MASSES*, Phys. Lett. **153B** (1985) 311–314.
- [129] G. R. Farrar et al., *Limit on the mass of a long-lived or stable gluino*, JHEP **02** (2011) 018, arXiv: [1011.2964 \[hep-ph\]](#).
- [130] M. Aaboud et al., *Search for heavy long-lived charged R-hadrons with the ATLAS detector in 3.2 fb^{-1} of proton–proton collision data at $\sqrt{s} = 13$ TeV*, Phys. Lett. **B760** (2016) 647–665, arXiv: [1606.05129 \[hep-ex\]](#).
- [131] C. Collaboration, *Search for heavy stable charged particles with 12.9 fb^{-1} of 2016 data* (2016).
- [132] S. Agostinelli et al., *GEANT4: A Simulation toolkit*, Nucl. Instrum. Meth. **A506** (2003) 250–303.
- [133] R. Mackeprang and D. Milstead, *An Updated Description of Heavy-Hadron Interactions in GEANT-4*, Eur. Phys. J. **C66** (2010) 493–501, arXiv: [0908.1868 \[hep-ph\]](#).
- [134] J. Alwall et al., *MadGraph 5 : Going Beyond*, JHEP **06** (2011) 128, arXiv: [1106.0522 \[hep-ph\]](#).
- [135] J. Alwall et al., *The automated computation of tree-level and next-to-leading order differential cross sections, and their matching to parton shower simulations*, JHEP **07** (2014) 079, arXiv: [1405.0301 \[hep-ph\]](#).
- [136] C. Degrande et al., *UFO - The Universal FeynRules Output*, Comput. Phys. Commun. **183** (2012) 1201–1214, arXiv: [1108.2040 \[hep-ph\]](#).
- [137] P. Artoisenet et al., *Automatic spin-entangled decays of heavy resonances in Monte Carlo simulations*, JHEP **03** (2013) 015, arXiv: [1212.3460 \[hep-ph\]](#).
- [138] T. Sjöstrand et al., *An Introduction to PYTHIA 8.2*, Comput. Phys. Commun. **191** (2015) 159–177, arXiv: [1410.3012 \[hep-ph\]](#).
- [139] D. Curtin et al., *Illuminating Dark Photons with High-Energy Colliders*, JHEP **02** (2015) 157, arXiv: [1412.0018 \[hep-ph\]](#).
- [140] S. Knapen et al., *Triggering Soft Bombs at the LHC*, JHEP **08** (2017) 076, arXiv: [1612.00850 \[hep-ph\]](#).
- [141] *Search for long-lived neutral particles decaying in the hadronic calorimeter of ATLAS at $\sqrt{s} = 13$ TeV in 3.2 fb^{-1} of data*, tech. rep. ATLAS-CONF-2016-103, Geneva: CERN, 2016.

- [142] ATLAS Collaboration, *Search for pair-produced long-lived neutral particles decaying in the ATLAS hadronic calorimeter in pp collisions at $\sqrt{s} = 8$ TeV*, Phys. Lett. B **743** (2015) 15, arXiv: [1501.04020](#).
- [143] G. Aad et al., *Search for long-lived, weakly interacting particles that decay to displaced hadronic jets in proton-proton collisions at $\sqrt{s} = 8$ TeV with the ATLAS detector*, Phys. Rev. D **92.1** (2015) 012010, arXiv: [1504.03634 \[hep-ex\]](#).
- [144] M. Aaboud et al., *Search for long-lived, massive particles in events with displaced vertices and missing transverse momentum in $\sqrt{s} = 13$ TeV pp collisions with the ATLAS detector* (2017), arXiv: [1710.04901 \[hep-ex\]](#).
- [145] C. Collaboration, *Inclusive search for new particles decaying to displaced jets at $\sqrt{s} = 13$ TeV* (2017).
- [146] V. Khachatryan et al., *A search for pair production of new light bosons decaying into muons*, Phys. Lett. B **752** (2016) 146–168, arXiv: [1506.00424 \[hep-ex\]](#).
- [147] R. Aaij et al., *Updated search for long-lived particles decaying to jet pairs* (2017), arXiv: [1705.07332 \[hep-ex\]](#).
- [148] R. Aaij et al., *Search for Higgs-like bosons decaying into long-lived exotic particles*, Eur. Phys. J. C **76.12** (2016) 664, arXiv: [1609.03124 \[hep-ex\]](#).
- [149] *Performance of the reconstruction of large impact parameter tracks in the ATLAS inner detector*, tech. rep. ATL-PHYS-PUB-2017-014, Geneva: CERN, 2017.
- [150] ATLAS Collaboration, *Triggers for displaced decays of long-lived neutral particles in the ATLAS detector*, JINST **8** (2013) Po7015, arXiv: [1305.2284](#).
- [151] ATLAS Collaboration, *Standalone vertex finding in the ATLAS muon spectrometer*, JINST **9** (2014) Po2001, arXiv: [1311.7070](#).
- [152] V. Khachatryan et al., *Search for Long-Lived Neutral Particles Decaying to Quark-Antiquark Pairs in Proton-Proton Collisions at $\sqrt{s} = 8$ TeV*, Phys. Rev. D **91.1** (2015) 012007, arXiv: [1411.6530 \[hep-ex\]](#).
- [153] C. Csaki et al., *Searching for displaced Higgs boson decays*, Phys. Rev. D **92.7** (2015) 073008, arXiv: [1508.01522 \[hep-ph\]](#).
- [154] C. Vasquez Sierra, *Snapshot of current long-lived particle results at LHCb*, https://indico.cern.ch/event/649760/contributions/2689322/attachments/1542518/2419630/LHCb_LLP_CVS.pdf.
- [155] A. Coccaro et al., *Data-driven Model-independent Searches for Long-lived Particles at the LHC*, Phys. Rev. D **94.11** (2016) 113003, arXiv: [1605.02742 \[hep-ph\]](#).

- [156] V. Khachatryan et al., *Search for long-lived particles that decay into final states containing two electrons or two muons in proton-proton collisions at $\sqrt{s} = 8$ TeV*, Phys. Rev. **D91.5** (2015) 052012, arXiv: [1411.6977 \[hep-ex\]](#).
- [157] C. Collaboration, *Search for long-lived particles that decay into final states containing two muons, reconstructed using only the CMS muon chambers* (2015).
- [158] G. Aad et al., *Search for long-lived neutral particles decaying into lepton jets in proton-proton collisions at $\sqrt{s} = 8$ TeV with the ATLAS detector*, JHEP **11** (2014) 088, arXiv: [1409.0746 \[hep-ex\]](#).
- [159] *Search for long-lived neutral particles decaying into displaced lepton jets in proton–proton collisions at $\sqrt{s} = 13$ TeV with the ATLAS detector*, tech. rep. ATLAS-CONF-2016-042, Geneva: CERN, 2016.
- [160] G. Aad et al., *A search for prompt lepton-jets in pp collisions at $\sqrt{s} = 8$ TeV with the ATLAS detector*, JHEP **02** (2016) 062, arXiv: [1511.05542 \[hep-ex\]](#).
- [161] R. Aaij et al., *Search for hidden-sector bosons in $B^0 \rightarrow K^{*0}\mu^+\mu^-$ decays*, Phys. Rev. Lett. **115.16** (2015) 161802, arXiv: [1508.04094 \[hep-ex\]](#).
- [162] R. Aaij et al., *Search for long-lived scalar particles in $B^+ \rightarrow K^+\chi(\mu^+\mu^-)$ decays*, Phys. Rev. **D95.7** (2017) 071101, arXiv: [1612.07818 \[hep-ex\]](#).
- [163] R. Aaij et al., *Search for dark photons produced in 13 TeV pp collisions* (2017), arXiv: [1710.02867 \[hep-ex\]](#).
- [164] J. A. Evans and J. Shelton, *Long-Lived Staus and Displaced Leptons at the LHC*, JHEP **04** (2016) 056, arXiv: [1601.01326 \[hep-ph\]](#).
- [165] R. Aaij et al., *Tesla : an application for real-time data analysis in High Energy Physics*, Comput. Phys. Commun. **208** (2016) 35–42, arXiv: [1604.05596 \[physics.ins-det\]](#).
- [166] E. Izaguirre and B. Shuve, *Multilepton and Lepton Jet Probes of Sub-Weak-Scale Right-Handed Neutrinos*, Phys. Rev. D **91.9** (2015) 093010, arXiv: [1504.02470 \[hep-ph\]](#).
- [167] R. Aaij et al., *Search for massive long-lived particles decaying semileptonically in the LHCb detector*, Eur. Phys. J. **C77.4** (2017) 224, arXiv: [1612.00945 \[hep-ex\]](#).
- [168] R. Aaij et al., *Search for Majorana neutrinos in $B^- \rightarrow \pi^+\mu^-\mu^-$ decays*, Phys. Rev. Lett. **112.13** (2014) 131802, arXiv: [1401.5361 \[hep-ex\]](#).
- [169] B. Shuve and M. E. Peskin, *Revision of the LHCb Limit on Majorana Neutrinos*, Phys. Rev. **D94.11** (2016) 113007, arXiv: [1607.04258 \[hep-ph\]](#).

- [170] D. Gorbunov and M. Shaposhnikov, *How to find neutral leptons of the ν MSM?* JHEP **10** (2007), [Erratum: JHEP11,101(2013)] 015, arXiv: [0705.1729 \[hep-ph\]](#).
- [171] D. Milanes, N. Quintero, and C. E. Vera, *Sensitivity to Majorana neutrinos in $\Delta L = 2$ decays of B_c meson at LHCb*, Phys. Rev. **D93.9** (2016) 094026, arXiv: [1604.03177 \[hep-ph\]](#).
- [172] J. Helo, M. Hirsch, and S. Kovalenko, *Heavy neutrino searches at the LHC with displaced vertices*, Phys. Rev. D **89** (2014) 073005, arXiv: [1312.2900 \[hep-ph\]](#).
- [173] P. Mermod, *Right-handed neutrinos: the hunt is on!* Proceedings of Prospects in Neutrino Physics (NuPhys2016) (2017), arXiv: [1704.08635 \[hep-ex\]](#).
- [174] S. Antusch, E. Cazzato, and O. Fischer, *Sterile neutrino searches via displaced vertices at LHCb*, Phys. Lett. B **774** (2017) 114, arXiv: [1706.05990](#).
- [175] M. Gronau, C. N. Leung, and J. L. Rosner, *Extending Limits on Neutral Heavy Leptons*, Phys. Rev. D **29** (1984) 2539.
- [176] LHCb Collaboration, *Search for massive long-lived particles decaying semileptonically in the LHCb detector*, Eur. Phys. J. C **77.4** (2017) 224, arXiv: [1612.00945 \[hep-ex\]](#).
- [177] NA62 Collaboration, *The Beam and detector of the NA62 experiment at CERN*, JINST **12.05** (2017) Po5025, arXiv: [1703.08501 \[physics.ins-det\]](#).
- [178] SHiP Collaboration, *A facility to Search for Hidden Particles (SHiP) at the CERN SPS*, CERN-SPSC-2015-016 (2015), arXiv: [1504.04956 \[physics.ins-det\]](#).
- [179] T. Asaka and M. Shaposhnikov, *The nuMSM, dark matter and baryon asymmetry of the universe*, Phys. Lett. B **620** (2005) 17, arXiv: [hep-ph/0505013 \[hep-ph\]](#).
- [180] L. Canetti et al., *Dark Matter, Baryogenesis and Neutrino Oscillations from Right Handed Neutrinos*, Phys. Rev. D **87** (2013) 093006, arXiv: [1208.4607 \[hep-ph\]](#).
- [181] P. Mermod, *Hidden sector searches with SHiP and NA62*, Proceedings of International Workshop on Neutrinos from Accelerators (NuFact2017) (2017), arXiv: [1712.01768 \[hep-ex\]](#).
- [182] G. Aad et al., *Search for nonpointing and delayed photons in the diphoton and missing transverse momentum final state in 8 TeV pp collisions at the LHC using the ATLAS detector*, Phys. Rev. **D90.11** (2014) 112005, arXiv: [1409.5542 \[hep-ex\]](#).
- [183] G. Aad et al., *Search for nonpointing photons in the diphoton and E_T^{miss} final state in $\sqrt{s} = 7\text{TeV}$ proton-proton collisions using the ATLAS detector*, Phys. Rev. **D88.1** (2013) 012001, arXiv: [1304.6310 \[hep-ex\]](#).
- [184] C. Collaboration, *Search for long-lived neutral particles in the final state of delayed photons and missing energy in proton-proton collisions at $\sqrt{s} = 8\text{ TeV}$* (2015).

- [200] L. Horyn, *ATLAS Fast TracKer (FTK) – Overview of triggering constraints*, https://indico.cern.ch/event/649760/contributions/2748921/attachments/1542873/2420596/Horyn_LLP_FTK.pdf.
- [201] G. Aad et al., *Search for long-lived stopped R-hadrons decaying out-of-time with pp collisions using the ATLAS detector*, Phys. Rev. **D88.11** (2013) 112003, arXiv: [1310.6584](https://arxiv.org/abs/1310.6584) [hep-ex].
- [202] V. Khachatryan et al., *Search for Decays of Stopped Long-Lived Particles Produced in Proton–Proton Collisions at $\sqrt{s} = 8$ TeV*, Eur. Phys. J. **C75.4** (2015) 151, arXiv: [1501.05603](https://arxiv.org/abs/1501.05603) [hep-ex].
- [203] *Search for long-lived particles that stop in the CMS detector and decay to muons at $\sqrt{s} = 13$ TeV*, tech. rep. CMS-PAS-EXO-17-004, Geneva: CERN, 2017.
- [204] *Muon Reconstruction and Identification Improvements for Run-2 and First Results with 2015 Run Data* (2015).
- [205] B. Acharya et al., *Search for magnetic monopoles with the MoEDAL prototype trapping detector in 8 TeV proton-proton collisions at the LHC*, JHEP **08** (2016) 067, arXiv: [1604.06645](https://arxiv.org/abs/1604.06645) [hep-ex].
- [206] A. De Roeck et al., *Sensitivity of LHC Experiments to Exotic Highly Ionising Particles*, Eur. Phys. J. **C72** (2012) 1985, arXiv: [1112.2999](https://arxiv.org/abs/1112.2999) [hep-ph].
- [207] J. Kang and M. A. Luty, *Macroscopic Strings and ‘Quirks’ at Colliders*, JHEP **11** (2009) 065, arXiv: [0805.4642](https://arxiv.org/abs/0805.4642) [hep-ph].
- [208] V. M. Abazov et al., *Search for New Fermions (‘Quirks’) at the Fermilab Tevatron Collider*, Phys. Rev. Lett. **105** (2010) 211803, arXiv: [1008.3547](https://arxiv.org/abs/1008.3547) [hep-ex].
- [209] M. Farina and M. Low, *Constraining Quirky Tracks with Conventional Searches*, Phys. Rev. Lett. **119.11** (2017) 111801, arXiv: [1703.00912](https://arxiv.org/abs/1703.00912) [hep-ph].
- [210] S. Knapen et al., *Tracking down Quirks at the Large Hadron Collider* (2017), arXiv: [1708.02243](https://arxiv.org/abs/1708.02243) [hep-ph].
- [211] J. S. Bullock, *Notes on the Missing Satellites Problem*, ArXiv e-prints (Sept. 2010), arXiv: [1009.4505](https://arxiv.org/abs/1009.4505) [astro-ph.CO].
- [212] M. Boylan-Kolchin, J. S. Bullock, and M. Kaplinghat, *Too big to fail? The puzzling darkness of massive Milky Way subhaloes*, Monthly Notices of the Royal Astronomical Society **415** (July 2011) L40–L44, arXiv: [1103.0007](https://arxiv.org/abs/1103.0007) [astro-ph.CO].
- [213] D. H. Weinberg et al., *Cold dark matter: controversies on small scales*, Proc. Nat. Acad. Sci. **112** (2014), [Proc. Nat. Acad. Sci. **112**,2249(2015)] 12249–12255, arXiv: [1306.0913](https://arxiv.org/abs/1306.0913) [astro-ph.CO].
- [214] B. Famaey and S. McGaugh, *Challenges for Λ CDM and MOND*, Journal of Physics: Conference Series **437.1** (2013) 012001.

- [215] P. Schwaller, D. Stolarski, and A. Weiler, *Emerging Jets*, JHEP **05** (2015) 059, arXiv: [1502.05409 \[hep-ph\]](#).
- [216] N. Daci et al., *Simplified SIMPs and the LHC*, JHEP **11** (2015) 108, arXiv: [1503.05505 \[hep-ph\]](#).
- [217] C. Collaboration, *The Phase-2 Upgrade of the CMS Tracker*, tech. rep. CERN-LHCC-2017-009. CMS-TDR-014, Geneva: CERN, 2017.
- [218] C. Lourenco, *The Phase-2 Upgrade of the CMS Barrel Calorimeters Technical Design Report*, tech. rep. CERN-LHCC-2017-011. CMS-TDR-015, This is a dummy submission so that we get the LHCC reference number to be added in the cover page of the document. We will then proceed with the real submission. It would be good to have the submission workflow changed so as to avoid this extra complication., Geneva: CERN, 2017.
- [219] C. Lourenco, *The Phase-2 Upgrade of the CMS Muon Detectors*, tech. rep. CERN-LHCC-2017-012. CMS-TDR-016, This is a dummy submission, just to get the LHCC reference number., Geneva: CERN, 2017.
- [220] C. Lourenco, *The Phase-2 Upgrade of the CMS L1 Trigger Interim Technical Design Report*, tech. rep. CERN-LHCC-2017-013. CMS-TDR-017, Geneva: CERN, 2017.
- [221] CMS Collaboration, *Estimated Sensitivity for New Particle Searches at the HL-LHC*, CMS Physics Analysis Summary CMS-PAS-FTR-16-005, 2017.
- [222] Y. Gershtein, *CMS Hardware Track Trigger: New Opportunities for Long-Lived Particle Searches at the HL-LHC*, Phys. Rev. **D96.3** (2017) 035027, arXiv: [1705.04321 \[hep-ph\]](#).
- [223] *LHCb VELO Upgrade Technical Design Report*, LHCb-TDR-013, Geneva, 2013.
- [224] *LHCb Tracker Upgrade Technical Design Report*, LHCb-TDR-015, Geneva, 2014.
- [225] P. Ilten et al., *Proposed Inclusive Dark Photon Search at LHCb*, Phys. Rev. Lett. **116.25** (2016) 251803, arXiv: [1603.08926 \[hep-ph\]](#).
- [226] P. Ilten et al., *Dark photons from charm mesons at LHCb*, Phys. Rev. **D92.11** (2015) 115017, arXiv: [1509.06765 \[hep-ph\]](#).
- [227] A. Pierce et al., *Searching for Confining Hidden Valleys at the LHC(b)* (2017), arXiv: [1708.05389 \[hep-ph\]](#).
- [228] G. F. Giudice and A. Romanino, *Split supersymmetry*, Nucl. Phys. **B699** (2004), [Erratum: Nucl. Phys.B706,487(2005)] 65–89, arXiv: [hep-ph/0406088 \[hep-ph\]](#).
- [229] H. Pagels and J. R. Primack, *Supersymmetry, Cosmology and New TeV Physics*, Phys. Rev. Lett. **48** (1982) 223.

- [230] L. Covi, J. E. Kim, and L. Roszkowski, *Axinos as cold dark matter*, Phys. Rev. Lett. **82** (1999) 4180–4183, arXiv: [hep-ph/9905212 \[hep-ph\]](#).
- [231] L. J. Hall et al., *Freeze-In Production of FIMP Dark Matter*, JHEP **03** (2010) 080, arXiv: [0911.1120 \[hep-ph\]](#).
- [232] K. M. Zurek, *Asymmetric Dark Matter: Theories, Signatures, and Constraints*, Phys. Rept. **537** (2014) 91–121, arXiv: [1308.0338 \[hep-ph\]](#).
- [233] <https://twiki.cern.ch/twiki/bin/view/LHCPhysics/InterpretingLHCResults>.
- [234] N. Arkani-Hamed et al., *MARMOSET: The Path from LHC Data to the New Standard Model via On-Shell Effective Theories* (2007), arXiv: [hep-ph/0703088 \[HEP-PH\]](#).
- [235] J. Alwall, P. Schuster, and N. Toro, *Simplified Models for a First Characterization of New Physics at the LHC*, Phys. Rev. D**79** (2009) 075020, arXiv: [0810.3921 \[hep-ph\]](#).
- [236] D. Alves, *Simplified Models for LHC New Physics Searches*, J. Phys. **G39** (2012), ed. by N. Arkani-Hamed et al. 105005, arXiv: [1105.2838 \[hep-ph\]](#).
- [237] H. Okawa, *Interpretations of SUSY Searches in ATLAS with Simplified Models, Particles and fields. Proceedings, Meeting of the Division of the American Physical Society, DPF 2011, Providence, USA, August 9-13, 2011*, 2011, arXiv: [1110.0282 \[hep-ex\]](#).
- [238] S. Chatrchyan et al., *Interpretation of Searches for Supersymmetry with simplified Models*, Phys. Rev. D**88.5** (2013) 052017, arXiv: [1301.2175 \[hep-ex\]](#).
- [239] G. Busoni et al., *Recommendations on presenting LHC searches for missing transverse energy signals using simplified s-channel models of dark matter* (2016), ed. by A. Boveia et al., arXiv: [1603.04156 \[hep-ex\]](#).
- [240] S. Kraml et al., *SModelS: a tool for interpreting simplified-model results from the LHC and its application to supersymmetry*, Eur. Phys. J. C**74** (2014) 2868, arXiv: [1312.4175 \[hep-ph\]](#).
- [241] F. Ambrogi et al., *SModelS v1.1 user manual* (2017), arXiv: [1701.06586 \[hep-ph\]](#).
- [242] M. Papucci et al., *Fastlim: a fast LHC limit calculator*, Eur. Phys. J. C**74.11** (2014) 3163, arXiv: [1402.0492 \[hep-ph\]](#).
- [243] F. Ambrogi et al., *On the coverage of the pMSSM by simplified model results* (2017), arXiv: [1707.09036 \[hep-ph\]](#).
- [244] M. Drees et al., *CheckMATE: Confronting your Favourite New Physics Model with LHC Data*, Comput. Phys. Commun. **187** (2015) 227–265, arXiv: [1312.2591 \[hep-ph\]](#).
- [245] D. Dercks et al., *CheckMATE 2: From the model to the limit*, Comput. Phys. Commun. **221** (2017) 383–418, arXiv: [1611.09856 \[hep-ph\]](#).

- [246] E. Conte et al., *Designing and recasting LHC analyses with MadAnalysis 5*, Eur. Phys. J. **C74**.10 (2014) 3103, arXiv: [1405.3982 \[hep-ph\]](#).
- [247] B. Dumont et al., *Toward a public analysis database for LHC new physics searches using MADANALYSIS 5*, Eur. Phys. J. **C75**.2 (2015) 56, arXiv: [1407.3278 \[hep-ph\]](#).
- [248] A. Buckley et al., *Rivet user manual*, Comput. Phys. Commun. **184** (2013) 2803–2819, arXiv: [1003.0694 \[hep-ph\]](#).
- [249] C. Balíkzs et al., *ColliderBit: a GAMBIT module for the calculation of high-energy collider observables and likelihoods*, Eur. Phys. J. **C77**.11 (2017) 795, arXiv: [1705.07919 \[hep-ph\]](#).
- [250] J. de Favereau et al., *DELPHES 3, A modular framework for fast simulation of a generic collider experiment*, JHEP **02** (2014) 057, arXiv: [1307.6346 \[hep-ex\]](#).
- [251] *Simplified likelihood for the re-interpretation of public CMS results*, tech. rep. CMS-NOTE-2017-001, Geneva: CERN, 2017.
- [252] V. Khachatryan et al., *Constraints on the pMSSM, AMSB model and on other models from the search for long-lived charged particles in proton-proton collisions at $\sqrt{s} = 8$ TeV*, Eur. Phys. J. **C75**.7 (2015) 325, arXiv: [1502.02522 \[hep-ex\]](#).
- [253] G. Belanger et al., *Probing U(1) extensions of the MSSM at the LHC Run I and in dark matter searches*, JHEP **09** (2015) 151, arXiv: [1505.06243 \[hep-ph\]](#).
- [254] D. Barducci et al., *Status and prospects of the nMSSM after LHC Run-1*, JHEP **01** (2016) 050, arXiv: [1510.00246 \[hep-ph\]](#).
- [255] F. Spite and M. Spite, *Abundance of lithium in unevolved halo stars and old disk stars: Interpretation and consequences*, Astron. Astrophys. **115** (1982) 357–366.
- [256] R. H. Cyburt, B. D. Fields, and K. A. Olive, *An Update on the big bang nucleosynthesis prediction for Li-7: The problem worsens*, JCAP **0811** (2008) 012, arXiv: [0808.2818 \[astro-ph\]](#).
- [257] M. Fairbairn et al., *Stable massive particles at colliders*, Phys. Rept. **438** (2007) 1–63, arXiv: [hep-ph/0611040 \[hep-ph\]](#).
- [258] S. Chatrchyan et al., *Search for heavy long-lived charged particles in pp collisions at $\sqrt{s} = 7$ TeV*, Phys. Lett. **B713** (2012) 408–433, arXiv: [1205.0272 \[hep-ex\]](#).
- [259] G. Aad et al., *Searches for heavy long-lived sleptons and R-Hadrons with the ATLAS detector in pp collisions at $\sqrt{s} = 7$ TeV*, Phys. Lett. **B720** (2013) 277–308, arXiv: [1211.1597 \[hep-ex\]](#).
- [260] M. Aaboud et al., *Search for metastable heavy charged particles with large ionization energy loss in pp collisions at $\sqrt{s} = 13$ TeV using the ATLAS experiment*, Phys. Rev. **D93**.11 (2016) 112015, arXiv: [1604.04520 \[hep-ex\]](#).

- [261] G. R. Farrar and P. Fayet, *Phenomenology of the Production, Decay, and Detection of New Hadronic States Associated with Supersymmetry*, Phys. Lett. **B76** (1978) 575–579.
- [262] T. Sjöstrand, S. Mrenna, and P. Skands, *PYTHIA 6.4 Physics and Manual*, JHEP **05** (2006) 026, arXiv: [hep-ph/0603175](#).
- [263] E. Bagnaschi et al., *Likelihood Analysis of Supersymmetric SU(5) GUTs*, Eur. Phys. J. **C77**.2 (2017) 104, arXiv: [1610.10084](#) [hep-ph].
- [264] J. Heisig et al., *Trilinear-Augmented Gaugino Mediation*, JHEP **05** (2017) 003, arXiv: [1701.02313](#) [hep-ph].
- [265] A. G. Hessler et al., *Probing the scotogenic FIMP at the LHC*, JHEP **01** (2017) 100, arXiv: [1611.09540](#) [hep-ph].
- [266] J. Heisig and A. Lessa, *in preparation*, 2018.
- [267] V. Khachatryan et al., *Search for Displaced Supersymmetry in events with an electron and a muon with large impact parameters*, Phys. Rev. Lett. **114**.6 (2015) 061801, arXiv: [1409.4789](#) [hep-ex].
- [268] *Search for Displaced SUSY in Dilepton Final States*, CMS-PAS-B2G-12-024, 2014.
- [269] *Displaced SUSY Parametrisation Study For User*, <https://twiki.cern.ch/twiki/bin/view/CMSPublic/DisplacedSusyParametrisationStudyForUser>, 2014.
- [270] P. W. Graham et al., *Displaced Supersymmetry*, JHEP **07** (2012) 149, arXiv: [1204.6038](#) [hep-ph].
- [271] *Les Houches Workshop Series*, *in preparation*, 2018.
- [272] Y. Cui, *Natural Baryogenesis from Unnatural Supersymmetry*, JHEP **12** (2013) 067, arXiv: [1309.2952](#) [hep-ph].
- [273] *Search for long-lived neutral particles decaying to dijets*, tech. rep. CMS-PAS-EXO-12-038, Geneva: CERN, 2013.
- [274] M. Dine and W. Fischler, *A Phenomenological Model of Particle Physics Based on Supersymmetry*, Phys. Lett. **110B** (1982) 227–231.
- [275] M. Freytsis, D. J. Robinson, and Y. Tsai, *Galactic Center Gamma-Ray Excess through a Dark Shower*, Phys. Rev. **D91**.3 (2015) 035028, arXiv: [1410.3818](#) [hep-ph].
- [276] M. Freytsis et al., *Gamma-rays from Dark Showers with Twin Higgs Models*, JHEP **05** (2016) 018, arXiv: [1601.07556](#) [hep-ph].
- [277] *Search for long-lived, heavy particles in final states with a muon and a multi-track displaced vertex in proton-proton collisions at $\sqrt{s} = 8\text{TeV}$ with the ATLAS detector*. Tech. rep. ATLAS-CONF-2013-092, Geneva: CERN, 2013.
- [278] https://atlas.web.cern.ch/Atlas/GROUPS/PHYSICS/PAPERS/SUSY-2016-08/hepdata_info.pdf, 2017.

- [279] B. C. Allanach et al., *Prompt Signals and Displaced Vertices in Sparticle Searches for Next-to-Minimal Gauge Mediated Supersymmetric Models*, Eur. Phys. J. **C76**.9 (2016) 482, arXiv: [1606.03099 \[hep-ph\]](https://arxiv.org/abs/1606.03099).
- [280] M. Cacciari, G. P. Salam, and G. Soyez, *FastJet User Manual*, Eur. Phys. J. **C72** (2012) 1896, arXiv: [1111.6097 \[hep-ph\]](https://arxiv.org/abs/1111.6097).
- [281] M. Cacciari and G. P. Salam, *Pileup subtraction using jet areas*, Phys. Lett. **B659** (2008) 119–126, arXiv: [0707.1378 \[hep-ph\]](https://arxiv.org/abs/0707.1378).
- [282] D. Bertolini et al., *Pileup Per Particle Identification*, JHEP **10** (2014) 059, arXiv: [1407.6013 \[hep-ph\]](https://arxiv.org/abs/1407.6013).
- [283] M. Cacciari, G. P. Salam, and G. Soyez, *SoftKiller, a particle-level pileup removal method*, Eur. Phys. J. **C75**.2 (2015) 59, arXiv: [1407.0408 \[hep-ph\]](https://arxiv.org/abs/1407.0408).
- [284] E. Conte, B. Fuks, and G. Serret, *MadAnalysis 5, A User-Friendly Framework for Collider Phenomenology*, Comput. Phys. Commun. **184** (2013) 222–256, arXiv: [1206.1599 \[hep-ph\]](https://arxiv.org/abs/1206.1599).
- [285] C. Collaboration, *Search for displaced leptons in the e-mu channel* (2016).
- [286] *Search for pair-production of second-generation scalar leptoquarks in pp collisions at $\sqrt{s} = 13$ TeV with the CMS detector*, tech. rep. CMS-PAS-EXO-16-007, Geneva: CERN, 2016.
- [287] *Search for pair-production of second-generation scalar leptoquarks in pp collisions at $\sqrt{s} = 13$ TeV with the CMS detector*, <http://cms-results.web.cern.ch/cms-results/public-results/preliminary-results/EXO-16-007/>, 2016.

